

Amphiphilic Block Copolymers of Poly(ethylene oxide) and Poly(perfluorohexylethyl methacrylate): from Synthesis to Applications

Dissertation

zur Erlangung des akademischen Grades

Doktor-Ingenieur (Dr. -Ing.)

genehmigt durch

Mathematisch-Naturwissenschaftlich-Technische Fakultät

(Ingenieurwissenschaftlicher Bereich)

der Martin-Luther-Universität Halle-Wittenberg

von Herrn M.Phil. Hazrat Hussain

geb. am 05.01.1973 in Nawan Killi (Pakistan)

Gutachter:

1. Prof. Dr. J. Kressler
2. Prof. Dr. K. Mäder
3. Prof. Dr. S. Förster

Halle (Saale), den 19-08-2004

urn:nbn:de:gbv:3-000007140

[<http://nbn-resolving.de/urn/resolver.pl?urn=nbn%3Ade%3Agbv%3A3-000007140>]

Dedicated to My Loving Parents

Acknowledgement

I would like to express my deep sense of gratitude, sincere thanks to my advisor Prof. Dr. Jörg Kressler for his valuable suggestions, discussions, continued encouragement and inspirations through out my stay here, and providing me an opportunity to work in his group.

I am also obliged to Prof. Dr. R. Neubert (Halle), Prof. Dr. A. Blume (Halle), Prof. Dr. H. J. Radosch (Halle), Dr. S. Höring (Halle), Dr. N. M. Nubarov (Moscow, Russia), Dr. P. Phol (Berlin), Dr. R. Thomann (Freiburg), Dr. Y. Mrestani (Halle), Dr. A. Kerth (Halle) Dr. M. Janich (Halle) and Dr. O. Kryolova (Berlin) for their help and cooperation over the course of my work in their laboratories.

I am grateful to all colleagues, Dr. K. Busse, Dr. J. Vogel, Dr. H. Kausche, Dr. Z. Funke, Dr. H. Budde, Dr. C. Schwinger, N. Mahmood, B. Borisova, C. Peetla, S. Kaiser, for their cooperation and nice company during my stay.

Special thanks and appreciation are due to Dr. K. Busse and my former colleague Dr. T. Menke not only for their fruitful discussions related to my research work, but also for their help in solving my day to day problems which any student might face in a foreign land.

I would like to acknowledge DFG and BMBF for financial support of this work.

Finally, I wish to pay my gratitude to my loving family members for their encouragement throughout my studies.

M.Phil. Hazrat Hussain

This dissertation is based on the following publications:

1. H. Hussain, K. Busse, A. Kerth, A. Blume, N. S. Melik-Nubarov, and J. Kressler “Interaction of poly(ethylene oxide) and poly-(perfluorohexylethyl methacrylate) containing block copolymers with biological systems” (submitted)
2. H. Hussain, A. Kerth, A. Blume, J. Kressler “Amphiphilic block copolymers of poly(ethylene oxide) and poly(perfluorohexylethyl methacrylate) at the water surface and their penetration into the lipid monolayer” *J. Phys. Chem. B* **2004**, *108*, 9962.
3. H. Hussain, A. Kerth, K. Busse, A. Blume, J. Kressler “Block copolymers in contact with lipid monolayer” *Polym. Mater. Sci. Engi.* **2004**, *90*, 563.
4. H. Hussain, K. Busse, J. Kressler, Poly(ethylene oxide) and Poly(perfluorohexylethyl methacrylate) Containing Amphiphilic Block Copolymers: Association Properties in Aqueous Solution” *Macromol. Chem. Phys.* **2003**, *204*, 936.
5. H. Hussain, H. Budde, S. Höring, K. Busse, J. Kressler, “Synthesis and characterization of poly(ethylene oxide) and poly(perfluorohexylethyl methacrylate) containing triblock copolymers” *Macromol. Chem. Phys.* **2002**, *203*, 2103.
6. K. Busse, H. Hussain, H. Budde, S. Höring, J. Kressler, “Micelle formation of perfluorinated triblock copolymers in water” *Polym. Prep.* **2002**, *43*, 366.
7. K. Busse, J. Kressler, H. Hussain, O. O. Krylova, P. Pohl, S. Höring, H. Budde, “Behavior of amphiphilic block copolymers at model membranes” *Polym. Mater. Sci. Engi.* **2001**, *84*, 100.

8. H. Hussain, C. Peetla, J. Kressler, N. M. Nubarov, P. Pohl, “Interaction of amphiphilic block copolymers with model bilayer membranes and encapsulation of a model hydrophobic drug by block copolymer micelles: potential pharmaceutical applications” (to be submitted).

Contents

1. Introduction	1
1.1. Block copolymers	1
1.2. Block copolymers in solid state	2
1.3. Block copolymers in solution	6
1.4. Applications of block copolymers	11
2. Synthesis and characterization of bulk properties of poly(ethylene oxide) and poly(perfluorohexylethyl methacrylate) containing block copolymers	14
2.1. Introduction	14
2.2. Experimental section	16
2.2.1. Materials	16
2.2.2. Synthesis by atom transfer radical polymerization	16
2.2.3. Experimental techniques	17
2.3. Results and discussion	20
2.3.1. Molecular characterization	20
2.3.2. Microphase separation in bulk	23
2.3.3. Effect of poly(perfluorohexylethyl methacrylate) block on crystallinity and thermal properties of the block copolymers	27
2.4. Conclusion	34
3. Behavior of poly(ethylene oxide) and poly(perfluorohexylethyl methacrylate) containing block copolymers in aqueous solution	36
3.1. Introduction	36
3.2. Experimental section	39
3.2.1. Surface tension measurements	39
3.2.2. Dynamic light scattering	39
3.2.3. Transmission electron microscopy	40
3.3. Results and discussion	41

3.3.1. Micelle formation	41
3.3.2. Effect of concentration, temperature, ultrasonic treatment, and time	45
3.3.3. Morphology of solvent evaporated samples	52
3.4. Conclusion	56
4. Amphiphilic block copolymers of poly(ethylene oxide) and poly(perfluoro- hexylethyl methacrylate) on water surface and their penetration into lipid monolayer	57
4.1. Introduction	57
4.2. Experimental section	60
4.2.1. Materials	60
4.2.2. Surface pressure measurements	60
4.2.3. Infrared reflection absorption spectroscopy setup	61
4.3. Results and discussion	63
4.3.1. Interfacial properties of the block copolymers at the air/water interface	63
4.3.2. Penetration of lipid monolayer by block copolymer chains	67
4.3.3. Infrared reflection absorption spectroscopy investigations	70
4.4. Conclusion	78
5. Potential pharmaceutical applications of amphiphilic block copolymers of poly(ethylene oxide) and poly(perfluorohexylethyl methacrylate) or poly(<i>n</i>-decylmethacrylate)	80
5.1. Introduction	80
5.2. Experimental section	84
5.2.1. Cytotoxicity measurements	84
5.2.1.1. Purification of the copolymers	84
5.2.1.2. Cell culturing	84
5.2.2. Interaction of block copolymers with lipid bilayers	85
5.2.2.1. Planar bilayer membranes	85

5.2.2.2. Liposomes	86
5.2.3. Encapsulation of a model hydrophobic drug by block copolymer micelles	88
5.2.3.1. Preparation of drug loaded micelles	88
5.2.3.2. Quantitative evaluation of the encapsulated drug content in dried micelles	90
5.2.3.3. Effect of freeze-thawing on drug loaded micelle size distribution	91
5.3. Results and discussion	92
5.3.1. Cytotoxicity results	92
5.3.2. block copolymers in contact with lipid bilayers	93
5.3.2.1. Interaction with planar lipid bilayer	93
5.3.2.2. Interaction with liposomes	95
5.3.3. Encapsulation of testosterone undecanoate as model hydrophobic drug by block copolymer micelles	98
5.4. Conclusion	104
6. Summary and perspectives	106
7. Zusammenfassung	113
Literature	119
Resume	131

Abbreviations and symbols

PEO	Poly(ethylene oxide)
PFMA	Poly(perfluorohexylethyl methacrylate)
PDMA	Poly(<i>n</i> -decylmethacrylate)
PE- <i>b</i> -PEE	Poly(ethylene- <i>b</i> -ethylethylene)
PCL- <i>b</i> -PB	Poly(ϵ -caprolactone- <i>b</i> -butadiene)
PEO- <i>b</i> -PBO	Poly(ethylene oxide- <i>b</i> -butylene oxide)
PEO- <i>b</i> -PEE	Poly(ethylene oxide- <i>b</i> -ethylethylene)
PEO- <i>b</i> -PEP	Poly[(ethylene oxide)- <i>b</i> -(ethylene- <i>alt</i> -propylene)]
PEO- <i>b</i> -PHMA	Poly(ethylene oxide- <i>b</i> -hexyl methacrylate)
PEO- <i>b</i> -PS	Poly(ethylene oxide- <i>b</i> -styrene)
PMMA	Poly(methyl methacrylate)
PPO	Poly(propylene oxide)
ATRP	Atom transfer radical polymerization
DPhPC	1, 2-Diphytanoyl- <i>sn</i> -glycero-3-phosphocholine
DPhPS	1,2-Diphytanoyl- <i>sn</i> -glycero-3-[phospho-L-serine]
THF	Tetrahydrofuran
MeOH	Methanol
DMF	Dimethyl formamide
DMSO	Dimethyl sulfoxide
KOH	Potassium hydroxide
HEPES	N-2-Hydroxyethylpiperazine-N'-2-ethanesulfonic acid
PMDETA	Pentamethyldiethylene triamine
EDTA	Ethylenediaminetetraacetic acid
MMT	Methyl tetrazolium
Tris	Tris (hydroxymethyl)aminoethane
PC	Phosphatidylcholine
bpy	2,2-Bipyridine
CaH ₂	Calcium hydride
CDCl ₃	Deuterated chloroform

RuO ₄	Ruthenium tetroxide
hpc	Hexagonally packed cylinders
bcc	Body centered cube
lam	Lamellae
hpl	Hexagonally perforated lamellae
G	Gyroid
ΔG°	Standard Gibbs free energy change
ΔH°	Standard enthalpy change
ΔS°	Standard entropy change
χ	Flory-Huggins interaction parameter
N	Degree of polymerization
R _G	Radius of gyration
ODT	Order-to-disorder transition
MST	Microphase separation transition
CMC	Critical micelle concentration
CMT	Critical micelle temperature
SSAL	Self-similar adsorbed layer
TEM	Transmission electron microscopy
PLM	Polarized light microscopy
DSC	Differential scanning calorimetry
SAXS	Small angle X-ray scattering
SANS	Small angle neutron scattering
WAXS	Wide angle X-ray scattering
DLS	Dynamic light scattering
NMR	Nuclear magnetic resonance
PGSE (NMR)	pulsed gradient spin-echo (NMR)
SEC	Size exclusion chromatography
PSS	Polymer Standard Service
GPC	Gel permeation chromatography
PCS	Photon correlation spectroscopy
IRRAS	Infrared reflection absorption spectroscopy

MCT	Mercury-cadmium-tellurium (HgCdTe)
HMWSP	Hydrophobically modified water-soluble polymers
λ	Wavelength
q	Scattering vector
I	Scattering intensity
T	Temperature
T_m	Melting temperature
T_c	Crystallization temperature
X_c	Crystallinity (weight percent)
M_n	Molar mass (number average)
M_w	Molar mass (weight average)
ppm	Parts per million
d	Long period
q^*	Maximum of the first peak in SAXS profile
a	Lattice constant
π	Surface pressure
I_a & I_c	Area under amorphous halos and crystalline reflections respectively in WAXS traces.
f	PEO weight fraction in block copolymer
ΔH_f	Enthalpy of fusion
ΔH_f°	Enthalpy of fusion of a perfect PEO crystal
D_{app}	Apparent diffusion coefficient
n	Refractive index
$R_{h,app}$	Apparent hydrodynamic radius
k	Boltzmann constant
η	Viscosity
Γ	Relaxation rate of the correlation function
ζ	Zeta potential
ε and ε_0	Permittivity of free space and relative permittivity of the medium

Chapter 1

Introduction

1.1. Block copolymers

Block copolymers are macromolecules that consist of different and often incompatible blocks obtained from chemically different monomers. Block copolymers represent a subject of broad current research interest across the full spectrum of macromolecular chemistry and physics, ranging from the development of new synthetic strategies and molecular architectures to application of advanced theoretical and computational

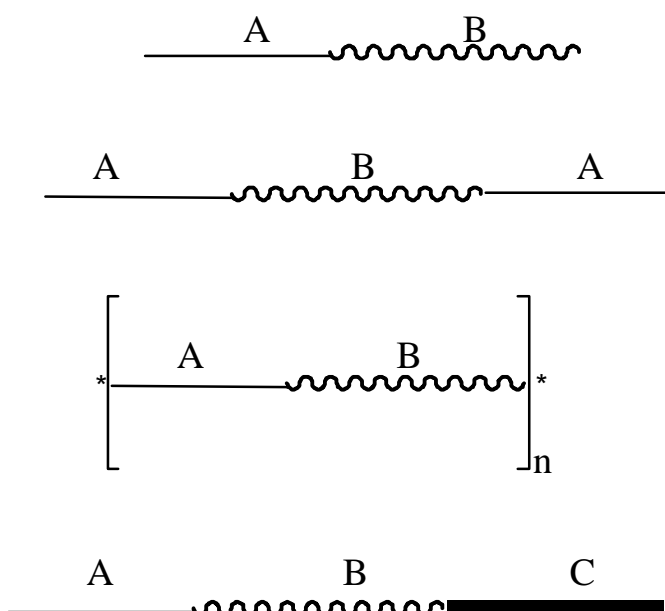


Figure 1.1. Schematic representation of different types of linear block copolymer architectures.

methods. Almost fifty years after the preparation of the first laboratory block copolymer sample (styrene and isoprene block copolymer) by living anionic polymerization,

scientific interest in block copolymers continues to grow, as does the global market for these materials.

A variety of molecular architectures of linear block copolymers are available, such as diblock (A-B), triblock (A-B-A), and multi-block or segmented copolymer (A-B)_n, where n is the number of A-B segments. When a third type of block is added, a linear ABC triblock copolymer can be synthesized. Schematic representation of different types of linear block copolymer architectures can be seen in Figure 1.1. The most suitable method for the synthesis of block copolymers with definite structures is anionic polymerization.² However, the more recent techniques of controlled radical polymerization, such as atom transfer radical polymerization and nitroxide-mediated polymerization have been successfully adopted as well to synthesize block copolymers with well-defined compositions, and molar masses.³⁻⁵

The immiscibility of the constituent blocks leads to the phase separation in block copolymers, however, unlike polymer blends, where the constituting polymers separate at macroscopic scale, phase separation only in the nanometre range is possible in block copolymers due to the covalent bonding between the constituting blocks, which confines them to microdomains of molecular dimension. The very same immiscibility of the constituent blocks is responsible for the characteristic behavior of block copolymers in solvent (selective for one of the block) and at the interface (e.g. air/liquid and liquid/solid) as well. Thus, block copolymers get adsorbed onto the interface and self-assemble to form micellar aggregates in selective solvent. This makes these materials useful for a variety of applications. It is, therefore, not surprising that block copolymers have attracted worldwide attention of physicists, chemists, pharmacists, and engineers.

1.2. Block copolymers in solid state

Block copolymers with immiscible blocks exhibit characteristic morphological behavior and interesting properties. The material (bulk) properties of the block copolymers are dominated by the tendency for the blocks to spontaneously segregate into microphases

when the temperature is lowered. Microphase separation occurs as a result of a reduction in enthalpy as the blocks demix, but at the cost of a loss of entropy as the blocks are arranged in ordered structures.⁶ Strongly segregated or microphase separated block copolymers form a variety of ordered structures. The commonly observed microphase separated block copolymer structures are lamellar (lam), hexagonally packed cylinders

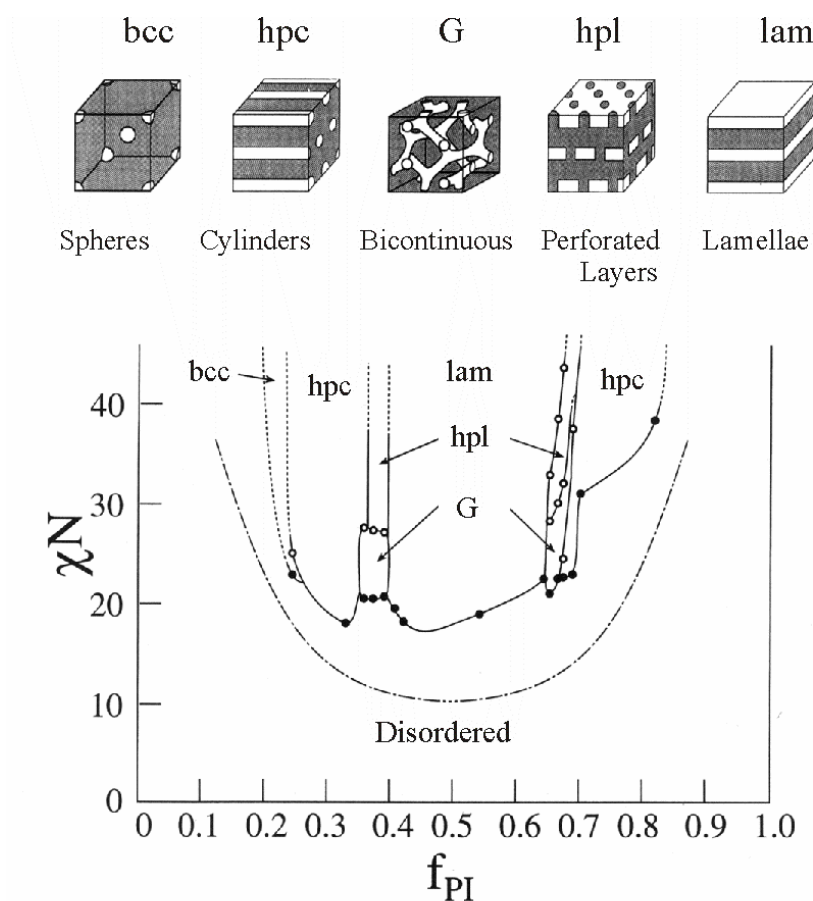


Figure 1.2. Experimental phase diagram for polyisoprene-*block*-polystyrene copolymers, the open and filled circles represent the order-order transitions (OOT) (i.e. transitions between the two ordered phases), and order-disorder transitions (ODT) (i.e. transitions between the ordered and disordered phases), respectively. The dash-dot curve is the mean field approximation for the ODT.⁹ [The Figure is reproduced from Khandpur et al.].¹⁰

(hpc), and spheres (bcc).⁷⁻⁸ Additionally, a variety of complex phases such as hexagonally perforated lamellar (hpl) and gyroid (G) phases have been observed recently in weakly segregated diblock copolymers.¹⁰⁻¹¹ The most common phase-separated structures of spheres, hexagonally-packed cylinders, and lamellae, also some times called as the classical ones, are generally observed in all block copolymers. On the contrary, less is known about the more complex hexagonally perforated layer and the gyroid mesophases. Theoretically, these structures are not generally found to be the lowest energy (equilibrium) structures. However, the more recent theoretical studies of Masten et al.¹² predict the gyroid mesophase to be stable.

The bulk properties in block copolymers can be controlled by three factors: the overall degree of polymerization (N), the volume fraction and the segment-segment Flory-Huggins interaction parameter (χ). The key parameter that dictates the block copolymer microphase separation is the product χN . Figure 1.2 shows the phase diagram in terms of χN and copolymer composition, f (i.e. volume fraction), and the corresponding schematic representation of the microphase separated block copolymer structures of spheres (bcc), hexagonally packed cylinders (hpc), lamellae (lam), hexagonally perforated lamellar (hpl), and gyroid (G) phases.

On the basis of the χN values three different limiting regimes can be recognized for the diblock copolymer melt: (1) the disordered state with unperturbed Gaussian chain statistics ($R_G \sim N^{1/2}$) at $\chi N < 1$, (2) the ordered state in the weak segregation limit (WSL) at $\chi N \sim 10$, the theory¹³⁻¹⁴ predicts fluctuations in the disordered phase as the WSL is approached, with a characteristic dimension scaling as $N^{4/5}$, and immediately beyond the WSL, limited demixing of the constituting blocks occurs to form microphase separated structure, and (3) the ordered state in the strong segregation limit ($\chi N \gg 10$), where strong repulsive forces between the constituting blocks result in a sharp interface separating nearly pure domains of the corresponding blocks with pronounced stretching of the chains ($R_G \sim N^{3/2}$). The relation between the phase behavior of the block

copolymer and the numeric value of χN strictly depends on the architecture of the block copolymer, i.e. diblock, triblock, multiblock, or graft. The value of 10 as discussed above pertains to a linear symmetric diblock copolymer architecture, while for symmetric ring diblock copolymer systems a value close to 18 has been reported.¹⁵ Several groups have reported the influence of block copolymer architecture on the phase diagram by computer based simulation.¹⁶ The microphase-separation behavior in block copolymers becomes more complicated if one or more of the blocks are crystallizable. In the melt, ordered structures are formed similar to those of amorphous copolymers, however, the process of crystallization of the respective block/s is expected to compete with microphase separation at low temperatures.¹⁷ The investigations on the microphase separation of crystalline-amorphous block copolymers have attracted a considerable attention recently.

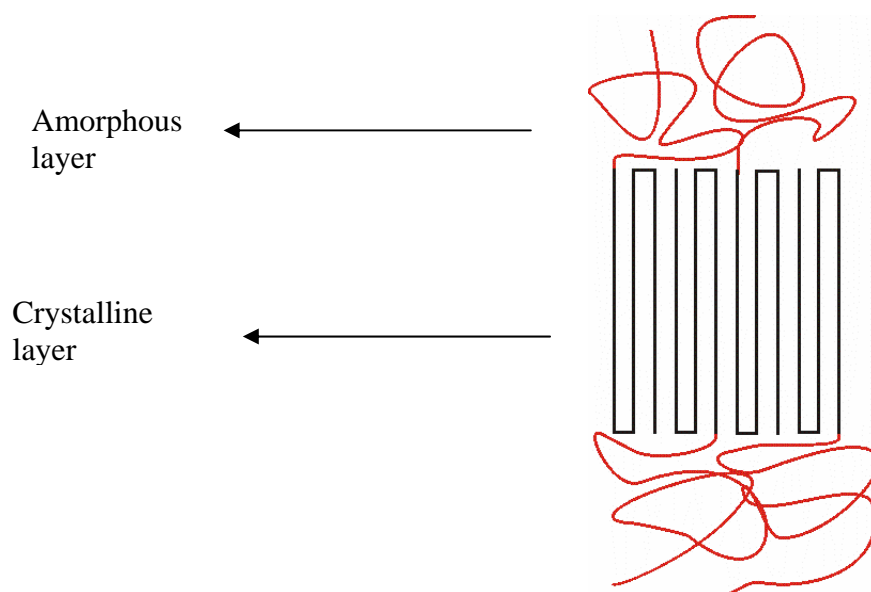


Figure 1.3. Theoretical model for symmetric crystalline-amorphous diblock copolymer morphology.¹⁸

These studies can help understand the fundamental physics of polymer crystallization, in general, as well as crystallization in confined geometry. The proposed theoretical

model¹⁹⁻²¹ concerning the morphology of crystalline-amorphous block copolymers as shown in Figure 1.3 assumes an alternating crystalline and amorphous layer structure. In the crystalline layer, there is a regular chain folding with the chain stems oriented perpendicular to the interface with the amorphous layer. Many diblock copolymers with a crystallizable block such as poly(ethylene),²² poly(ethylene oxide),²³ and poly(ϵ -caprolactone)²⁴ have been investigated for their microphase separation behavior. The final morphology in such systems depends on a number of factors. For example, it has been reported that the crystallization from a strongly segregated melt is confined to the nanodomains of the amorphous state.²⁵ However, in contrast to strongly segregated system, crystallization from a weakly segregated melt has been observed to destroy the microphase separated structure to form a layered structure consisting of alternating crystalline and amorphous layers.²⁶ Furthermore, the morphology in such systems has been reported to be heavily influenced by the kinetic factors as well.²⁷

Different experimental techniques such as transmission electron microscopy (TEM), and small angle scattering techniques such as X-ray (SAXS), neutron (SANS), and light (SALS) have been used extensively to understand the morphological behavior and nanoscopic domains of the component blocks.^{7,28} Electron microscopy is one of the best techniques for studying the morphology and determining mesomorphic structure and domain size. The small angle X-ray scattering technique has been developed to a high degree of perfection as well.²⁹ Valuable information about the structure of block copolymers in the solid state can be obtained by differential scanning calorimetry, polarization microscopy, and dynamic mechanical analysis and many more as well.¹⁵

1.3. Block copolymers in solution

Block copolymers often consist of blocks that have affinity either toward water or toward oil and hence behave like typical amphiphiles when dissolved in a selective solvent (i.e. a good solvent for one block but a precipitant for the other) and associate reversibly to

form micelles with a core composed of the insoluble block and a corona of solvated soluble blocks. The micelles are usually spherical with narrow size distribution but may change in shape and size distribution under certain conditions. Though the micelles are made of a core of the insoluble block surrounded by the shell of soluble block, however,

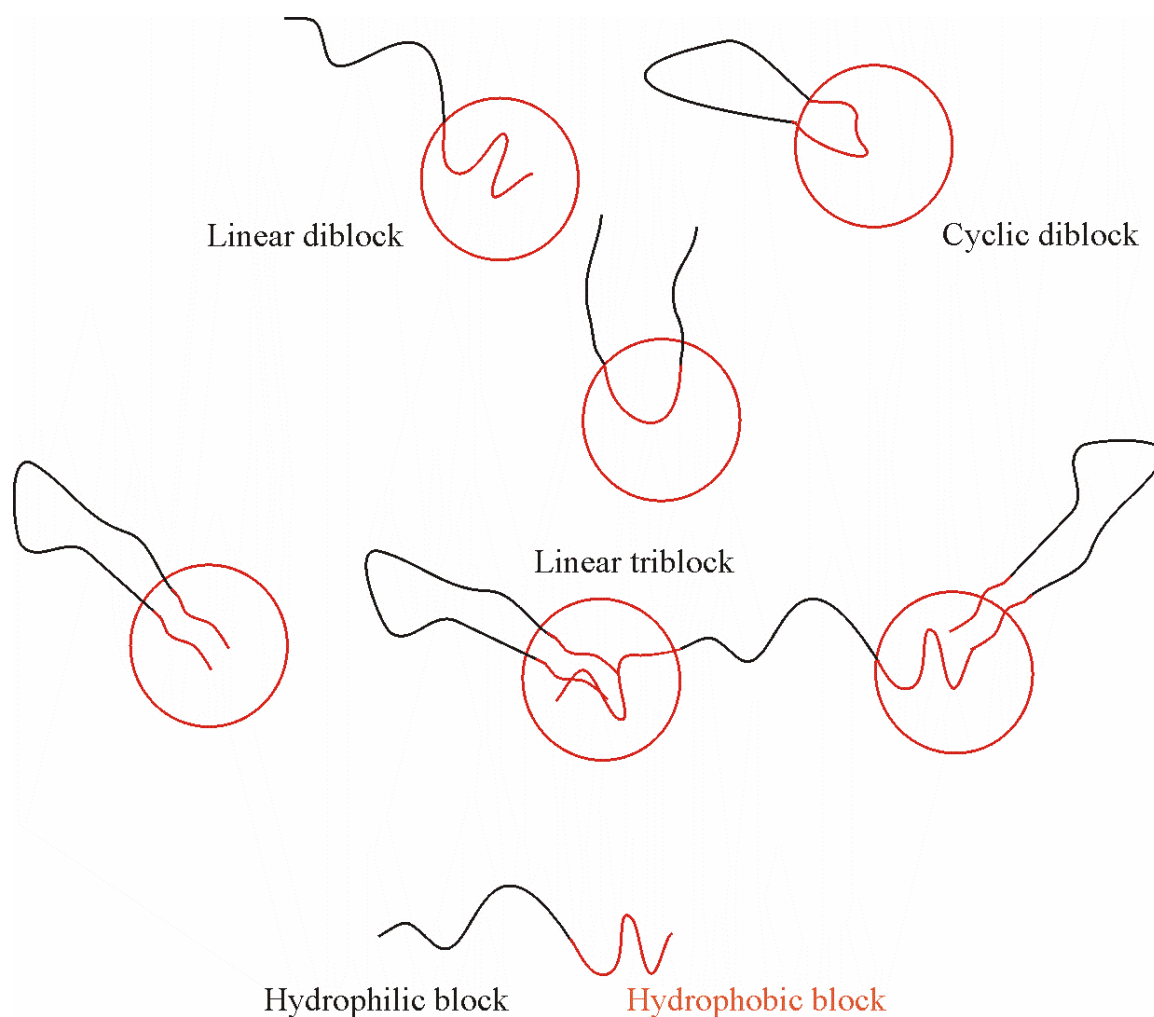


Figure 1.3. Schematic representation of chain conformations in micelles formed by block copolymers of different architectures in selective solvent.³⁰

as for as the chain conformation of the soluble block in the micelle fringe is concerned, there is a definite difference in structure between A-B and A-B-A copolymers on the one side and B-A-B (with B being the insoluble block) on the other as shown schematically in Figure 1.3. In fact, B-A-B copolymers have a tendency to form ‘flower-like micelles’ or to lead to micellar bridging.³¹⁻³²

The self-assembled micellar structures have been the subject of extensive investigations ever since the pioneering work of Merrett et al.,³³ Climie et al.,³⁴ and Burnett et al.³⁵ Briefly, the micellization in block copolymer aqueous solution can be initiated either at a given temperature by increasing the concentration beyond the critical micelle concentration (CMC) (i.e. the concentration at which the micelle formation starts in solution) or at a given concentration by increasing the temperature beyond the critical micelle temperature (CMT) (i.e. the copolymer solution temperature at which the micelles formation starts). Both the CMC and CMT are the fundamental parameters, which characterize the block copolymer solution behavior. The phenomenon of micellization was already well established for low molar mass surfactants but amphiphilic block copolymers offered potential advantages such as extremely low critical micelle concentration, larger and more robust assemblies and micellization in any desired organic or aqueous solvent. However, the micellization of amphiphilic block copolymers is inherently more complex than that of conventional, low molar mass surfactants. The composition polydispersity could be appreciable even for a copolymer with a narrow molar mass distribution and accordingly, no sharp CMC or CMT has been observed for block copolymers.³⁶ In practice, a certain CMC range with some notable uncertainty is usually detected. A large difference often occurs between the CMC values determined by different methods because the sensitivity of the techniques to the quantity of molecularly dissolved copolymers (unimers) present in solution may vary.³⁷ Initial studies on block copolymer micellization was primarily concerned with organic solvents, however, more recently micellization in aqueous solution has attracted a great deal of attention.³⁸

From thermodynamic viewpoint, the micellization of block copolymers in organic medium is an exothermic process (enthalpic-driven).³⁹⁻⁴⁰ The negative standard Gibbs energy (ΔG°)

$$\Delta G^\circ = \Delta H^\circ - T\Delta S^\circ \quad (1.1)$$

of micellization in organic solvent results from the dominant negative ΔH° values with respect to negative ΔS° values. The positive contribution of the entropic term ($T\Delta S^\circ$), i.e. unfavorable to micellization, arises from the entropy loss because of the less swollen state of copolymer chains in the micelles than in the unassociated state and furthermore, the number of possible conformations is also decreased due to the restriction of the block junctions at the core/shell interface of the micelle. The negative values of ΔH° arise from the exothermic energy interchange, which results from the replacement of polymer/solvent interactions by polymer/polymer and solvent/solvent interactions in the formation of the micelle core (i.e. the main contribution to the exothermic process is the formation of the micelle core).⁴⁰ In contrast, the micellization in aqueous medium, for low molar mass surfactants as well as for amphiphilic block copolymers is an endothermic process (entropy-driven process, (i.e. ΔH° and ΔS° are positive)).^{39,41-42} According to Liu et al.⁴³ the positive ΔS° values are due to the destruction of the ordered hydrogen bonded water structure in the vicinity of the polymer chains. At higher temperatures, the polymer chains become more hydrophobic due to the disruption of hydrogen bonds, and hence the solvent quality for the block decreases (i.e. the micelle formation takes place).

As for as morphology of the micelles is concerned, in addition to typical spherical, other micellar morphologies such as slightly elliptic, rod-like, vesicles, crew-cut micelles, flower-like micelles, worm like micelles and temperature induced sphere-rod transitions have also been reported.⁴⁴⁻⁴⁷ Yuan et al.⁴⁸ have recently reported multiple morphologies of polystyrene-*b*-poly(ethylene oxide)-*b*-polystyrene block copolymer self-assembly, including vesicles, large compound vesicles, large compound micelles

(LCMs), and so on, by altering the solvent, solvent composition, annealing time, and copolymer composition.

Different techniques have been used to study the CMC and the micelles of block copolymers. For block copolymers that form micelles in water, surface tension measurement is commonly used to determine the CMC. The surface tension of block copolymer solution below CMC decreases with increasing concentration and attains a constant value as the concentration exceeds CMC. Other experimental methods such as light scattering, differential scanning calorimetry, size exclusion chromatography (SEC) and spectroscopic methods such as fluorescence, ^{13}C - and ^1H -NMR have also been used for this purpose as reviewed in^{30,40} and references there in. Micelle properties such as aggregation number, shape and size have been largely characterized by static and dynamic light scattering techniques.⁴⁹⁻⁵⁰ Additionally, supporting information for hydrodynamic radius have been obtained from pulsed gradient spin-echo (PGSE) NMR,⁵¹ and SEC as well.⁵² More recently electron microscopy and small angle scattering (X-rays and neutron) have provided detailed information about micellar morphology and internal structure.^{28,53}

The immisibility of the constituting segments in block copolymers makes these materials interfacially active (i.e. the block copolymer chains adsorb at the interface). Amphiphilic block copolymers have been widely studied for their ability to form monolayer at the air/water interface.⁵⁴ Adsorption of block copolymers at the interface plays an important role in many industrial applications such as adhesion, lubrication, and stabilization of colloidal systems.⁵⁵ The block copolymer monolayer at the air/water interface is constituted of hydrophobic block anchoring the chains at the interface and of a hydrophilic block, which protrude toward the bulk solution, forming either mushrooms, brushes, or tail-loop-train distributions, depending on the surface coverage and on whether the hydrophilic block has an attractive interaction with the interface. However, the formation of block copolymer monolayer is not restricted to air/water interface, it can form at any solvent/air interface where one of the block is soluble in the solvent and the

other block being in a bad solvent acting as a buoy for the polymer chain at air/solvent interface. The block copolymer chains at the interface can be studied by several experimental techniques, such as infrared reflection absorption spectroscopy (IRRAS),⁵⁶ ellipsometry,⁵⁷ neutron and X-ray reflection,⁵⁸ and by measuring the pressure-area isotherms of the adsorbed monolayer.⁵⁷

1.4. Application of block copolymers

Block copolymers are an important class of materials both from commercial and academic viewpoint. Over the last several decades block copolymers have found numerous applications ranging from thermoplastic elastomers, adhesives, sealants, compatibilizer in polymer blends, emulsifiers, to more recent advances in their medical applications in cancer treatment.⁵⁹⁻⁶¹

The self-assembled structures formed by the block copolymers have attracted a great deal of attention for their pharmaceutical applications in the area of enhanced drug solubility and delivery, improved drug stability in the formulation, sustained and controlled release of the drug after administration etc.⁶² The block copolymer micelle size (10-100 nm), stability, low toxicity, and ability to solubilize hydrophobic compounds make them suitable for drug delivery application. Many groups are working actively on exploring the block copolymer micelles as drug carrier systems.⁶³⁻⁶⁴ At present, three different types of drug delivery systems based on block copolymers have been investigated. These are: (1) micelle forming block copolymer conjugates, (2) non-covalent (physical entrapment) incorporation of drug in block copolymer micelles, and (3) block ionomer complexes, where the drug and block copolymer are linked through electrostatic interactions. The most important commercially available amphiphilic block copolymers are poly(ethylene oxide) (PEO) and poly(propylene oxide) (PPO) containing block copolymers (Pluronic or also known as Poloxamer). Due to their easily availability, low toxicity, and unique characteristic of reducing the adsorption of serum

protein when adsorbed on the surface of the colloidal drug carriers, pluronic copolymers have been investigated extensively for various pharmaceutical applications.

The pluronic type copolymers have been shown to influence the transport and activity of the anticancer agents in multi drug resistance (MDR) tumor cells.⁶¹⁻⁶² MDR is often found in many types of human tumors that have relapsed after initial positive response to chemotherapy. Pluronic block copolymers were found to sensitize the MDR tumors with respect to various anticancer agents.⁶⁵ The influx of the anticancer agent into MDR tumor improves significantly in presence of the pluronic copolymers. In contrast, under similar conditions, the influx in sensitive cells was not altered at all or was increased less significantly.⁶⁰⁻⁶¹ In this regard, the formulation containing doxorubicin and pluronic block copolymers (a mixture of L61, and F127) developed for the cancer treatment is undergoing Phase II clinical trials.⁶⁶

One of the most useful consequences of the amphiphilic nature of block copolymers is their tendency to accumulate at different surfaces. Thus, block copolymers sterically stabilize colloidal system by adsorption onto the particle surface, i.e. emulsion droplets, liposomes, polymer nanoparticles, such that the hydrophobic block act as anchor resulting into adsorption where as the hydrophilic blocks remain flexible and extend out in the medium.⁶² Important biomedical applications of amphiphilic block copolymers, particularly those having PEO as the hydrophilic block, include to modify adhesion properties of surfaces. For example, the grafting of such block copolymers to hydrophobic surfaces is a very promising way to avoid non-desired protein adsorption onto specific surfaces.⁶⁷ This type of surface modification has great potential in increasing the biocompatibility of various materials. In another example, the grafting of PEO containing block copolymers onto liposome surface has been found to increase the longevity of these liposomes in blood stream, making them practical vehicles for drug delivery.⁶⁸

Amphiphilic block copolymers are also attracting attention for their applications in separation systems.⁶⁹ The micelle formation exhibited by block copolymers offers the

possibility to solubilize hydrophobic compounds in micelle core. In other words the aqueous solution of amphiphilic block copolymers are potential alternative to organic solvents for the extractions of organic molecules.⁷⁰ Hence, organic pollutants in water can be removed by solubilization into block copolymer micelles.

Chapter 2

Synthesis and characterization of bulk properties of poly(ethylene-oxide) and poly(perfluorohexylethyl methacrylate) containing block copolymers

2.1. Introduction

Fluoropolymers have long been known as an important class of materials due to their low surface energy, low coefficient of friction, nonflammability, low dielectric constant, and solvent and chemical resistance.⁷¹ Block copolymers containing fluorinated and non-fluorinated segments are of potential interest as they exhibit typical surfactant properties in selective solvents,⁷²⁻⁷⁴ excellent chemical and thermal stability, low surface energy and a dielectric constant which cannot be achieved by the corresponding non-fluorinated materials.⁷⁵ They have many uses as emulsifier in liquid and supercritical carbon dioxide⁷⁶⁻⁷⁷ and as surfactant for stabilization of polyurethane foams.⁷⁸

So far, few attempts have been made to prepare semifluorinated block copolymers by means of anionic,⁷⁹ cationic,^{71,80} ring opening metathesis,⁸¹ living radical,⁸² group transfer,⁸³⁻⁸⁴ atom transfer radical polymerization,⁸⁵⁻⁸⁶ and by selective addition of perfluoroalkyl iodides to C-C double bond.⁸⁷ Most of the studies that have been carried out on semifluorinated block copolymers discuss their behavior at surfaces/interfaces.^{71, 79,83,88-91} However, it is of equal interest to investigate their bulk properties as well.

Block copolymers composed of crystalline and amorphous blocks are interesting materials to study the crystal structure, morphology, crystallization kinetics and dynamics. The covalent bonding between the dissimilar blocks (amorphous and crystalline), results in a new material whose properties are not a simple function of the individual homopolymers.⁹² In general, semicrystalline block copolymers with

polyethylene (PE),^{25, 93} poly(ϵ -caprolactone) (PCL),⁹⁴⁻⁹⁵ and poly(ethylene oxide) (PEO)⁹⁶⁻⁹⁷ as the semicrystalline component have been used frequently for bulk studies. These block copolymers have been found to form ordered melt morphology depending on the composition. However, in semicrystalline state they possess more complicated phase behavior due to the crystallization of the crystallizable component. Many semicrystalline block copolymers such as poly(ethylene-*b*-ethylethylene) (PE-*b*-PEE),^{26,98} poly(ϵ -caprolactone-*b*-butadiene) (PCL-*b*-PB),²⁴ poly(ethylene oxide-*b*-butylene oxide) (PEO-*b*-PBO),⁹⁶ poly(ethylene oxide-*b*-ethylethylene) (PEO-*b*-PEE) and poly[(ethylene oxide)-*b*-(ethylene-*alt*-propylene)] (PEO-*b*-PEP),⁹⁹ poly(ethylene oxide-*b*-hexyl methacrylate) (PEO-*b*-PHMA),¹⁰⁰ poly(ethylene oxide-*b*-styrene) (PEO-*b*-PS),²³ and others have been reported with respect to their phase behavior. It was found that disregarding the ordered melt morphology, the crystallization of the crystallizable segment destroys the initial phase morphology and imposes the crystalline lamellar structure. It has also been reported recently that crystallization of the crystallizable component can be confined to the preformed melt microdomains.^{23,95,97}

In this chapter, the synthesis by atom transfer radical polymerization (ATRP), and the general behavior in bulk of poly(ethylene oxide) (PEO) and poly(perfluorohexylethyl methacrylate) (PFMA) containing amphiphilic di- and triblock copolymers have been discussed. Wide- and small-angle X-ray scattering (WAXS, SAXS) studies have been carried out to investigate their bulk properties. In addition, polarized light microscopy (PLM) was used to study the effect of PFMA end blocks on the crystallization behavior of PEO middle blocks in PFMA-*b*-PEO-*b*-PFMA triblock copolymers. DSC has been used to investigate the thermal behavior of the copolymers.

2.2. Experimental section

2.2.1. Materials

Perfluorohexylethyl methacrylate, (IUPAC: 1H, 1H, 2H, 2H-tridecafluorooctylmethacrylate) (95%, Clariant) was distilled under reduced pressure, stirred over CaH₂ for one week at room temperature and then distilled under vacuum before use. *n*-Butylacetate (99.5%, Merck) was stirred over CaH₂ for three days at room temperature and distilled under vacuum. THF (99%, Merck) was dried over KOH, distilled, stirred over CaH₂ for three days and finally distilled under reflux with Na/benzophenone. Poly(ethylene oxide) monools and diols (99%, Fluka) with different molar masses ranging from 2 000 to 20 000 g/mol were used as received. 2-Bromopropionylbromide (95.5%, Fluka) and pentamethyldiethylene-triamine (PMDETA) (>98%, Merck) were distilled before use. CuBr (97%, Merck) and 2,2-bipyridine (bpy) (>99.5%, Merck) were used as received.

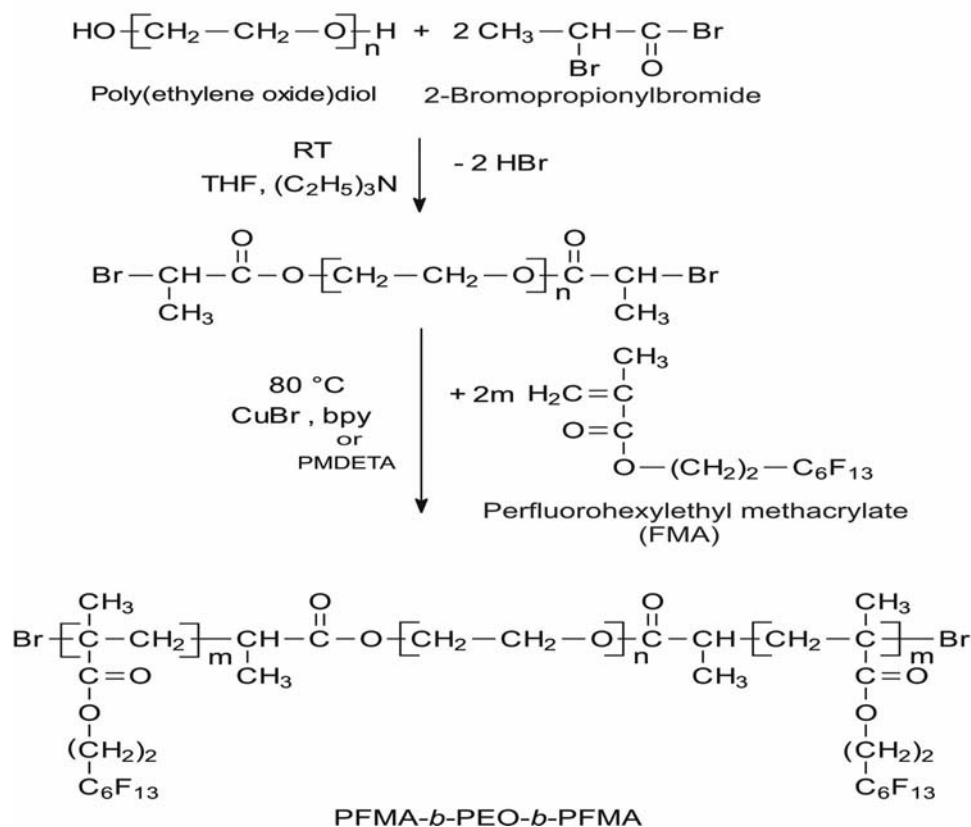
2.2.2. Synthesis by atom transfer radical polymerization

In a typical experiment for the synthesis of triblock copolymers, poly(ethylene oxide) macroinitiator was obtained from poly(ethylene oxide) diol and 2-bromopropionylbromide according to the procedure outlined in Scheme 2.1.

30.0 g (3.0 mmol, calculated for OH-groups) of poly(ethylene oxide) diol were dissolved in 500 ml dried THF. 0.5 g (5.0 mmol) of triethylamine was added and 1.08 g (5.0 mmol) of 2-bromopropionylbromide were introduced dropwise to the stirred solution. After 24 h, the product was isolated by evaporating the solvent in a rotary evaporator, filtered over silica gel, precipitated in *n*-hexane and dried under vacuum at 40°C over night. The product was analyzed by size exclusion chromatography (SEC) and ¹H-NMR spectroscopy. Polymerization was carried out in a Schlenk line, in flame dried glass tubes with a magnetic stirrer, using typical procedure for ATRP¹⁰¹⁻¹⁰² as described below:

0.4 mmol of PMDETA (complexing agent) was added to a stirred solution of macroinitiator (0.2 mmol, calculated for end groups) and CuBr (0.2 mmol, as catalyst) in

10 mL of *n*-butylacetate. The tubes were degassed in vacuum and flushed with Argon several times. Perfluorohexylethyl methacrylate (FMA) was introduced to the stirred reaction mixture. Polymerization was carried out at 85°C. The reaction solution was filtered over silica gel to remove catalyst complex, precipitated in *n*-hexane, and dried under vacuum at 35°C.



Scheme 2.1. Synthesis of triblock copolymers of EO and FMA by ATRP.

2.2.3. Experimental techniques

¹H-NMR spectra were recorded using Varian 300 MHz spectrometer at 20°C in CDCl₃. The composition of the block copolymers was determined from ¹H-NMR spectra. Molar masses of the, macroinitiators and block copolymers were measured by SEC at ambient temperature using a Waters GPC equipped with a Knauer pump, two PSS columns and

RI detector (W410) using THF as eluent. Poly(ethylene oxide) calibration was used to calculate the molar masses. Characteristic data of the block copolymers are given in Table 2.1. For the polymers under investigation the abbreviation scheme PEO_xF_y has been used, where x represents the PEO molar mass (kg/mol) and y represents the PFMA wt.-% in the block copolymer, and $-D$ has been added when a monofunctional macroinitiator was used. That means, e.g. $\text{PEO}_{20}\text{F}_{62}$ is a triblock copolymer with 62 wt.-% PFMA in the outer blocks and a 20 kg/mol PEO middle block.

SAXS measurements were performed in an evacuated Kratky compact camera (Anton Paar K.G.) with an 80 μm entrance slit. Cu K_α radiation with a wavelength of $\lambda = 0.15418$ nm was used. The scattered intensity I , was recorded by a scintillation counter in a step-scanning mode at room temperature and in the melt at 80°C. The scattering vector q is defined by $q = (4\pi/\lambda)\sin\theta$. The obtained scattering profiles were corrected for background scattering, desmeared,¹⁰³ and Lorentz corrected.

WAXS measurements were carried out at room temperature with a URD63 (Seifert) diffractometer using Cu K_α radiation. The experiments were carried out at room temperature on isothermally crystallized block copolymer samples.

DSC experiments were carried out with Perkin-Elmer DSC-2 to evaluate melting temperature T_m of PEO blocks and PEO crystallinity (weight percentage) X_c in the block copolymers. The DSC was calibrated with In and Pb Standards. Sample masses below 10 mg are chosen for DSC measurement. The heating thermograms were obtained at 5 K/min after standard cooling to -50°C (-20 K/min).

A LEO 912 transmission electron microscope (TEM) was used with an acceleration voltage of 120 kV. Isothermally crystallized samples were microtomed with a Leica Ultramicrotome at -100°C using a diamond knife to obtain thin sections (< 100 nm) for TEM studies. The specimens were stained with RuO_4 .

A Leica DMRX polarizing optical microscope equipped with a Leitz-1350 hot stage was used to observe the spherulite formation behavior of the samples. The samples

were prepared as follows: a small amount of the material was first melted between the glass slides on the hot stage at 80°C for a few minutes to erase any previous thermal history. The samples were then cooled at 30 K/min to a preselected crystallization temperature. The subsequent spherulite formation was observed between the crossed polarizers.

Table 2.1. Characteristic data of the block copolymers. In the abbreviation scheme PEO_xF_y *x* represents the PEO molar mass (kg/mol) and *y* the PFMA wt.-% in block copolymer, and -*D* has been added when a monofunctional macroinitiator was used.

Sample code	M_n (kg/mol) (SEC results)	Wt.-% PFMA (¹ H-NMR results)	M_w/M_n
PEO ₂	1.99	0.0	1.0
PEO ₂ F13-D	2.3	12	1.1
PEO ₂ F19-D	1.7	19	1.1
PEO ₅	3.7	0.0	1.0
PEO ₅ F15-D	4.9	15	1.0
PEO ₅ F19-D	4.3	19	1.1
PEO ₅ F25-D	5.2	25	1.1
PEO ₆	6.5	0.0	1.0
PEO ₆ F20	9.9	20	1.5
PEO ₆ F23	7.2	23	1.1
PEO ₆ F35	8.4	35	1.4
PEO ₆ F53	8.7	53	1.2
PEO ₆ F60	6.3	60	1.5
PEO ₁₀	12.1	0.0	1.1
PEO ₁₀ F5*	11.5	5	1.1
PEO ₁₀ F9	15.6	9	2.1
PEO ₁₀ F11	17.6	11	1.9
PEO ₁₀ F15	16.8	15	1.8
PEO ₁₀ F18*	10.9	18	1.3
PEO ₂₀	24.1	0.0	1.2
PEO ₂₀ F4	27.2	4	1.4
PEO ₂₀ F9	26.5	9	1.3
PEO ₂₀ F14	22.3	14	1.2
PEO ₂₀ F21*	18.7	21	1.5
PEO ₂₀ F24	25.4	24	1.4
PEO ₂₀ F41*	27.7	41	1.4
PEO ₂₀ F62*	32.0	62	1.3

* 2,2-bipyridine was used as complexing agent for the synthesis, while pentamethyldiethylene-triamine was used for other samples.

2.3. Results and discussion

2.3.1. Molecular characterization

PEO and PFMA based block copolymers have been synthesized by atom transfer radical polymerization. The reaction was carried out in solution using *n*-butylacetate as solvent. The block copolymerization procedure has been described already in the experimental

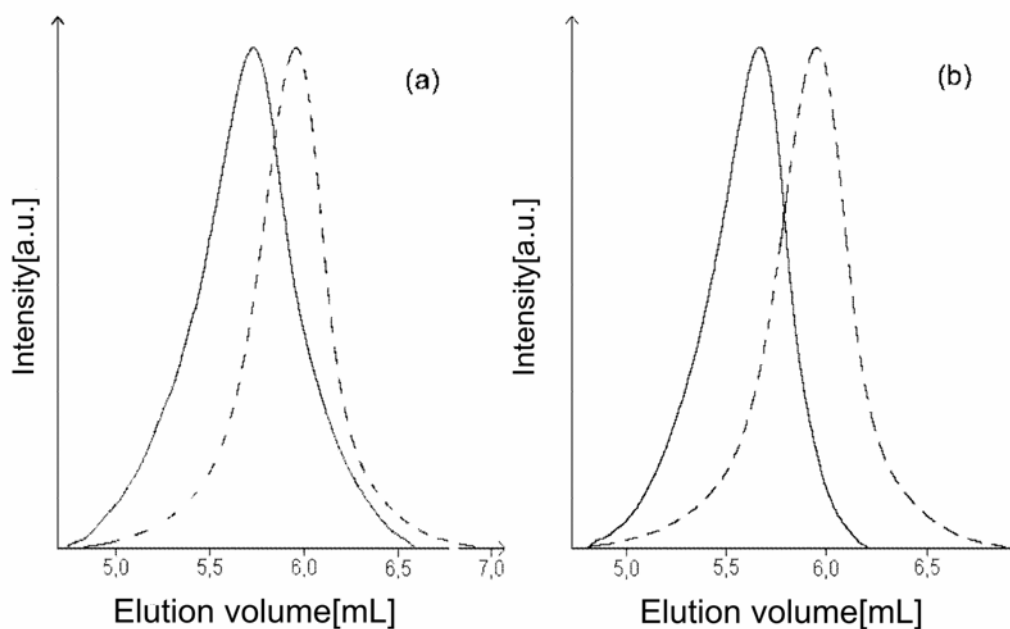


Figure 2.1. SEC traces of PEO macroinitiator of 20 000 g/mol (- - -) and the synthesized block copolymers (a) PEO₂₀F21 and (b) PEO₂₀F62 block copolymer (—).

section. The whole reaction is outlined in Scheme 2.1. Both the macroinitiator and the resulting block copolymers were characterized with SEC and ¹H-NMR spectroscopy. The SEC curves of the macroinitiator and the resulting triblock copolymers are shown for two samples in Figure 2.1. The shift of SEC traces of macroinitiator (dashed line) to lower elution volumes after polymerization suggests the successful synthesis of the block

copolymers. The produced block copolymers (full line), (a) PEO₂₀F21 and (b) PEO₂₀F62, have a significantly lower elution volume and therefore higher molar masses compared to the macroinitiator. Moreover, the monomodal and relatively narrow molar mass distribution also suggest a low degree of permanent termination or activity loss by any side reactions.⁹⁴ The relative high polydispersity for some of the samples might be due to the physical aggregation of a number of chains. We can exclude a chemical bonding, as in other solvents (e.g. water for water soluble species) the polydispersity was for these polymers much lower [for sample PEO₁₀F9 the polydispersity was 2.1 in THF and 1.4 in water (data not shown)]. Comparing block copolymers with low polydispersity with the pure PEO samples (macroinitiator), the obtained masses seem to be too low, e.g. PEO₁₀F5 has a 'weight' of 11.5 kg/mol whereas the PEO middle block has a weight of 12.1 kg/mol. This discrepancy can be explained by the lowering of the hydrodynamic volume, due to the presence of fluorine containing blocks.

Furthermore, ¹H-NMR spectroscopy was employed to characterize the obtained block copolymers in more detail. The ¹H-NMR spectra and assignment of the signals for the macroinitiator Br-PEO-Br and PEO₂₀F62 triblock copolymer are shown in Figure 2.2. Signals due to terminal methyl group protons *a* are seen at approximately 1.8 ppm, while signals due to protons *b* and *c* appear at 4.4 and 4.3 ppm respectively in ¹H-NMR spectrum of macroinitiator (Figure 2.2a). Clear signals of both PFMA and PEO blocks can be seen in ¹H-NMR spectrum of the block copolymer (Figure 2.2b). PEO block protons *d* produce signals in the region 3.4-3.8 ppm while the signals, at approximately 0.89, 1.02 ppm (due to protons *e*), 1.65 and 4.2 ppm (due to protons *f* and *i* respectively) represent the PFMA block. Copolymer composition was determined from the integrals of signals due to protons *i*, *c* (one integral for both the signals) and *d* in Figure 2.2b. No signals for the protons associated with double bond of unreacted FMA could be detected in the NMR spectra.

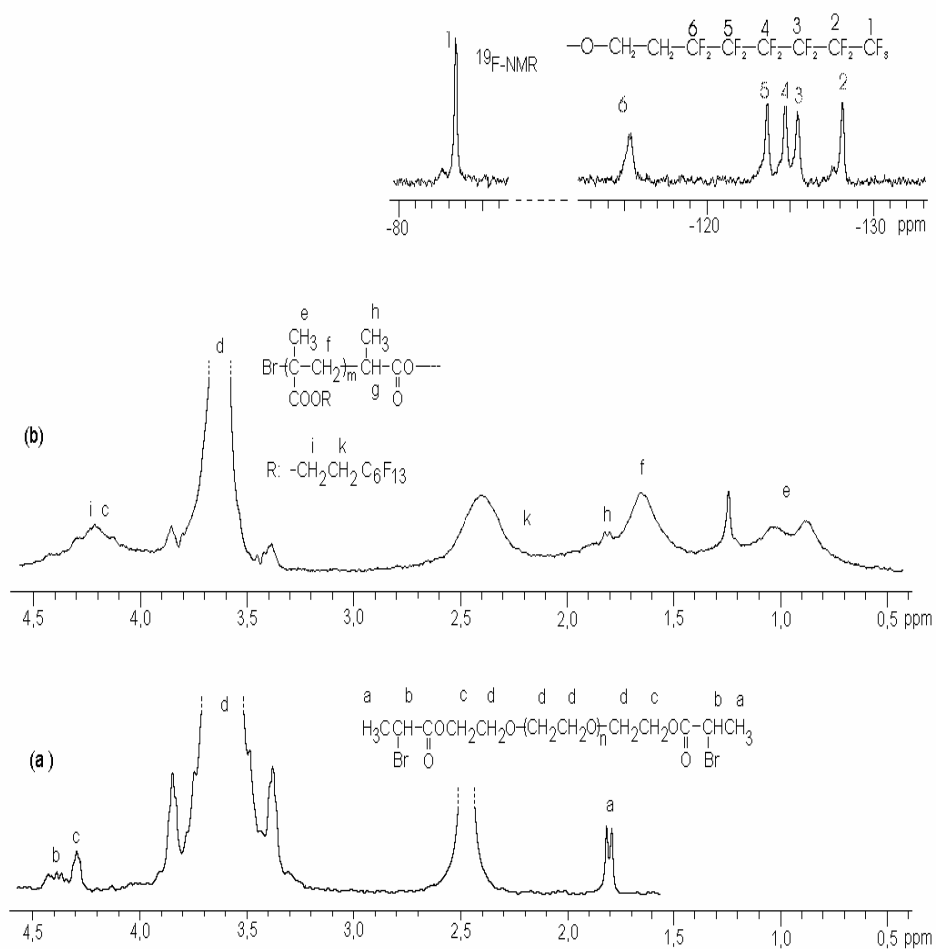


Figure 2.2. ^1H -NMR spectra of Br-PEO₂₀-Br macroinitiator (a) and PEO₂₀F62 (b). The upper right trace shows the ^{19}F -NMR spectrum of the respective block copolymer. The peaks are assigned to the chemical groups in the perfluoroethyl group as indicated.

2.3.2. Microphase separation in bulk

Microphase separation of the block copolymers, both in melt and solid state was investigated by SAXS. For high temperature measurement, the samples were heated at

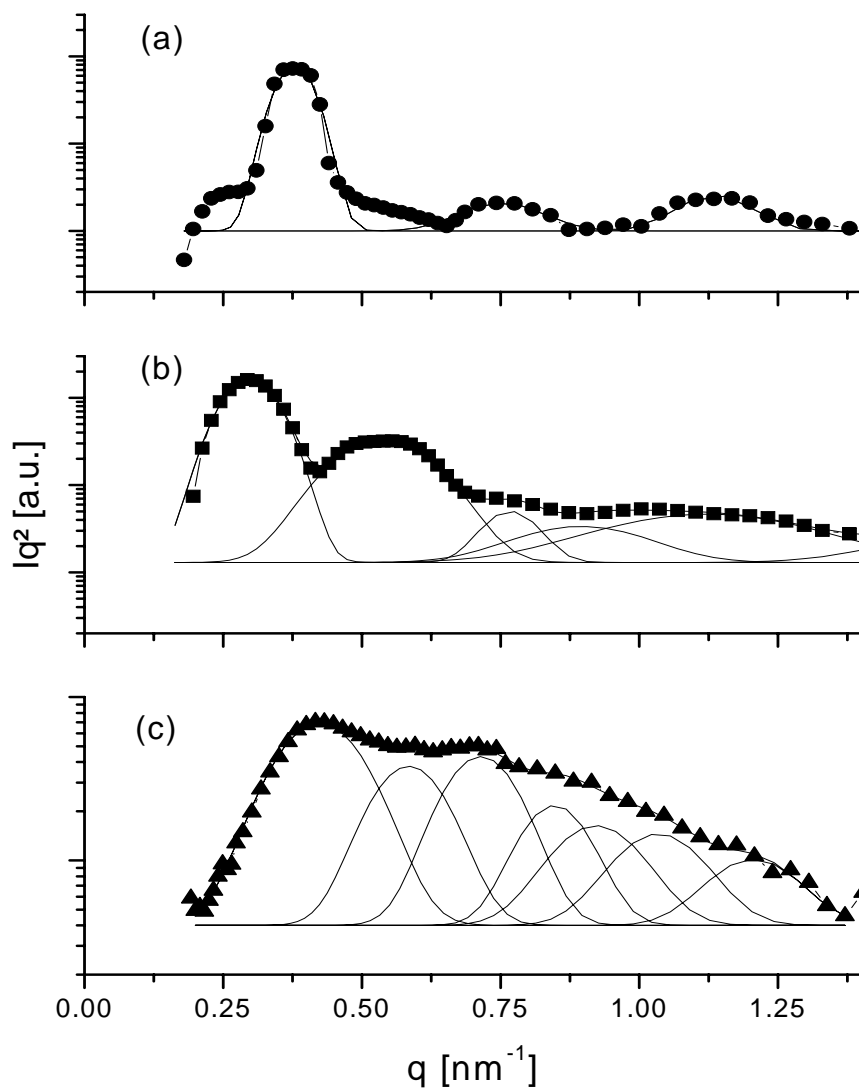


Figure 2.3. SAXS traces of triblock copolymers (a) PEO₆F53, (b) PEO₂₀F24 and (c) PEO₂₀F4 in the melt ($T = 80^{\circ}\text{C}$). Depending on the composition, (a) lamellae, (b) hexagonally packed cylinders, and (c) cubic lattice are the detected morphologies.

90°C for a few minutes and subsequent measurement was carried out at 80°C (above the melting temperature of pure PEO). Lorentz-corrected SAXS curves for three samples with varying PFMA content are shown in Figure 2.3. To identify the morphology, which should be either lamellar, cylindrical (hexagonal), spherical (bcc or other cubic lattice) or gyroidal for our types of polymers,⁸ a best fit for each trace is included. As some of the higher order peaks are poorly resolved for some samples, the relative positions for the peaks are fixed (e.g. 1 : 2 : 3 for lamellar morphology), only q^* for the first peak and all widths and heights are used for the fitting procedure. With these assumptions, we can distinguish at least between these morphologies unambiguously. The nearly symmetric copolymer PEO₆F53 has lamellar morphology as can be seen in Figure 2.3a by the higher order reflections with relative positions 1 : 2 : 3 in the ordered liquid phase. The long period is $d = 16.6$ nm corresponding to $q^* = 0.378$ nm⁻¹. In contrast, PEO₂₀F24 melt forms hexagonal arrangement of PFMA cylinders (Figure 2.3b) as the fit result points out relevant peaks with relative positions 1 : $\sqrt{3}$: $\sqrt{7}$: $\sqrt{9}$. The first order peak is at $q^* = 0.296$ nm⁻¹. SAXS data of PEO₂₀F4 melt (see Figure 2.3c) show a first order peak at $q^* = 0.42$ nm⁻¹. Higher order peaks are found with relative positions 1 : $\sqrt{2}$: $\sqrt{3}$ indicating the formation of spheres arranged in body center cubic (bcc) structure. According to the composition the melt morphology of this copolymer may be described as PFMA spheres packed onto a bcc lattice in PEO matrix. However, crystallization can destroy the ordered melt structure as shown in Figure 2.4. The hexagonally packed cylindrical morphology of PEO₂₀F24 in the melt (full squares in Figure 2.4) is destroyed after crystallization. SAXS trace of isothermally crystallized sample PEO₂₀F24 (at 40°C for 1 week, measured at room temperature, full circles in Figure 2.4) shows four orders of reflections observed at q / q^* ratios of 1 : 2 : 3 : 4, characteristic of lamellar structure. Transformation from prior ordered melt morphology to lamellar morphology in solid can be due to the crystallization as discussed for different systems in the literature.^{26,96,98-99} It is clear from the observation that crystallization overwhelms the delicate balance between the

interfacial energy and chain stretching which determines the phase state of amorphous copolymers. Crystallization of PEO segment in block copolymer has been observed also with other techniques and will be discussed latter. The long period for both melt and solid state of sample PEO₂₀F24 is approximately $d = 21.1$ nm, corresponding to the first maximum in the SAXS trace. This suggests that while transforming morphology from

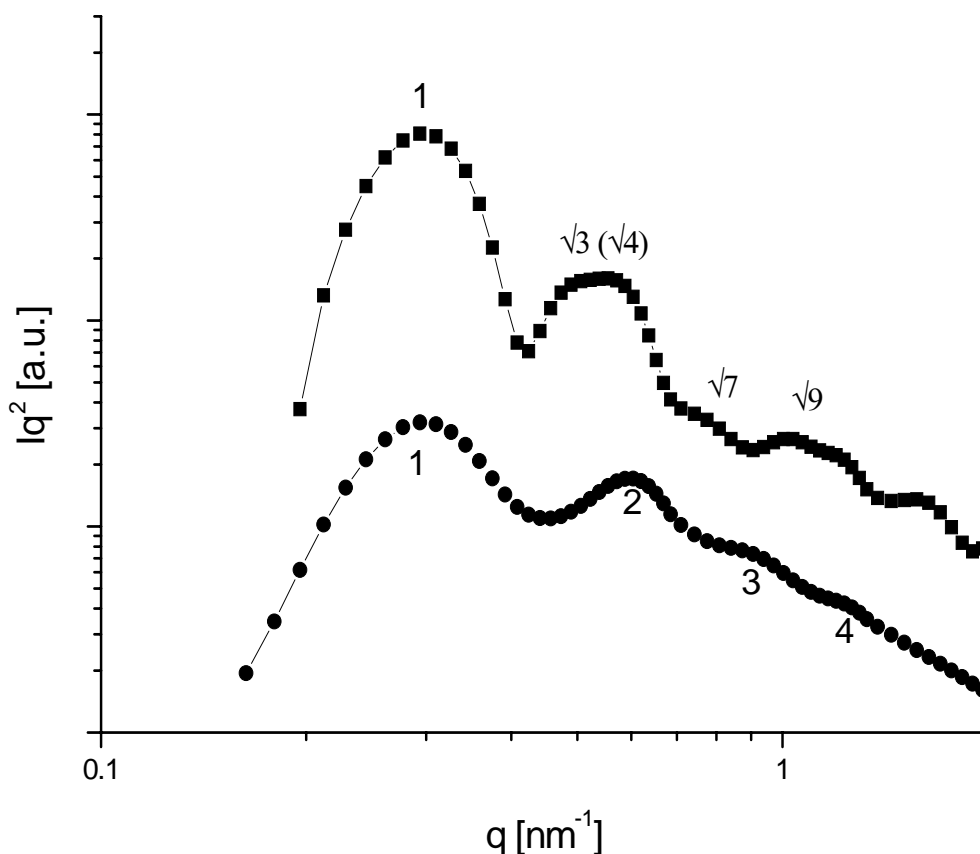


Figure 2.4. SAXS traces of PEO₂₀F24 copolymer, showing a melt structure of hpc (■) ($T = 80^\circ\text{C}$) and lamellar solid structure (●) (crystallized at 40°C).

cylinders to layers there was no further deformation in the material. Such epitaxy between the length scales in the melt of hexagonally ordered specimens and lamellar

ordered solids has been previously observed for ethylene oxide/butylene oxide diblock copolymers,⁹⁶ and polyolefin diblock copolymers.¹⁷ Furthermore, for the hpc structure it is possible to calculate the lattice constant a from the relation $a = 2d/\sqrt{3}$. Accordingly, the lattice constant is 24.5 nm. The lamellar morphology can also be observed by TEM as depicted in Figure 2.5.

Figure 2.5 is a TEM picture showing the semicrystalline morphology of the sample PEO₂₀F24. The block copolymer was crystallized isothermally at 40°C and the

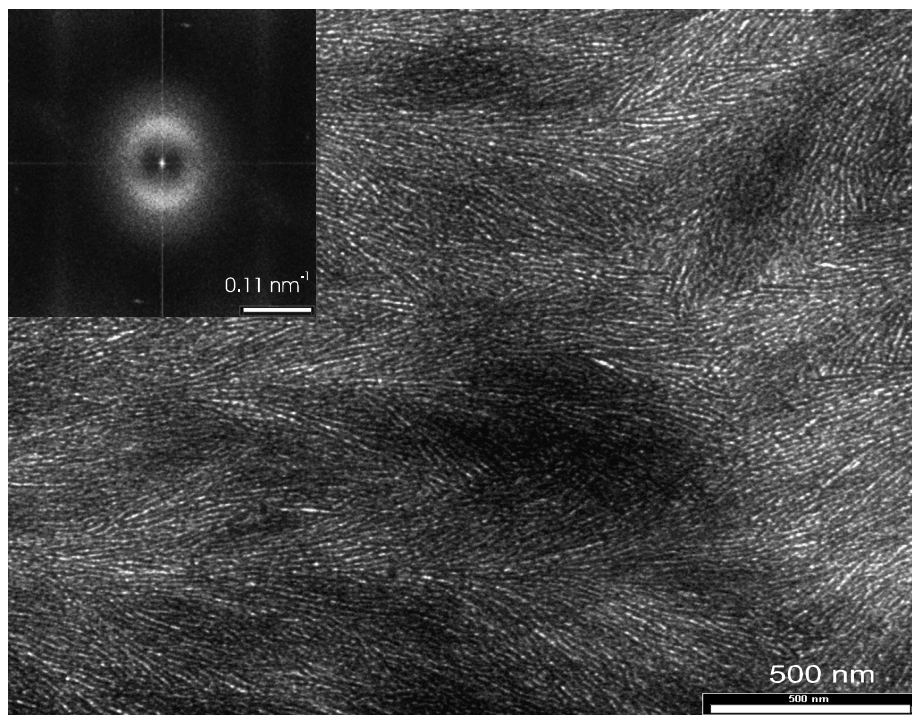


Figure 2.5. TEM micrograph of PEO₂₀F24 block copolymer. Fourier transformation is shown as inset. The obtained long period is approximately 20 nm.

sample was prepared as discussed in the experimental part. Again the picture reveals a layered crystalline structure with a long period of ~ 20 nm, obtained from the Fourier transformation of this image as shown as inset in Figure 2.5. This length is comparable to SAXS results of the sample. The brighter lines are assumed to represent PEO crystalline

lamellae and the dark layers are caused by PFMA and the amorphous part of the PEO chains due to preferential staining by ruthenium reagent.

2.3.3. Effect of poly(perfluorohexylethyl methacrylate) block on crystallinity, and thermal properties of block copolymers

The influence of PFMA end blocks on the crystal structure of PEO can be observed by WAXS investigations. Figure 2.6 shows WAXS profiles for PEO₂₀F24 and PEO₂₀F62.

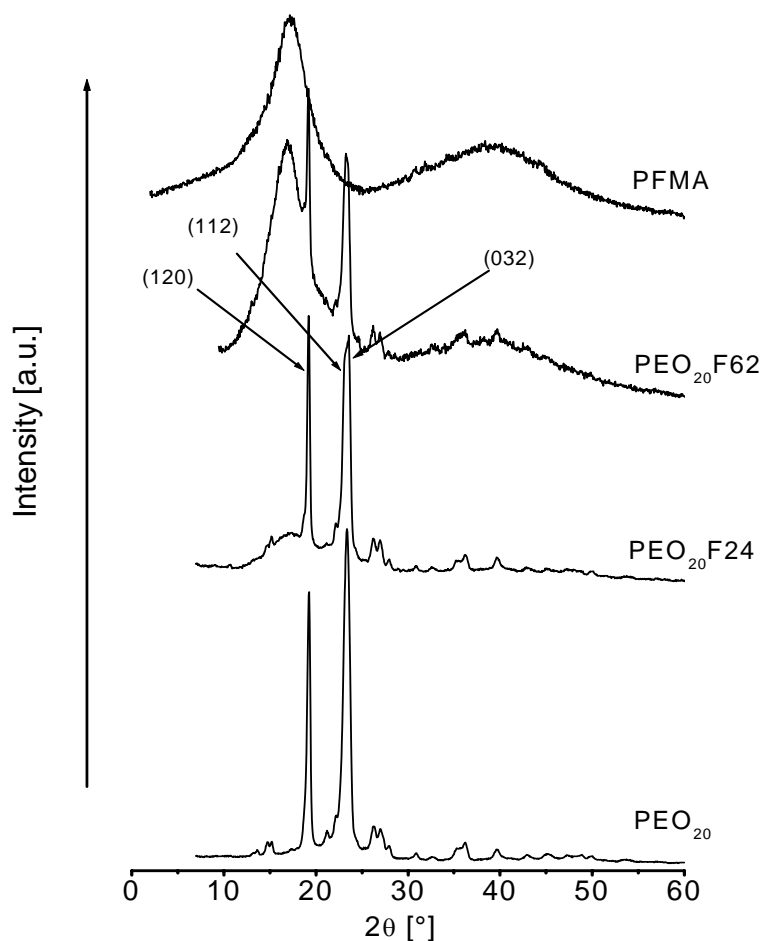


Figure 2.6. WAXS traces of PEO₂₀F24 and PEO₂₀F62 copolymers, along with PEO and PFMA homopolymers. Each graph is scaled separately to see the difference more clear.

The samples for WAXS were first melted at 100°C for a few minutes and then crystallized isothermally at 40°C at least for one week. For comparison, WAXS traces of PEO and PFMA homopolymers are also included. WAXS traces of the copolymers show sharp scattering peaks at $2\theta = 19.2^\circ$ (index 120) and $2\theta = 23.3^\circ$ (indices 112 and 032) and others, similar to PEO homopolymer. This indicates that PEO block crystallizes in the same crystallographic structure as the pure PEO (monoclinic crystal structure).¹⁰⁴ However, with increasing PFMA content two amorphous halos appear with maximum at approximately 17° and 38° superimposed by the sharp crystalline peaks. The former halo ($2\theta = 17^\circ$) is, however, more prominent than the latter. Intensities of the amorphous halos increase with increasing of PFMA content in block copolymer. It is clear from Figure 2.6 that the halos in the block copolymer WAXS traces originate mainly from the PFMA block scattering behavior. The maxima of the amorphous halos represent characteristic distances of $d_1 = 0.52$ nm and $d_2 = 0.24$ nm respectively. The characteristic distance of 0.52 nm can be assigned to the intermolecular distance between the fluorocarbon side groups.¹⁰⁵ Donth et al.¹⁰⁶ have also reported a scattering peak in WAXS trace of poly(*n*-alkyl methacrylate) at approximately $q \sim 13$ nm⁻¹ comparable to the halo observed here at $q \sim 12$ nm⁻¹ ($2\theta = 17^\circ$). Their interpretation is that this may reflect either chain to chain or side chain to side chain distance. The WAXS data reveal the crystallization of the PEO block in copolymers. However, the scattering intensity of the sharp crystalline peaks decreases with increasing PFMA content in the block copolymer, which may be due to lower degree of crystallinity and smaller crystallites. The weight fraction degree of crystallinity (X_c) of the block copolymers can be calculated from the area under the amorphous halos (I_a) and crystalline reflections (I_c) as:

$$X_c = I_c / (I_c + I_a) \cdot 1 / f \quad (2.1)$$

where f is the weight fraction of PEO in the copolymer. The values obtained from this procedure for PEO₂₀Fy block copolymer samples are depicted in Table 2.2. The

crystallinity decreases with increase in PFMA content in the block copolymer except for the sample PEO₂₀F24 that has shown relatively high X_c value. It is evident from the WAXS data that PFMA end blocks do not affect the local crystal structure of the PEO middle block; however, it affects the crystallinity of PEO. Thermal behavior of PEO₆Fy triblock copolymers is shown in Figure 2.7a. For comparison the thermogram of pure PEO (6 000 g/mol) is also included. The peak maximum of the endotherm was taken as the melting temperature (T_m). The thermogram of PEO homopolymer shows a small secondary peak at lower temperature (~ 58°C). This gives evidence of limited fractionation. All the block copolymers even with high PFMA content (wt.-%>50), show

Table 2.2. Thermal and WAXS characterization of PEO_xFy block copolymers.

Sample code	T_m (°C)	ΔH_f (J/g) ^a	X_c ^b	$X_{c,w}$ ^c
PEO ₆	62	190	0.92	-
PEO ₆ F20	55	145	0.71	-
PEO ₆ F23	55	154	0.76	-
PEO ₆ F35	54	100	0.54	-
PEO ₆ F53	53	130	0.64	-
PEO ₆ F60	52	96.3	0.48	-
PEO ₁₀	65	190	0.92	-
PEO ₁₀ F5	58	160	0.79	-
PEO ₁₀ F11	59	144	0.71	-
PEO ₁₀ F15	58	142	0.69	-
PEO ₁₀ F18	58	156	0.76	-
PEO ₂₀	66	195	0.94	0.75
PEO ₂₀ F4	61	149	0.73	0.72
PEO ₂₀ F14	60	147	0.71	-
PEO ₂₀ F21	60	143	0.7	0.63
PEO ₂₀ F24	60	143	0.7	0.68
PEO ₂₀ F62	59	117	0.57	0.5

^aas reduced to PEO fraction in the block copolymer. ^bfractional crystallinity from DSC.

^cfractional crystallinity obtained from WAXS data.

a reasonable melting endotherm. As given in Table 2.2 the copolymers show depression in melting point as compared to PEO homopolymer; however, this depression was not strongly dependent on PFMA content in the copolymers. A similar trend was observed for all samples. Furthermore, crystallization was studied for all samples in the cooling

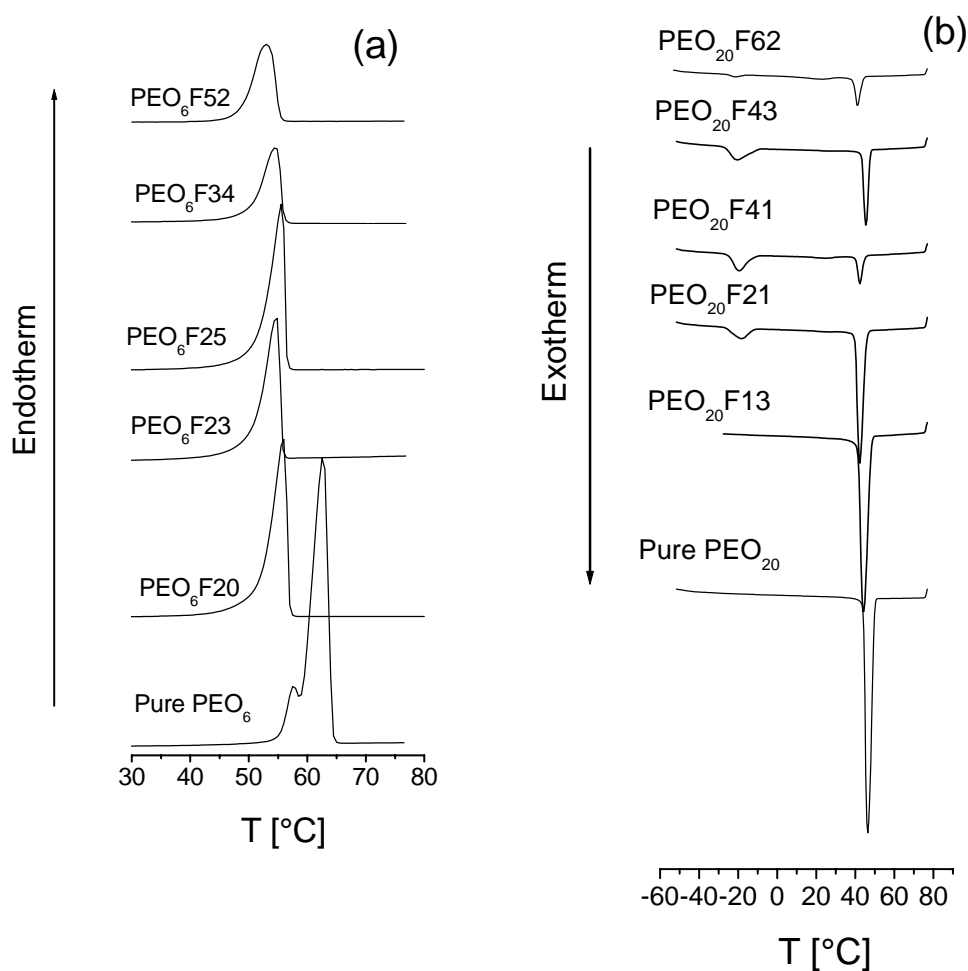


Figure 2.7. DSC traces of the block copolymers showing (a) melting endotherms for PEO homopolymer of 6 000 g/mol and PEO₆F_y block copolymers and (b) exotherms for PEO homopolymer of 20 000 g/mol and PEO₂₀F_y block copolymers.

phase. Crystallinity X_c (weight fraction crystallinity) was calculated from the peak area ΔH_f (reduced to PEO weight fraction in the copolymer) by

$$X_c = \Delta H_f / \Delta H_f^\circ \quad (2.2)$$

where ΔH_f° is the enthalpy of fusion of perfect (100 % crystalline) PEO crystal and can be calculated from¹⁰⁷ $\Delta H_f^\circ = 175 + 0.65T - 2.53 \times 10^{-3}T^2$, where T is the measured melting temperature of the sample. Heat of fusion ΔH_f (reduced to unit mass of PEO) and crystallinity (X_c) decrease in comparison to homopolymer as given in Table 2.2. A significant decrease in crystallinity can be seen only with high PFMA content. The end block length strongly affects the crystallization behavior of the PEO chains in the block copolymer. As reported by Donth et al.,¹⁰⁸ no crystallization of PEO chains was observed in triblock copolymers with long poly(methyl methacrylate) (PMMA) end blocks. They investigated the influence of the end block upon the crystallization of central PEO block. For PMMA-*b*-PEO-*b*-PMMA triblock copolymers with PEO block of 50 000 g/mol and each PMMA end block with 10 000 g/mol, they did not observe crystallization of PEO chains. The explanation was that long PMMA end blocks hinder the chain ends mobility of PEO block. However, the crystallization of PEO chains in the block copolymers reported here reveals that these samples do not have long enough PFMA end blocks to hinder PEO crystallization completely. Nevertheless, the influence of high PFMA content, i.e. long end blocks (~30 wt.-% or above) on PEO chain is evident from WAXS and DSC investigations on these samples. A peculiar crystallization behavior was observed in DSC cooling traces of PEO₂₀Fy copolymers with high PFMA content as shown in (Figure 2.7b). A second exotherm, not present in the PEO homopolymer and copolymer with low PFMA content was observed at a much larger super cooling (approximately $-15 \pm 3^\circ\text{C}$). These polymers show only one melting endotherm. Therefore, this phenomenon can be explained by considering that the first exotherm is produced by heterogeneous nucleation and the second exotherm by homogeneous nucleation as reported by other groups¹⁰⁹ for copolymers with low content of

crystallizable block. The effect of PFMA blocks on PEO crystallization can also be investigated with optical microscopy by observing spherulite texture of the copolymers.

Figure 2.8 shows PLM micrographs of two block copolymers with different PFMA content. Figure 2.8a is the PLM micrograph of PEO₁₀F9 block copolymer, isothermally crystallized at 40°C. The micrograph reveals the formation of a typical spherulitic texture after crystallization from the melt. The formation of large Maltese cross spherulitic texture on crystallization from the melt of block copolymer with low PFMA content is assumed to destroy completely⁹⁵ the preformed micro-phase separated melt structure as revealed for PEO₂₀F24 block copolymer by SAXS data (see Figure 2.4). The overall morphology of the block copolymer is dominated by the lamellar crystalline

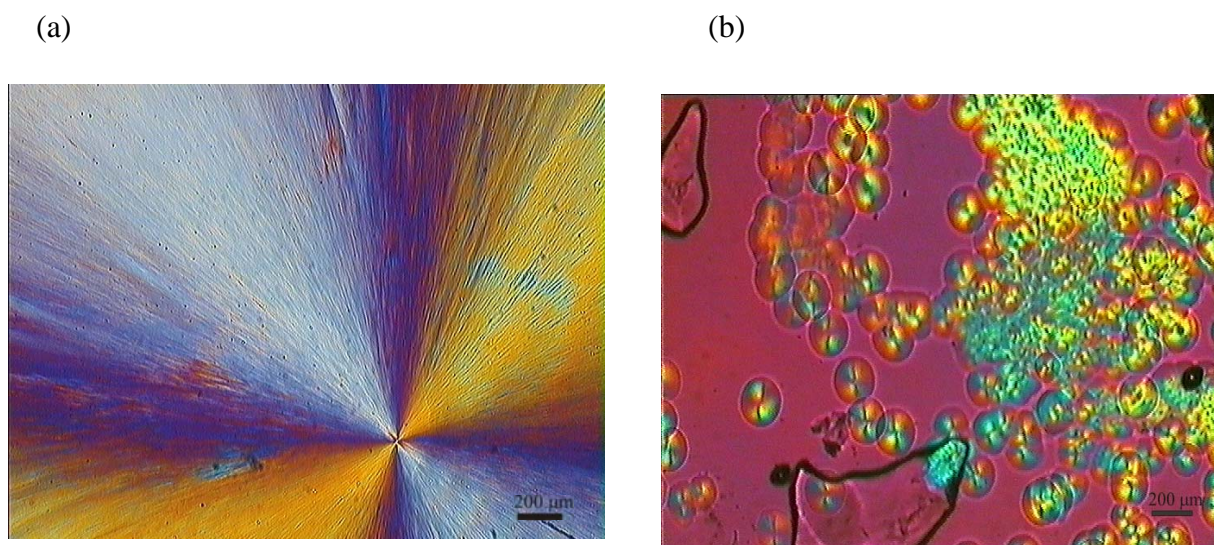


Figure 2.8. Optical micrographs of (a) PEO₁₀F9 and (b) PEO₆F35 block copolymer samples.

structure, with the amorphous phases lying between the crystalline lamellae. Low PFMA content (short block) offers less hindrance to PEO crystallization; however, relatively long PFMA blocks in the copolymer significantly arrest PEO chain movements resulting in relatively disordered spherulites as clearly seen in PLM micrograph (Figure 2.8b) of

PEO₆F35 block copolymer. This picture was taken while the crystallites were still growing at 40°C. Red color regions in the picture correspond to block copolymer in the molten state. The formation of large number of very small spherulites and a speckle-like final texture suggests that PFMA end blocks hinder PEO crystallization. The final texture lacks the typical Maltese cross. Similar texture has been reported¹¹⁰ for semicrystalline block copolymers and is termed as pseudomorphosis; a term that issued to describe crystallization confined within a pre-existing liquid crystalline texture. Detailed

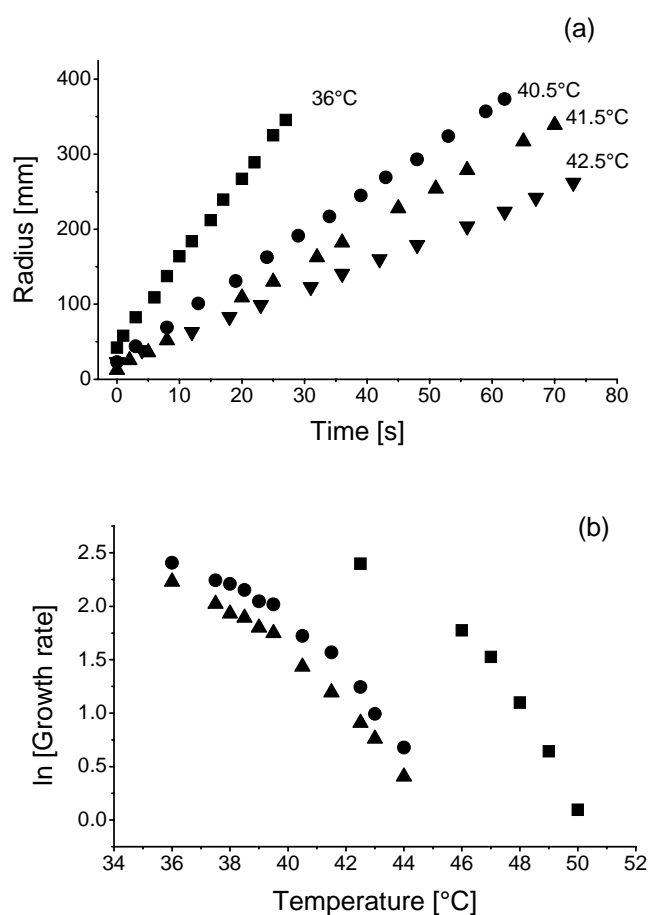


Figure 2.9. (a) Spherulite radius as function of time at different crystallization temperatures for PEO₁₀F9, (b) Calculated spherulite growth rate of PEO₁₀ homopolymer (■), PEO₁₀F9 (●), and PEO₁₀F15 (▲) copolymers as function of crystallization temperature.

investigations, however, are needed to explore the pseudomorphosis phenomenon in these block copolymers. The effect of PFMA block on PEO crystallization in PEO₁₀F9 and PEO₁₀F15 copolymers was also observed by monitoring the spherulite growth rate as shown in Figure 2.9. By measuring the spherulitic diameter as function of time under isothermal conditions at preselected crystallization temperatures, crystallization growth rates are calculated from the radius vs. time plots. Figure 2.9a shows plot of the spherulitic radius, against time at each crystallization temperature for PEO₁₀F9. For all the temperatures, the spherulitic radius increased linearly with time. Figure 2.9b shows the growth rates as function of the crystallization temperatures for PEO₁₀F9, PEO₁₀F15 and PEO₁₀ homopolymer. The data reveal a similar crystallization behavior of the PEO; both as homopolymer and as well as when chemically linked to PFMA block, however, the slower crystallization growth rates of the block copolymer samples, depending on the PFMA content, indicate a hindrance to PEO chain movement due to PFMA block as discussed above.

2.4. Conclusion

Atom transfer radical polymerization has been carried out successfully to synthesize novel poly(ethylene oxide) and poly(perfluorohexylethyl methacrylate) containing block copolymers using PEO as macroinitiator. SAXS studies on these block copolymers revealed the formation of different ordered melt morphologies, i.e. lamellae, hexagonal packed cylinders and spheres, depending on the composition. However, crystallization of PEO chains on cooling was found to destroy the ordered melt morphology and imposes a crystalline lamellar structure. For example, PEO₂₀F24 copolymer form hexagonal packed cylinders in bulk at temperature above the melting point of PEO block and lamellar morphology at room temperature. Epitaxial relationship was observed between hexagonal melt and lamellar solid phases for this sample as well. TEM has confirmed the crystalline lamellar morphology of the isothermally crystallize block copolymer sample. WAXS data show that PEO block in copolymers crystallizes in its usual monoclinic form.

Nevertheless, there is a reduction in crystallinity and depression in melting temperature (T_m) as compared to the homopolymer as revealed by WAXS and DSC data. These effects are more pronounced in block copolymers with long PFMA blocks. PFMA content in block copolymer affects the spherulitic texture and its growth rate. Low PFMA content (short block) offered less hindrance to PEO crystallization; however, relatively long PFMA block in the copolymer was found to arrest PEO chain movements significantly enough; resulting in relatively disordered spherulites as revealed by the PLM micrographs. The disordered spherulite texture was assumed to be due to confined PEO crystallization within the pre-existing microphase-separated melt domains.

Chapter 3

Behavior of poly(ethylene oxide) and poly(perfluorohexylethyl methacrylate) containing block copolymers in aqueous solution

3.1. Introduction

The ability of block copolymers to organize as micelles or other complex aggregates in selective solvents above a certain critical micelle concentration (CMC) has been studied for the last several decades.³⁸ Block copolymers with hydrophilic and hydrophobic segments in particular have been a rich field of research due to the structural diversity formed in solvents selective for one block. Thus, amphiphilic block copolymers form various supramolecular structures such as spherical micelles, vesicles, cylindrical micelles and other complex aggregates in solution.¹¹¹⁻¹¹³ The reason behind the keen interest in self-association of amphiphilic block copolymers has been their potential applications in different fields such as biomedical, pharmaceutical etc.¹¹⁴⁻¹¹⁵

Amphiphilic block copolymers with long hydrophilic block attached with small hydrophobic block at one or both ends are also known as hydrophobically modified water-soluble polymers (HMWSP). These polymers are important because they exhibit characteristic rheological features that are markedly different from unmodified parent polymers. In aqueous solutions, the hydrophobic blocks of these polymers tend to associate forming hydrophobic microdomains to minimize their interaction with the unfavorable aqueous surrounding and interdomain bridges (especially the systems where the hydrophilic block is attached with hydrophobic blocks at both the ends). These interdomain bridges are assumed responsible for the unusual rheological features of these polymers.¹¹⁶ Though both the diblock (hydrophilic polymer with hydrophobic block at one end) and triblock copolymer (hydrophilic polymer with hydrophobic block at both the ends) form micelle like aggregates in water, yet the associated structures of these

systems are significantly different. Diblock copolymers prefer to form individual micelles with little tendency for cluster formation, except at very high concentration, while the triblock copolymers have tendency to form intermicellar network structure, caused by bridges at higher concentration.¹¹⁷ Triblock copolymers in a solvent selective for the middle block are assumed to form flower-like micelles with the middle block looping in the micelle corona at low concentration,^{41,118} however, their existence is still controversial from both the theoretical and experimental point of view. There are conflicting reports in literature about the self-association behavior of triblock copolymers in solvent selective for the middle block.¹¹⁹⁻¹²¹ Entropy loss due to the loop formation of the middle block is considered to be the main barrier for such block copolymers to self associate into regular micelles. Several factors such as size of the molecule (molar mass), composition, architecture, and concentration of the amphiphilic block copolymer play a key role in aggregation behavior, size and shape of the microscopic self-assembled structures.¹²² Various methods can be used, to investigate the onset of micellization in solution, the structural parameters of the micelles and the effect of different factors such as mentioned above on the micellization process. Experimental techniques such as viscosimetry,¹²³ fluorescence,¹²⁴ surface tension measurements,⁷⁹ laser light scattering,¹²⁵ TEM¹²² etc. have been used.

Amphiphilic block copolymers with poly(ethylene oxide) (PEO) as hydrophilic block have been extensively studied for several years, especially pluronic type of block copolymers.^{30,122,126} PEO-based amphiphilic block copolymers with other hydrophobic blocks such as polystyrene,¹²⁷ poly(butylene oxide)¹²⁵ etc. have also been reported frequently. However, there are only a few reports dealing with fluorocarbon modified poly(ethylene oxide) systems.¹²⁸⁻¹²⁹

Amphiphilic block copolymers of PEO as hydrophilic block and fluorine containing hydrophobic block might be of great potential interest because of the very peculiar properties of fluorine-containing materials such as low surface energy, high contact angle, reduced coefficient of friction, bio-compatibility and oleo- and

hydrophobicity.⁷¹ However, most of the literature available on the fluorine containing amphiphilic systems addresses low molar mass molecules, probably due to the difficulty in the synthesis of fluorine containing amphiphilic block copolymers. Only scarce literature is available on water-soluble fluorine-containing amphiphilic block copolymers.^{79,89} However, a number of investigations have been carried out on aggregation behavior of fluoroalkyl ended poly(ethylene glycol).^{31,129-130}

In this chapter, self-association behavior of water-soluble fluorine containing amphiphilic di- and triblock copolymers having PEO as hydrophilic block and PFMA as hydrophobic block, synthesized by ATRP as explained in *chapter 1*, has been discussed. A diblock copolymer having PEO hydrophilic block and *n*-decylmethacrylate as hydrophobic block (PEO-*b*-PDMA), anionically synthesized has been included as well. The naming scheme for PEO and PDMA containing diblock copolymers is the same as that for PEO and PFMA containing diblock copolymers discussed in *Chapter 2*, i.e. PEO_xFy-D for PEO and PFMA and PEO_xDy-D for PEO and PDMA based block copolymers. Association properties in aqueous solution have been studied using surface tension measurements, dynamic light scattering (DLS) and transmission electron microscopy (TEM). Surface tension measurements have shown that the copolymers start aggregation above a characteristic concentration (CMC). DLS investigations were carried out above the CMC, where the existence of micelles could be expected. DLS studies reveal the existence of various scatterers in solution, including single chains, micelles and larger clusters. TEM investigations have shown spherical micelles; however, different initial concentrations have exhibited different morphologies.

3.2. Experimental section

3.2.1. Surface tension measurements

Surface tension measurements were carried out by pendant drop method using OCA 20 (Data Physics) at 20°C. For this purpose aqueous polymer solutions were prepared in double distilled water. Clear solutions were obtained after overnight stirring at room temperature. However, in some cases a few minute ultrasonic treatment in addition to stirring was given as well to get clear solutions. Freshly prepared stock solutions were diluted to different concentrations for surface tension measurements. The same solutions were also used for DLS and TEM studies.

3.2.2. Dynamic light scattering

DLS measurements were performed with ALV-5000 goniometer equipped with Nd:YAG DPSS-200 laser at a wavelength of 532 nm. The intensity time-correlation functions $g^2(\tau)$ were recorded with an ALV-5000E multiple-tau digital autocorrelator. The normalized field autocorrelation function $g^1(\tau)$ was derived from the $g^2(\tau)$ via Siegert relation.¹³¹ In the device, the thermostated sample cell is placed on a motor-driven precision goniometer ($\pm 0.01^\circ$) which enables the photomultiplier detector to be moved from 20° to 150° scattering angle. A refractive index matching toluene surrounded the scattering cell. Experiments were done on the block copolymer solutions having concentration above CMC. The samples were prepared by filtering the solutions through cellulose acetate filters with 0.2 μm pore size directly into the dust free quartz cells. Measurements were made at an angle of 90° , otherwise mentioned. The experimental duration for each experiment was 15 to 30 min depending upon the scattering intensity. The correlation functions from dynamic light scattering were analyzed by the CONTIN method,¹³² giving information on the distribution of decay rate (Γ). Apparent diffusion coefficients were obtained from $D_{\text{app}} = \Gamma/q^2$ [with $q = (4\pi n/\lambda)\sin(\theta/2)$, n = refractive index of the medium, λ = wavelength of the light, θ = scattering angle] and the

corresponding apparent hydrodynamic radii ($R_{h,app}$, radius of the hydrodynamically equivalent sphere) via Stokes-Einstein equation $R_{h, app} = kT / (6\pi\eta D_{app})$, where k is the Boltzmann constant and η is the water viscosity at temperature T .

3.2.3. Transmission electron microscopy

TEM images were obtained using a LEO 912 TEM operating at an acceleration voltage of 120 kV. Samples were prepared by dipping carbon coated copper TEM grid into the copolymer solution. Extra solution was blotted with filter paper. The samples were then stained with RuO_4 .

3.3. Results and discussion

3.3.1. Micelle formation

Surface tension measurement over a wide range of concentration is one of the several methods used for the CMC determination of low molar mass surfactant or amphiphilic block copolymers. Surface tension measurements were carried out on aqueous solutions of the block copolymers in order to obtain information on the surface activity and micelle formation by the block copolymers. Figure 3.1a depicts the decreasing surface tension with increasing copolymer (PEO₂F12-D) concentration. It is clear from the plot that the surface tension decreases linearly with the logarithm of the copolymer concentration according to the Gibbs adsorption isotherm, i.e. a usual behavior of surface-active compounds. At a characteristic concentration, there is a clear inflection point above which the surface tension remains almost constant. This is a significant indication for a CMC and occurs for this sample at 2.14 g/L at 20°C. However, two inflection points can be seen in Figure 3.1b for PEO₁₀F11 above which the surface tension is still slightly

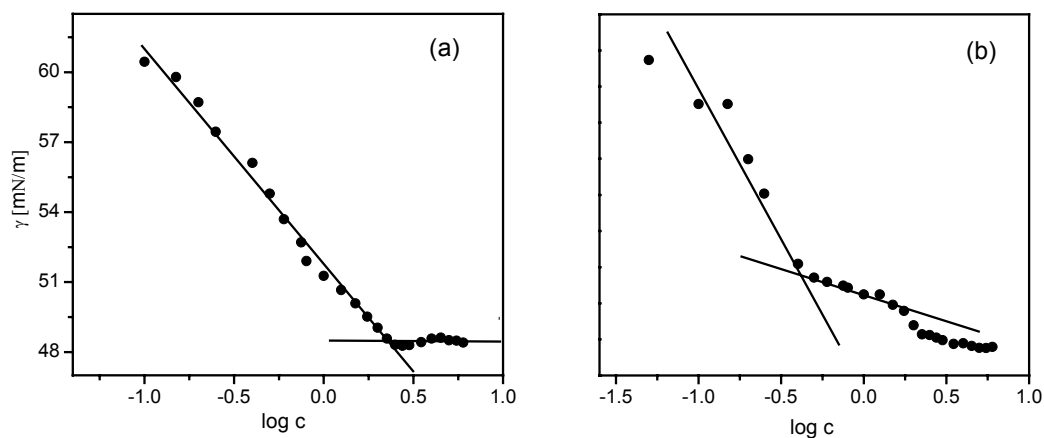


Figure 3.1. Surface tension vs. concentration plots for (a) PEO₂F12-D and (b) PEO₁₀F11 block copolymer solutions (the first inflection point is assumed as CMC.)

decreasing. For comparison, we took the first inflection point as the CMC of the sample. For triblock copolymers PEO₁₀F5, PEO₁₀F9 and PEO₁₀F11 having the same PEO block length but different PFMA contents, the CMC values were calculated to be 1.1, 0.7,

and 0.4 g/L, respectively. Therefore, the CMC decreases with increase in fluoro content in the block copolymer; in other words high fluoro content enhances the surface activity of the copolymer.

Direct evidence for the presence of micelles in solution can be obtained from DLS investigations. Hence, further investigations on the aggregation behavior of the block

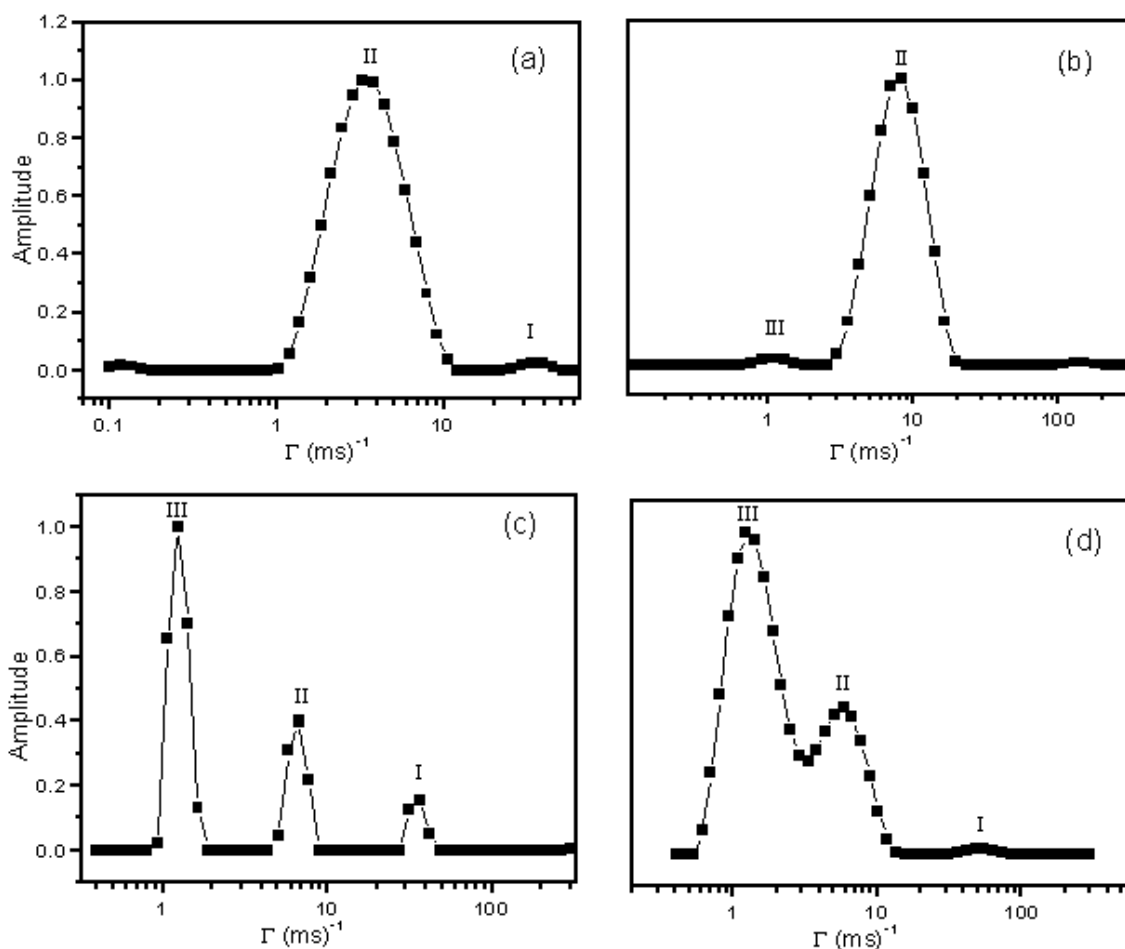


Figure 3.2. Decay-rate distributions for (a) PEO₁₀D₁₃-D ($c = 4$ g/L), (b) PEO₂F₁₂-D (4.0 g/L), (c) PEO₁₀F₅ (4.0 g/L), and (d) PEO₁₀F₁₁ (4.25 g/L) obtained from the respective time correlation functions, measured at $\theta = 90^\circ$, using CONTIN method.¹³² The measurements were carried out at 20°C.

copolymers were carried out with DLS. Distributions of decay rates (I) were obtained by analysis of the dynamic correlation functions $g^{(1)}(\tau)$ by CONTIN.¹³² Figure 3.2 shows decay rate distributions for different samples. The distribution for sample PEO₁₀D13-D reveals one prominent peak and another very small peak as shown in Figure 3.2a. The fast (I) and the intermediate (II) mode correspond to aggregates with apparent hydrodynamic radii $R_{h, app} = 2.7$ and 31 nm, respectively. Figure 3.2b, shows one prominent peak (II) for decay rate distribution for the sample PEO₂F12-D corresponding to aggregates of $R_{h, app} = 15$ nm and a very small peak (III) at lower decay rate distribution representing some large scatterers. The PEO block length in PEO₂F12-D is roughly five times shorter and $R_{h, app}$ is approximately half of the value for PEO₁₀D13-D copolymer. This suggests that the same scaling behavior as for Gaussian chains, $R_{h, app} \sim M_w^{0.5}$, is applicable. However, the length of an extended PEO chain with $M_w = 2\ 000$ g/mol, with approximate $R_{h, app}$ of 16 nm, is in the same range. Therefore, the PEO chains seem to be nearly full extended as no change in shape or structure of the micelles could be detected by TEM (discussed below). The triblock copolymers, however, show quite a different behavior. The I distributions are far from single mode as shown in Figure 3.2c and d for sample PEO₁₀F5 and PEO₁₀F11, respectively. Figure 3.2c clearly reveals three modes of decay rate representing three types of aggregates in the solution. Peak I, II, and III for fast, intermediate, and slow modes correspond to $R_{h, app} = 3, 16,$ and 85 nm, respectively. In Figure 3.2d three peaks are also identified, corresponding to aggregates of $R_{h, app} = 1.7, 18$ and 84 nm respectively. The aggregates of intermediate size, $R_{h, app} = 31, 15, 16, 18$ nm in the solutions of samples discussed above can be regarded as micelles with hydrophobic block making the core and hydrophilic PEO block constitutes the corona of the micelle. The fast mode (peak I in Figure 3.2a, c, and d) can be attributed to the single chains in the solution and the slow mode (peak III in Figure 3.2c and d) can be assigned to large clusters. The difference in the $R_{h, app}$ values of micelles for the triblock copolymers (PEO₁₀F11, PEO₁₀F5) (18 and 16 nm) and diblock

copolymer PEO₁₀D13-D (31 nm) with approximately the same PEO block length suggests that the PEO middle block in triblock copolymer micelles form loop in the micellar corona, resulting in the formation of flower-like micelles as has been suggested for block copolymers with this type of architecture,^{41,118} (i.e. hydrophilic middle block attached with hydrophobic blocks at its two ends). However, a very broad decay rate distribution peak for PEO₁₀D13-D and very small hydrophobic blocks in triblock copolymers makes it difficult to interpret the data with certainty. Several groups have reported the presence of large aggregates in addition to regular micelles in aqueous solution of PEO containing block copolymers.¹²⁶ However, in our investigations, the presence of large aggregates or clusters were more evident in triblock copolymer solution, an expected observation for this type of amphiphilic triblock copolymers.

Two opposing thermodynamic parameters play important role in the formation of flower-like micelles by the triblock copolymers; (i.e. having hydrophilic middle block and hydrophobic end blocks) the loss of entropy due to looping of the middle block and the free energy gain on the association of hydrophobic ends in the micellar core.¹¹⁸ The combined free energy of loop formation can be estimated from:

$$\Delta G_{\text{looping}} = \Delta G_{\text{back folding}} + \Delta G_{\text{hydrophobic}} \quad (3.1)$$

Stable flower-like micelles will form only when the net looping energy is negative. Alami et al.¹¹⁶ have reported such estimations for the hydrophobically modified poly(ethylene oxide) (C₁₂E₄₆₀C₁₂ systems). However, perfluorohexylethyl methacrylate blocks rather than *n*-alkyl groups, modify the PEO in the polymers discussed here. In this case, it becomes very much complicated to assess the net free energy of looping process. However, simplifying the case and taking into consideration that CF₂ is more hydrophobic than CH₂, i.e. 1 CF₂ ~ 1.7 CH₂,¹³³ 12 CH₂ groups can be assumed in each FMA unit. Using Equation 2 and 3, net looping energy ($\Delta G_{\text{looping}}$) can be calculated.

$$\Delta G_{\text{back folding}} = -2.6RT + 1.5RT \ln N_{\text{EO}} \quad (3.2)$$

$$\Delta G_{\text{hydrophobic}} = (-0.3 \text{ to } -0.5)RTN_{\text{CH}_2} \quad (3.3)$$

Hence, for PEO (10 000 g/mol) having 227 EO units and FMA with 12 CH₂ groups, $\Delta G_{\text{looping}} = -0.5RT$. This simple picture predicts that a single FMA unit at each end would be sufficient for the PEO chain of 227 EO units to make energetically stable loop. From the net composition of the copolymer, it can be calculated that each chain of PEO is attached to approximately 3-4 FMA units in total, i.e. there is a high probability to have at least one FMA unit at each end. Therefore, the formation of flower like micelles would be preferred by these triblock copolymers.

3.3.2. Effect of concentration, temperature, ultrasonic treatment, and time

For detailed DLS investigations, the PEO₁₀F11 sample was chosen due to its architecture and good scattering intensity as compared to other copolymers. Investigations were carried out over a range of concentration (above the CMC region) and each concentration was measured at several temperatures from 15°C to 50°C. Concentration dependent DLS data at two representative temperatures (30°C and 50°C) have been shown in Figure 3.3. Two large overlapping and one much smaller peak can be seen for all concentrations. The assignment of these peaks has been discussed earlier. The much smaller peak that appears at higher relaxation rate (I) corresponds to scattering species with $R_{h,\text{app}}$ in the range of 2.2 ± 0.5 nm for all concentrations. The value is close to that deduced from the empirical relationship for unmodified PEO in water at 30°C:¹³⁴

$$R_h = 0.0145M_w^{0.571 \pm 0.009} \text{ (nm)} \quad (3.4)$$

(M_w in g/mol). This relation gives $R_h = 2.79$ nm, for PEO with $M_w = 10$ 000 g/mol. A smaller value would be expected for copolymer chains where both the hydrophobic ends come close to each other to avoid interaction with unfavorable environment (water) with

the PEO loop in the surrounding. However, from the data it is difficult to assign this small peak either to single unassociated polymer chains or to unimolecular self-assembled structures. As the CONTIN program could not resolve the two overlapping peaks, the correlation functions were fitted to a bi-exponential function to obtain the apparent hydrodynamic radii for the intermediate and slow mode. A single exponential function could not fit the data. In order to check if real particles are detected by our measurements,

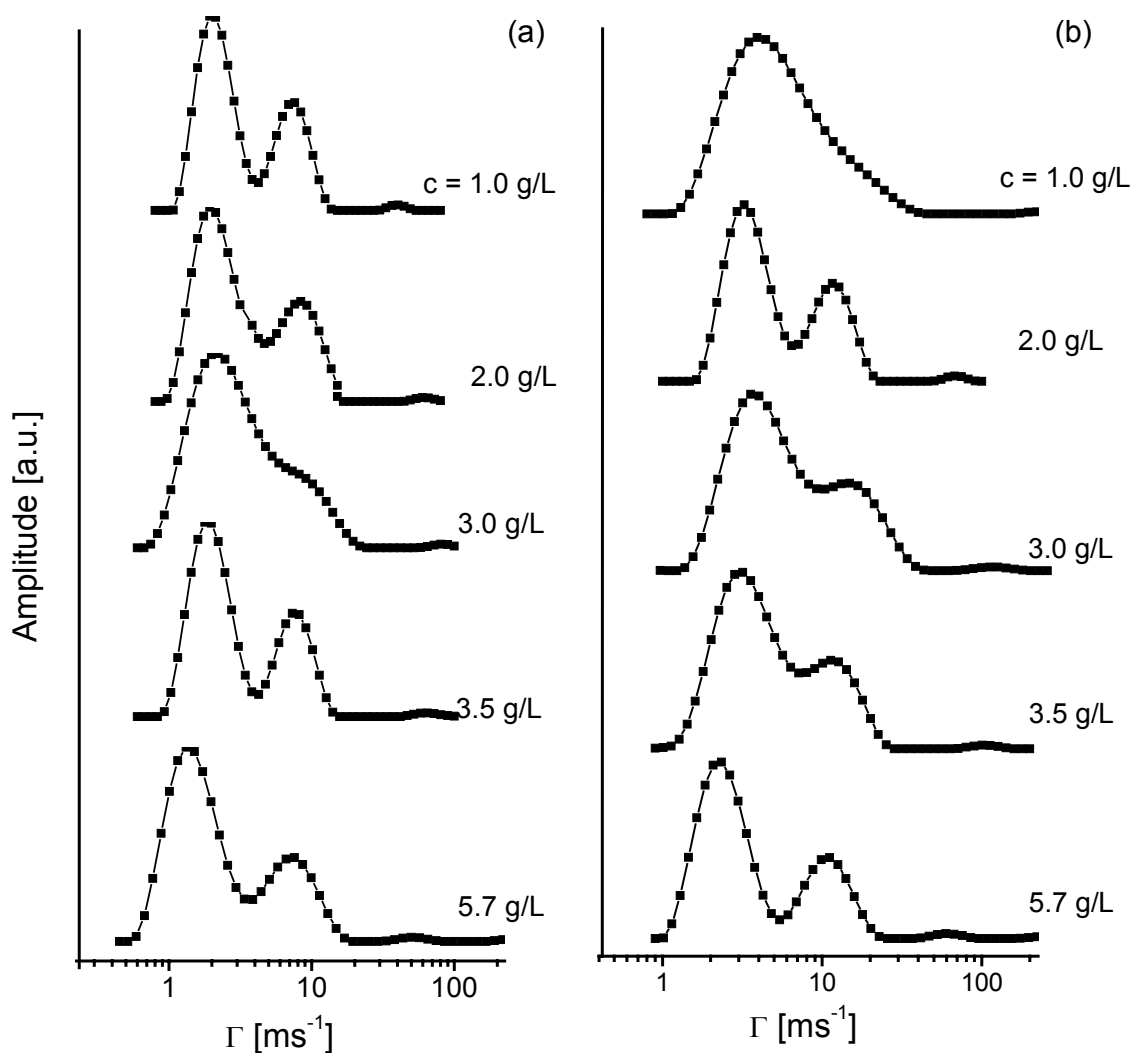


Figure 3.3. Decay rate distributions obtained by DLS for PEO₁₀F11 at different concentrations at (a) 30°C and (b) 50°C.

an angle dependent measurement of the decay rates was performed. Figure 3.4 shows that the relaxation rates of the fast and slow modes are proportional to the square of the scattering vector, indicating that the observed peaks come from diffusive aggregates. Therefore, the calculation of the apparent diffusion coefficient via $D_{\text{app}} = \Gamma/q^2$ is correct for these modes. Apparent hydrodynamic radii of the aggregates in solutions having

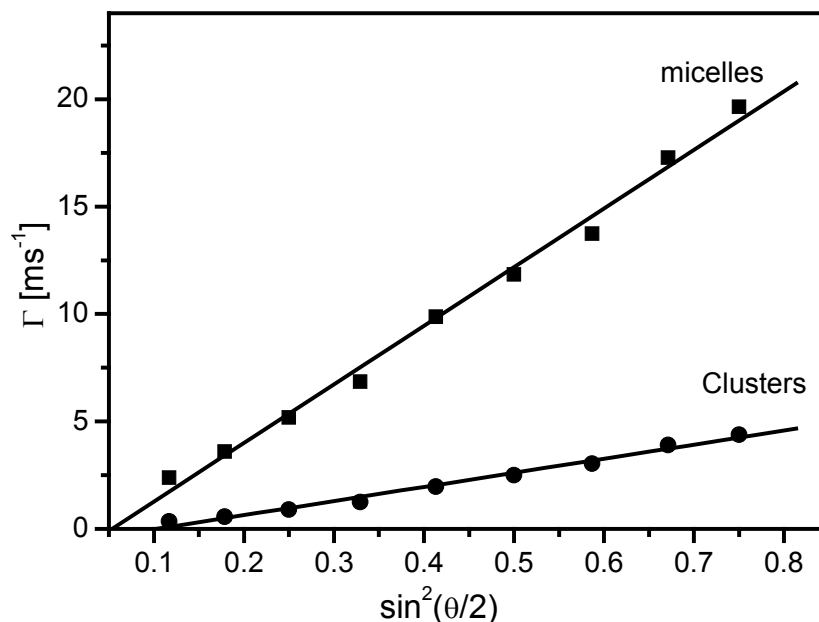


Figure 3.4. Plot of the relaxation rate as function of $\sin^2(\theta/2)$ for both the intermediate mode (micelles) (■) and slow mode (clusters) (●) at 20°C and $c = 3.0$ g/L. The data are derived from the bi-exponential fitting to the DLS data.

different concentrations were calculated from the data via Stokes-Einstein equation. Each concentration was measured at several temperatures between 15 and 50°C. Figure 3.5 shows the effect of concentration on the apparent hydrodynamic radius of the micelles and clusters for three temperatures. The error bars in the figure give the error on fitting the mean value. With concentration, a slight but significant increase (~ 2 nm) in the apparent hydrodynamic radius of micelles was observed for all the three temperatures. This effect can be due to the micellar structure, i.e. flower-like micelle having some

PFMA ends extended into the solvent. These extended chains may result in transient linking, providing an attractive contribution to intermicellar interaction. Yang et al. have reported similar results for ethylene oxide and butylene oxide containing triblock copolymers ($B_nE_mB_n$).¹³⁵ On the other hand, temperature had no effect on the micellar radii. Similar effect of temperature on PEO containing block copolymer micelles in water has been observed, and regarded as a compensation between an increase in aggregation

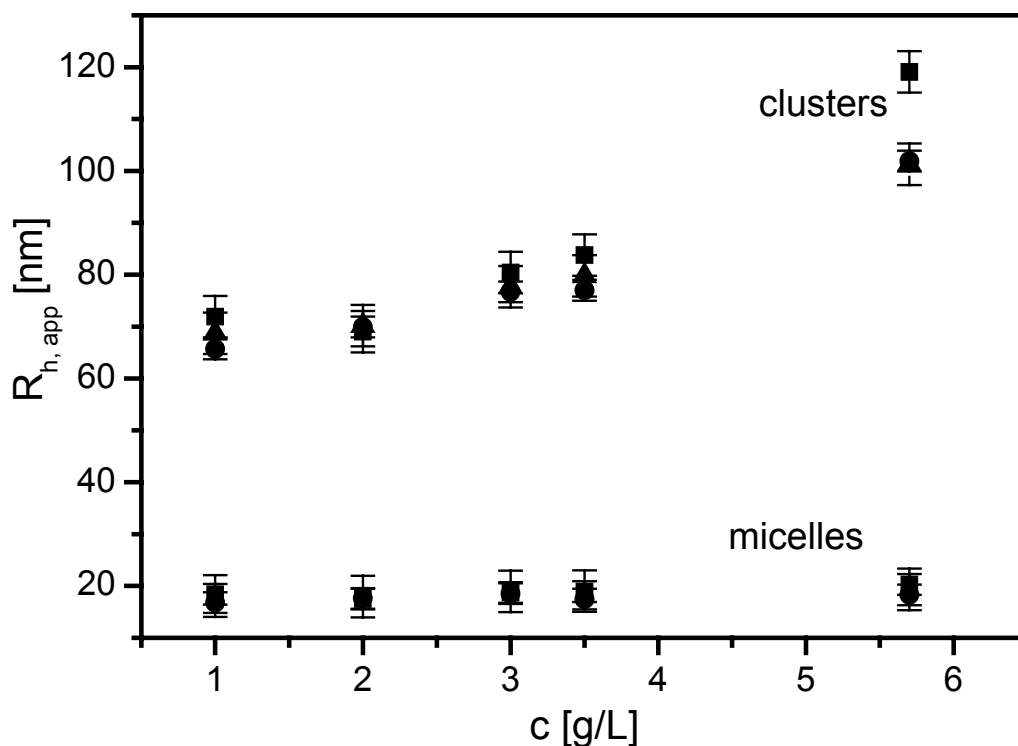


Figure 3.5. Effect of concentration on the apparent hydrodynamic radii of the clusters and micelles at 15°C (■), 30°C (●) and 50°C (▲).

number and a decrease in expansion of the PEO block fringe in the water that becomes poorer with temperature.³⁰ An effect of concentration on the clusters was even more significant as can be seen by an increase of the hydrodynamic radius. For the highest concentration under investigation (5.7 g/L), the apparent hydrodynamic radius increased to 119 nm, whereas at 1 g/L only 72 nm was obtained. This could be because of a

stronger attractive interaction among the clusters as compared to the micelles or to a real growth of the clusters. An effect of temperature can also be seen for clusters, at least at lower temperatures for higher concentrations. The value of $R_{h,app}$ changes from 119 nm at 15°C to 101 nm at 30°C and remains then almost constant. Different groups have reported the presence of larger aggregates of PEO homopolymer or copolymers of PEO in water and even in organic solvents such as methanol, acetonitrile.^{126,136} These are generally interpreted as loose aggregates, some kind of aggregates due to impurities in the sample, or incomplete dissolution of the polymer. Duval¹³⁷ has recently suggested that PEO aggregates as result of the history of preparation of the sample and that exposure of PEO to water at high temperatures greater than 89°C but lower than the critical solution temperature ($\sim 102^\circ\text{C}$) of PEO correlates with the observation of irreversible aggregation. To get more insight into the origin of the larger aggregates observed here; one solution (4.25 g/L) was treated with ultrasound for one hour at room temperature before the DLS experiments were carried out. Figure 3.6 shows the DLS data of the untreated solution (a) and immediately after one hour ultrasound treatment (b). The

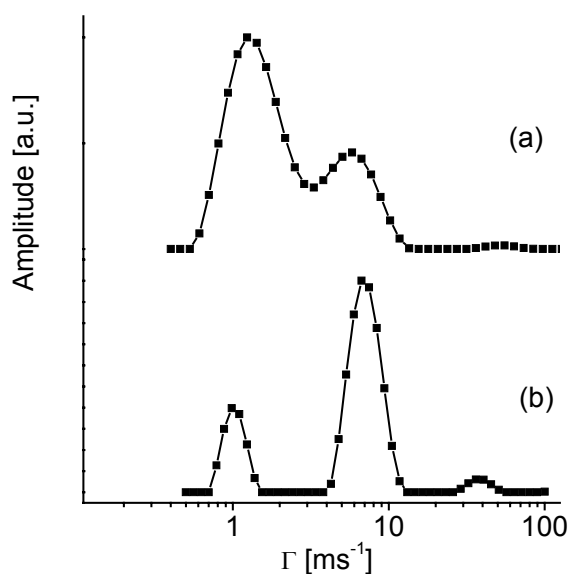


Figure 3.6. Effect of ultrasound treatment on the aggregates. Decay rate distribution (a) before ultrasound treatment and (b) after one hour ultrasound treatment at room temperature. The data in (b) were obtained immediately after the ultrasound treatment.

effect of ultrasound treatment was dramatic on the relative amplitude of the two main peaks. However, the existence of the clusters is still evident in the solution. In another experiment the copolymer solutions were stored at room temperature for several months. After approximately four months, DLS measurements were carried out on the solutions to study the effect of time on the aggregates in solutions. As shown in the Figure 3.7a and b for concentrations 2.0g/L and 3.0 g/L respectively. The decay rate distributions reveal the same two main scatterers, i.e. micelles and clusters, in solution as found before (Figure 3.3). However, by now the micelles are the main contributors to the scattering intensity of the solution. As discussed before, the DLS measurements after a limited time ultrasound

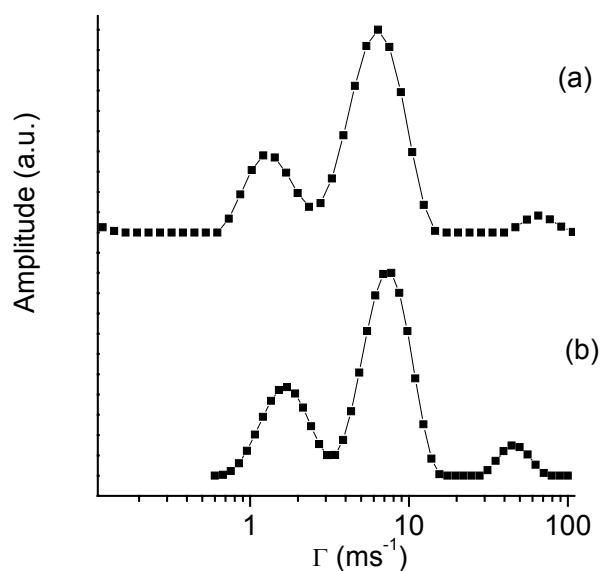


Figure 3.7. Decay rate distributions for aqueous solutions of PEO₁₀F11, stored for four months at room temperature, having concentration (a) 2.0 g/L and (b) 3.0 g/L.

treatment of solutions has produced similar results (see Figure 3.6). There are several reports on the aggregation behavior of the telechelic associative polymers, particularly on fluorocarbon associative polymers.^{31-32,138-140} From the literature as cited above, and the observation we have made on our triblock copolymer systems in water, it can be assumed that the observed large clusters in aqueous solution of the triblock copolymers are loose or random aggregates¹²⁰ formed by the intermicellar connection through bridges. Figure

3.8 shows the schematic illustration of the flower-like micelle and the intermicellar network (formed by the intermicellar bridges through the dangling chains) formation. The individual micelles are flower-like micelles with some free chains dangling in solution, which are responsible for the formation large clusters. The schematic presentation of a star-like micelle formation by the diblock copolymer in solution is also given in Figure 3.8. The intermicellar network is loose in the sense, that the bridges that hold the structure together break and form continuously, i.e. it can be regarded as equilibrium between the individual micelles and large clusters. However, this equilibrium shifts towards micelles with time (in untreated solutions) or by limited time high energy input (in the form of ultrasound) to the system.

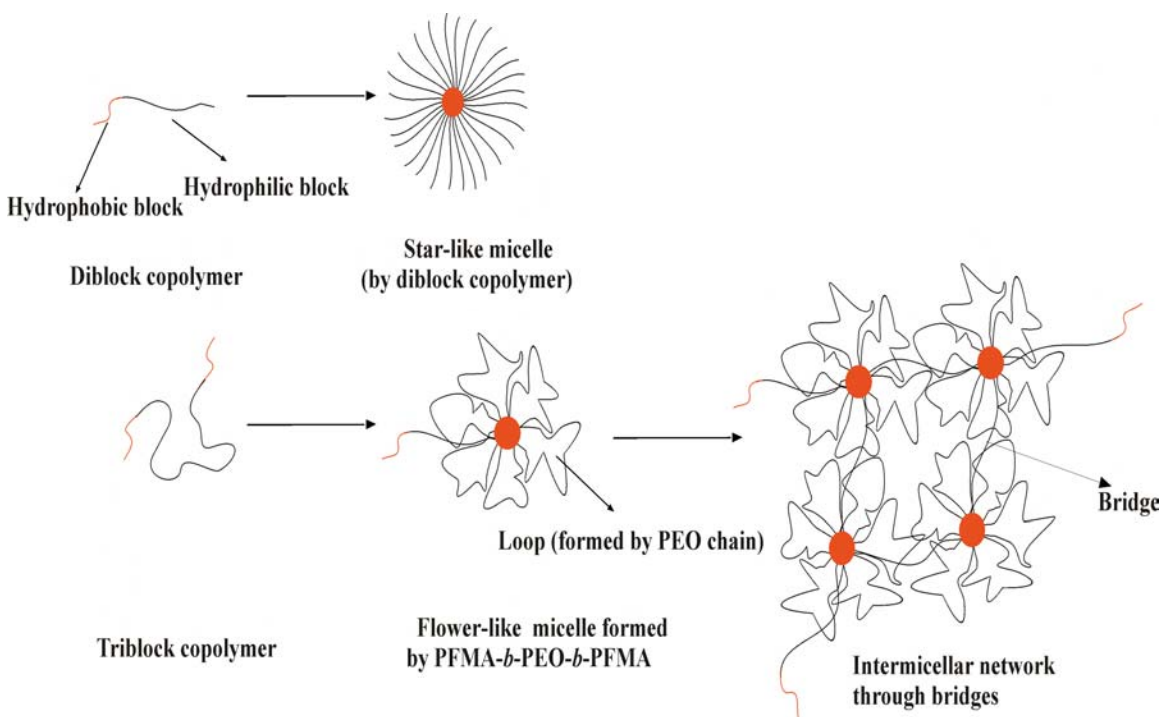


Figure 3.8. Schematic presentation of the star-like micelle formation by diblock copolymer, the flower-like micelle, and the intermicellar network formation by triblock copolymer (hydrophilic block having hydrophobic blocks attached at both the ends).

3.3.3. Morphology of solvent evaporated samples

The morphology of the copolymer aggregates in aqueous solution has been investigated by TEM after transferring the aqueous solution to carbon coated copper grids, as shown in Figure 3.9 and 3.10. The block copolymers mainly form spherical micelles. In Figure 3.9 TEM micrographs of sample (a) PEO₁₀D13-D and (b) PEO₂F12-D, obtained from initial concentration of 4.0 g/L for both the copolymers, are depicted. The mean radius of the aggregates as calculated from the pictures is 15.6 nm with a standard deviation of 2.8 nm and 21 nm with standard deviation of 2.9 nm for PEO₂F12-D and PEO₁₀D13-D

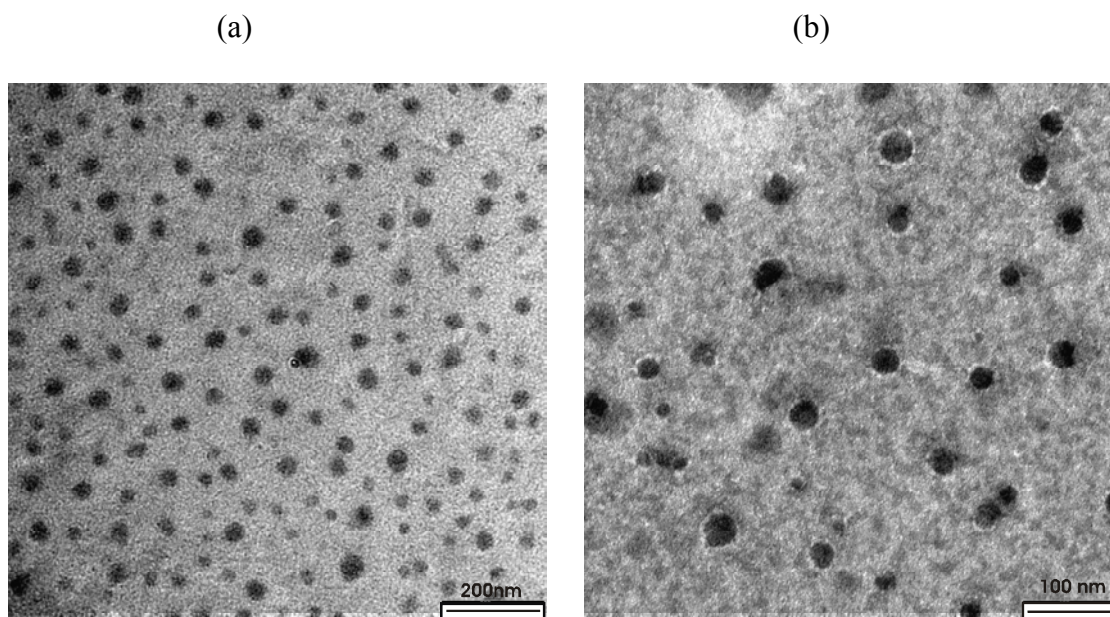


Figure 3.9. TEM pictures of sample (a) PEO₁₀D13-D and (b) PEO₂F12-D, after transferring the copolymer solutions to the carbon coated copper grids. The scale bars are 200 nm and 100 nm respectively.

copolymers respectively. For triblock copolymer PEO₁₀F11, TEM micrographs were obtained from different initial concentrations as shown in Figure 3.10. TEM picture (Figure 3.10a) from low initial concentration (2.5 g/L) reveals only small individual

micelles (average radius of the micelles calculated from the picture is $\sim 21 \pm 2.7$ nm), and a small incomplete network formation as shown with arrows in the picture, where the

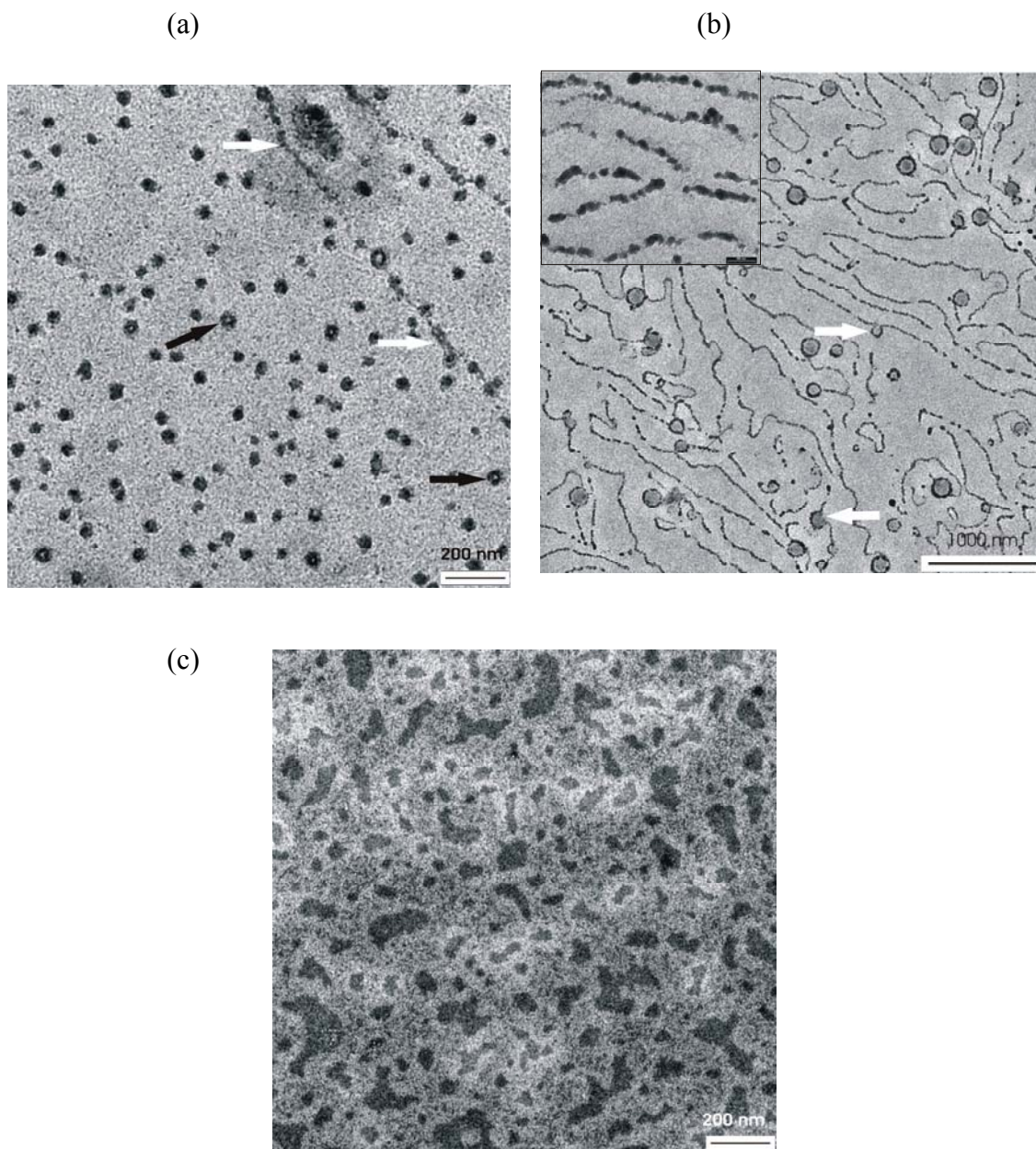


Figure 3.10. TEM micrographs of the associated structures of PEO₁₀F11 block copolymer obtained on a carbon coated copper grid after water evaporation from different initial concentrations 2.5 g/L (a), 3.5 g/L (b), and 5.7 g/L (c). The scale bar represents 200 nm (a), 1000 nm (b), and 200 nm (c). The inset in (b) shows the high magnification view of the fibrous network (scale bar 100 nm).

micelles are tending to coalesce together. By close observation, even some of the individual micelles, seem group of several individual micelles (as shown by dark arrow). Figure 3.10b with relatively high initial concentration (3.5 g/l) reveals a fibrous network and several large structures. Apparently, the fibrous network has the appearance of thread-like or worm-like micelles. However, in high magnification as shown as inset in Figure 3.10b, the network structure looks like a string of beads (single micelles). These can be assumed as individual micelles, connect with each other as the water evaporates. The apparent reason for this fusion could be the bridge formation as discussed earlier. Lee et al. have also reported similar fibrous network (formed by individual micelles) morphology for polypeptides.¹⁴¹ Looking to the details of the large spherical structures, it can be observed that the boundary wall is not smooth but appears a beaded ring. The origin of these structures is not yet clear. These could be simple rings of interconnected micelles formed as the water droplet evaporates or it could be spherical structures. The former idea, however, would be of more worth as there are some incomplete rings associated with the fibrous network (shown with arrow) and furthermore, even the complete ring-like structures are usually connected with the network structure. Different morphologies have been reported for block copolymer associated structures, like individual spherical micelles, vesicles, compound micelles, tubular, thread-like micelles.¹¹¹⁻¹¹³ However, the observed type of micellar arrangement is unique. It can be argued that with evaporation of the solvent, concentration of the solution increases, leading to an increase in the number density of the micelles and a corresponding decrease in their distance, and hence the formation of fibrous network occurs. However, this specific morphology was associated only when the initial concentration was 3.5 g/L. It implies that the initial concentration of the block copolymer solution plays an important role in fibrous network formation when the rate of evaporation of the solvent is fixed. Furthermore, still at higher concentration the tendency of film formation by the amphiphilic block copolymer is obvious as shown in Figure 3.10c. The block with the smaller interfacial tension to substrate compared to the other block tries to spread on the

surface. In this case, the spreading started but the polymer concentration of 5.7 g/L is not large enough to form a homogeneous film on the carbon film.

The ability of amphiphilic block copolymers to cover colloidal metal particles is used for many applications.¹⁴² To test the covering tendency of the polymers under investigation, colloidal particles can be added to the solutions.⁷⁹ The suitability for using the micelles as nanoreactors for producing metal particles in nanometre scale depends on

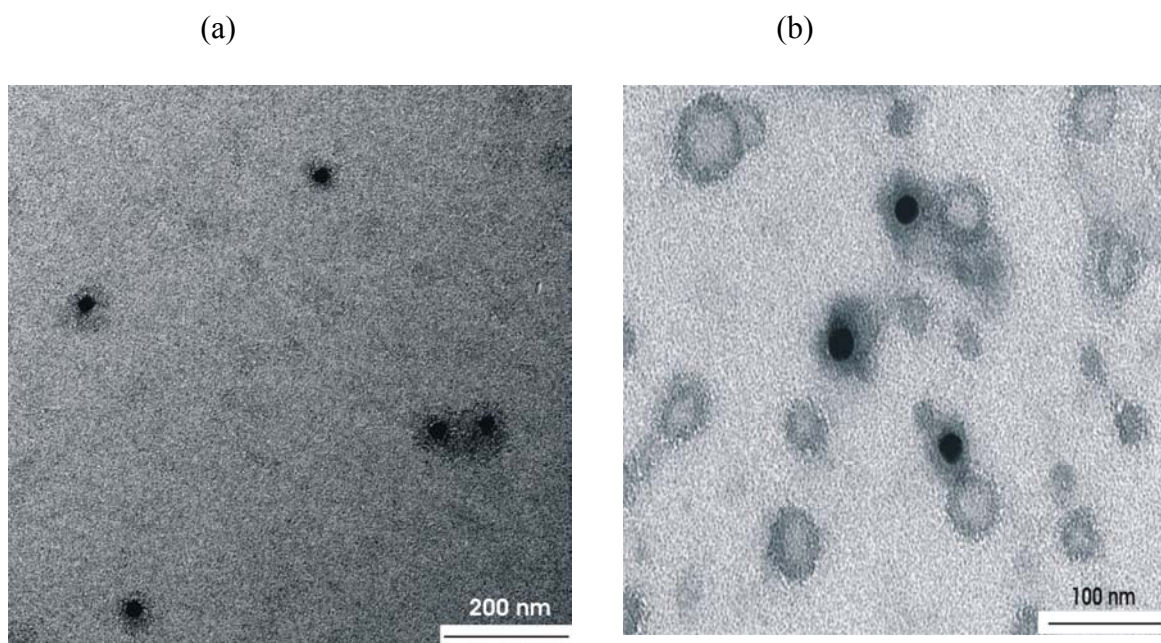


Figure 3.11. TEM images of gold colloid (dark particles) covered with (a) PEO₁₀D13-D and (b) PEO₁₀F11 block copolymer chains, obtained after transferring the water solutions to carbon coated copper grid. The scale bars are 200 nm and 100 nm respectively.

their affinity and stability. For this purpose, a dilute solution of colloidal gold (4.5×10^{-5} wt.-% in water) was mixed with the polymer solution. TEM investigations were carried out after approximately 10 min ultrasound treatment of the solutions at room temperature. Figure 3.11 depicts the TEM pictures of sample (a) PEO₁₀D13-D and (b) PEO₁₀F11 with gold colloids. The pictures reveal that the gold particles (dark circular spots in the

picture) are engulfed by the block copolymer (comparatively less dark surrounding). The effect of covering gold particles by amphiphilic block copolymers is well known and is used for the formation of nanoparticles.¹⁴²

3.4. Conclusion

Aggregation behavior of poly(ethylene oxide) and poly(perfluorohexylethyl methacrylate) containing amphiphilic block copolymers in aqueous solution has been investigated by different techniques. Surface tension measurements have shown a clear inflection point in surface tension vs. concentration plots. The concentration corresponding to the inflection point was interpreted as the CMC. The CMC decreased with an increase in the PFMA content in copolymers. Dynamic light scattering studies have revealed the existence of different types of aggregates in solutions, including single chains, micelles, and large clusters. However, the large clusters as the dominant scatterers were detected only in triblock copolymer solution. Micelle size was found resistant to changes in temperature, however, a slight but significant increase in apparent hydrodynamic radius was observed with an increase in concentration, while both the temperature and concentration affected the large clusters, especially in concentrated solution. TEM investigations, carried out after transferring the aqueous solutions to carbon coated copper grids, has shown that the initial concentration of samples used for TEM has an influence on the morphology of the aggregates formed. Depending upon the initial concentration, single micelles, a fibrous network with circular structures, and some irregular morphology (tendency towards film formation at high concentration) were revealed by TEM studies. Lastly, by adding colloidal gold particles to the copolymer solutions, the typical covering by the polymer was observed by TEM as well.

Chapter 4

Amphiphilic block copolymers of poly(ethylene oxide) and poly(perfluorohexylethyl methacrylate) on water surface and their penetration into lipid monolayer

4.1. Introduction

Block copolymer monolayers have attracted a great deal of attention during the last two decades.¹⁴³⁻¹⁴⁶ Amphiphilic block copolymers in selective solvents readily adsorb at the air/water interface forming monolayers. These are constituted of a hydrophobic block anchoring the copolymer chain at the interface and of a hydrophilic block, which extends into the solution. The adsorption from a selective solvent to the interface is assumed to be due to the immiscibility of the insoluble block with the solvent. However, monolayer formation is not only restricted to the air/water interface; it can also occur at the surface of other selective solvents as well. In contrast to lipid monolayers where a large variety of structural phase transitions have been reported during the film compression, only two phase transitions have been measured in copolymer monolayers.⁵⁴ The first transition during compression is a continuous phase transition between a mushroom conformation at low surface density where the chains do not overlap and a brush conformation at higher surface density where the steric interactions between the polymer chains result in an anisotropic stretching of the polymers from the surface. This behavior has been observed when the soluble block has no affinity for the interface such as poly(dimethylsiloxane)-polystyrene at the air/dioctyl phthalate interface.⁵⁸ The second possible phase transition, as predicted by Alexander¹⁴³ and Ligoure¹⁴⁷ for long chains adsorbed at the interface, is a first order transition between an adsorbed conformation at low surface density and a brush conformation at high surface density. This behavior

might be expected from block copolymers where the soluble block has an attractive interaction with the interface such as poly(ethylene oxide) containing block copolymers.^{57,148} The plateau in the isotherms of these copolymers has been reported as an evidence of a first order type transition.¹⁴⁹⁻¹⁵⁰

Though biomembranes are composed of a bilayer of lipids and peripheral and integral proteins, the Langmuir lipid monolayer system serves as a good model for the biomembrane.¹⁵¹⁻¹⁵² Studying the penetration of the lipid monolayer by amphiphilic molecules or other compounds yields information on the nature of the interactions between the membrane and the penetrant. There are many reasons for investigating such systems in the field of biophysics, biomedicine, and biotechnology.¹⁵³⁻¹⁵⁴ For example, one area of interest might be to understand the molecular mechanism of membrane sealing capabilities of block copolymer surfactants.¹⁵⁴ When exposed to nonionic block copolymer surfactants (poloxamers), the recovery rate of electrical or burn injuries have been found improved.¹⁵⁵⁻¹⁵⁶ Investigations on the penetration of monolayers by amphiphilic molecules have developed a better understanding of some complex physiological issues such as the function of lung surfactants in mammalian lungs, which has led to the development of therapeutic agents for the respiratory distress syndrome, a condition resulting from a deficiency of lung surfactants.¹⁵⁷⁻¹⁵⁹ Investigating the interaction of block copolymers with phospholipid mono- and bilayer systems would help understand the effects of Pluronic [poly(ethylene oxide) and poly(propylene oxide) containing block copolymers] copolymers on the transport and activity of the anticancer drugs in multidrug resistance (MDR) tumor cells.⁶⁰ MDR can be found in many human tumors that have relapsed after the initial positive response to chemotherapy.⁶⁵ For example, in a recent study the formulation of anthracyclines with pluronic copolymers (e.g. P85, L61) has been found to have a dramatic effect on the cytotoxicity of these drugs with respect to MDR cells.⁶⁰ A thorough discussion about the penetration of amphiphilic molecules into lipid monolayers can be found in a recent review by Vollhardt et al.¹⁶⁰

In this chapter, the behavior of PEO and PFMA containing amphiphilic block copolymers, and 1,2-diphytanoyl-*sn*-glycero-3-phosphocholine (DPhPC) at the air/water interface and the penetration of the lipid monolayer by the copolymers, using surface pressure (π)-area (A) isotherm measurements and infrared reflection absorption spectroscopy (IRRAS) has been discussed. DPhPC has often been used in studies of lipid-peptide interactions,¹⁶¹ electrophysiological measurements¹⁶² and membrane-channel activities,¹⁶³⁻¹⁶⁴ because of the general understanding that it forms highly stable bilayers with low ion leakage.¹⁶⁵ DPhPC monolayer π/A isotherms show the lipids being in the liquid expanded phase state. However, controversial reports have been published in the literature on the bulk phase behavior of DPhPC. Lindsey et al.¹⁶⁵ have reported that DPhPC does not show any phase transition over a temperature range of -120°C to 120°C , whereas Hsieh et al.¹⁶⁶ have found indications for a phase transition. However, only a few reports have been published on the behavior of DPhPC monolayers at the air/water interface and its interaction with amphiphilic molecules. Winterhalter et al.¹⁶⁷ have investigated the interaction of poly(ethylene glycols) with DPhPC monolayers, while Cseh et al.¹⁶⁸ reported the interactions of Phloretin with DPhPC monolayer using surface pressure and surface potential measurements. However, we are not aware of any investigations on the penetration of DPhPC monolayers at the air/water interface by amphiphilic block copolymers by using π/A measurements or IRRAS. The main aim of our study was (1) to get fundamental information about the behavior of the newly synthesized amphiphilic block copolymers at the air/water interface using π/A measurements and IRRAS, and (2) to gain insight into the penetration of DPhPC monolayers by block copolymers also using IRRAS. The intensity of $\nu(\text{O-H})$ band (from the water subphase) and $\nu(\text{C-O})$ band (from PEO) in the IRRAS spectra was analyzed to get qualitative information about the film thickness and hence the insertion and expulsion of block copolymer molecules from the lipid monolayer.

min after the spreading of the chloroform solution. For monolayer penetration experiments, the lipid monolayer was obtained as discussed above and then a known amount of the polymer solution in water was injected carefully through the film into the subphase. The π/A isotherm was measured after waiting for 30 min in each case. This waiting time was enough to get a constant surface pressure after the initial pressure jump directly after injection of the polymer solution. The same procedure was used to study the behavior of the block copolymer chains at the surface in the presence of lipid monolayer by IRRAS. Constant area experiments were performed on a home-built circular trough with an area of 7 cm² having no movable barriers. For constant area experiments, the DPhPC monolayers having different surface pressures were prepared in the circular trough. The increase in surface pressure of the lipid film with the injection of the copolymer aqueous solution into the subphase was measured. The final trough concentration of the block copolymer in each experiment was 0.22 μM .

4.2.3. Infrared reflection absorption spectroscopy setup

Infrared spectra were recorded with an Equinox 55 FT-IR spectrometer (Bruker, Karlsruhe, Germany) connected to an XA 511 reflection attachment (Bruker) with the above mentioned trough system and an external narrow band MCT detector. The IR beam can be directed along a system of mirrors onto the water surface at an angle of incidence of 40° with respect to the normal of the water surface. A computer controlled rotating KRS-5 polarizer (>98 % degree of polarization) is used to generate perpendicularly polarized light. The trough system is positioned on a moveable platform to be able to shuttle between the sample and the reference trough. This shuttle technique diminishes the spectral interference due to the water vapor absorption in the light beam.¹⁶⁹⁻¹⁷⁰ Schematic representation of the IRRAS setup is given in Figure 4.2. The monolayer films were compressed to a desired area per molecule, the barriers were then stopped and the IRRA spectra were recorded at a spectral resolution of 4 cm⁻¹ using Blackman-Harris-4-

Term apodization and a zero filling factor of 2. For each spectrum 1000 scans were summed over a total acquisition time of about 4.5 min. The single beam reflectance spectrum of the reference trough surface was ratioed as background to the single beam

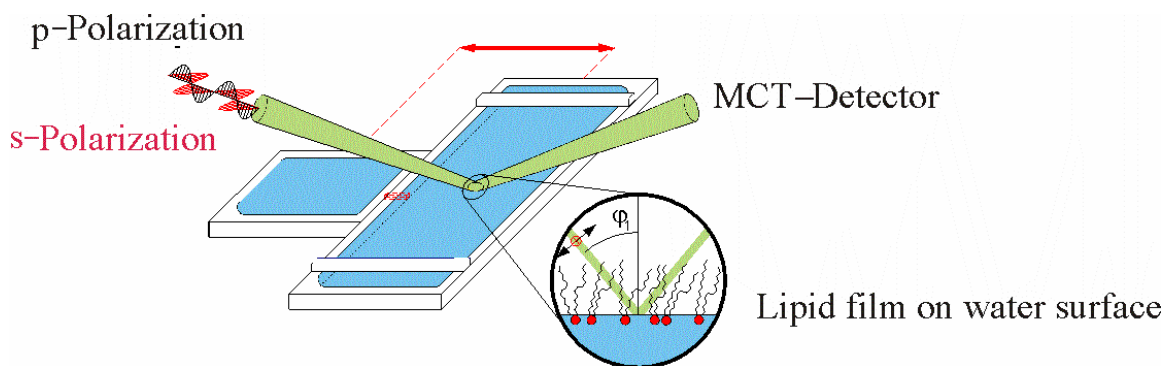


Figure 4.2. Schematic illustration of the IRRAS setup.

reflectance spectrum of the monolayer on the sample trough to calculate the reflection absorption spectrum as $-\log(R/R_0)$. The reflection-absorption of the $\nu(\text{O-H})$ band was calculated by an integration of the band between 3000 and 3500 cm^{-1} . In the region above 3500 cm^{-1} often a lower signal to noise ratio and/or superimposed rotational vibrational bands of water vapor were observed. This was therefore excluded from the integration procedure.¹⁷¹

4.3. Results and discussion

4.3.1. Interfacial properties of the block copolymers at the air/water interface

In order to obtain first information about the adsorption behavior of block copolymers at the air/water interface, different amounts of the aqueous solution of PEO₁₀F11 were

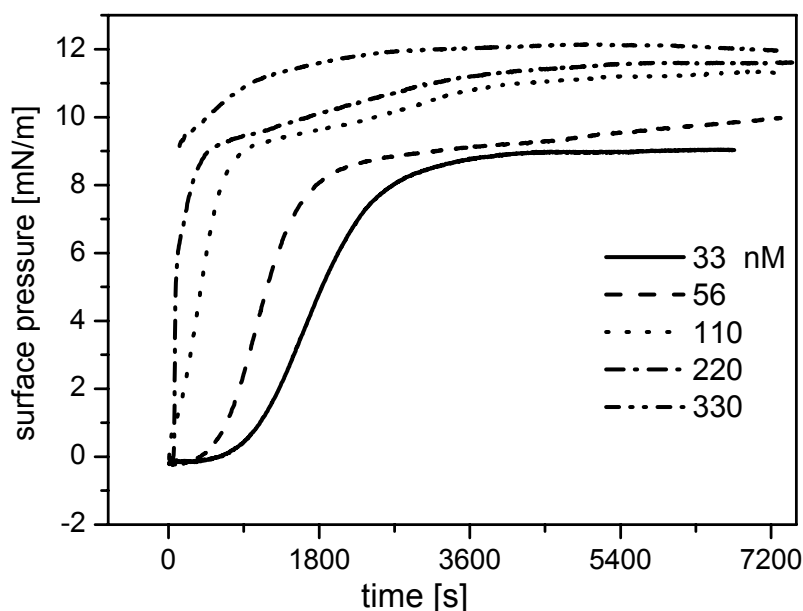


Figure 4.3. Adsorption of PEO₁₀F11 at the air/water interface. Different volumes of the aqueous solution were injected into the water filled circular trough. The corresponding total concentration of the block copolymer in the trough for each experiment is given in the inset.

injected into the water filled trough and the subsequent increase in surface pressure was monitored. These experiments were carried out in the small circular trough. Figure 4.3 shows the results from these experiments. Depending upon the initial injected volume, two different types adsorption behaviors were observed. First, an induction period, where no significant increase in surface pressure can be seen (when a small amount of the polymer solution is injected, i.e. 3 μ L and 5 μ L, with the corresponding copolymer

concentration in the trough of 33 nM and 56 nM, respectively). The induction period decreases with an increase in the copolymer concentration. After a sharp rise of the surface pressure (for 10 μ L, 20 μ L and 30 μ L, with the corresponding copolymer trough concentration of 110 nM, 220 nM, and 330 nM, respectively), a 'slow increase in surface pressure' which begins at approximately the same surface pressure (9.2 mN/m) in all the three respective isotherms, is observed prior to the plateau region (i.e. the almost constant surface pressure region of the isotherms). A similar behavior has been reported for a lipid monolayer penetration by proteins,¹⁶⁰ and that was assumed a first order phase transition which leads to the development of a two-dimensional condensed phase of the lipid monolayer. We suggest the 'slow increase regime' as a kind of phase transition of the polymer adsorbed layer at the water surface, involving the rearrangement of the polymer chains to attain a more stretched conformation in the water subphase to accommodate more polymer chains at the surface.

Figure 4.4 shows the experimental π/A isotherms for PEO₅F15-D, PEO₁₀F11, and PEO₂₀F14 block copolymers. Due to the limited compression range of our trough, the monolayer had to be deposited at several different surface areas to explore the complete isotherm. The overlapping of the different parts of the obtained isotherms was within the experimental error. The isotherms in Figure 4.4 have the same appearance irrespective of the architecture of the block copolymers. The collapse pressure of the monolayer was approximately 60 mN/m for all the three copolymers. For each copolymer isotherm, different regions can be distinguished; that correspond to different chain conformations or conformational transitions as described by scaling theories.¹⁷² A typical liquid expanded phase can be recognized at low surface pressures, where the PFMA hydrophobic segment anchors the polymer chain to the surface while the PEO due to its amphiphilic nature is assumed to adopt a flattened conformation at the interface. This phase can be considered as a self-similar adsorbed layer (SSAL) or due to its appearance as pancake. This is the characteristic phase for the attractive monomer case¹⁷³ (i.e. the

soluble block has an affinity for the water surface). In contrast, the non-attractive

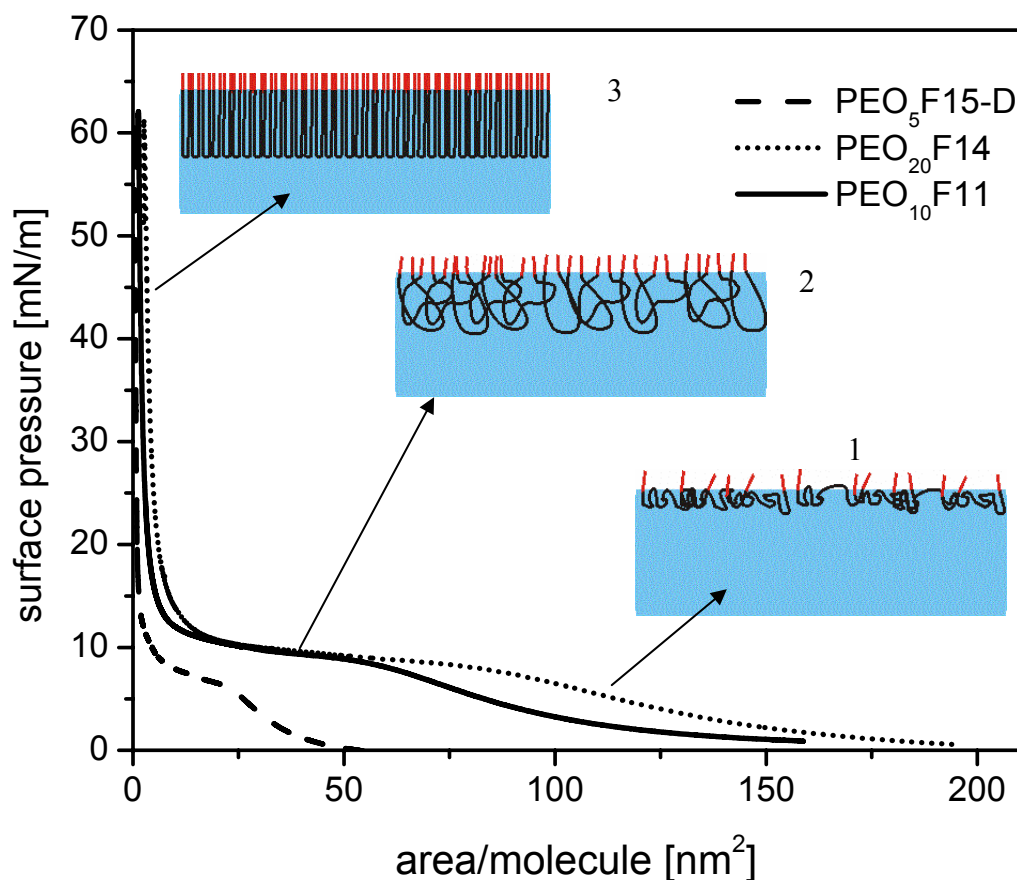


Figure 4.4. Surface pressure-area isotherms of three different block copolymers at 20°C. The schematic representation in the Figure shows the pancake (1), the plateau region (a transition regime from the pancake to the brush conformation) (2), and the brush conformation (3), respectively.

interfaces repel the soluble block from the surface already at low surface coverage, i.e. the mushroom regime. The adsorption of PEO at the water surface is also evident from the shift of the isotherms to larger areas per molecule with an increase in PEO chain length; $\text{PEO}_5\text{F15-D} < \text{PEO}_{10}\text{F11} < \text{PEO}_{20}\text{F14}$. A pseudo-plateau can be seen at a surface

pressure of approximately 9 mN/m for triblock and approximately 7 mN/m for the diblock copolymer, which does not exist in the nonattractive case. This pseudo-plateau has also been reported for the PEO homopolymer chains¹⁷⁴ and it is assumed to be associated with the dissolution of PEO chains into the water subphase with compression. A first order phase transition has been predicted by theories^{143,147} for such systems as discussed in the Introduction section above. However, with a slight but continuous variation of the surface pressure π with A in the present systems, it is difficult to interpret it as a true first order transition. There can be different reasons for this continuous variation of π with A such as the polydispersity of the PEO block.¹⁴⁹ In Figure 4.4, the plateau region is more pronounced for PEO₂₀F14, while for PEO₅F15-D with a much smaller PEO block, it is less distinct. Faure et al.⁵⁶ have reported similar behavior for poly(styrene)-*block*-poly(ethylene oxide) copolymers. They interpreted the phase transition corresponding to the plateau region as a first order transition for long PEO chain containing block copolymer (i.e. PS₃₂-PEO₇₀₀) with less and less first order character of the transition as the chain length decreases. In other words, as the PEO chain length decreases, the plateau of the isotherms become increasingly less pronounced, implying the transition increasingly deviates from first order.⁵⁴ At higher surface coverage the isotherms show a very large increase of the surface pressure. In this regime of the isotherm a brush conformation is expected. No additional plateau or change in the slope was observed in the brush regime of the isotherm. The brush can be viewed as tightly packed PEO chains in the water, anchored at the surface by the PFMA blocks. The area per molecule at the film collapse was calculated $\sim 0.31 \text{ nm}^2$, 1.31 nm^2 , and 2.65 nm^2 for PEO₅F15-D, PEO₁₀F11, and PEO₂₀F14 block copolymer film respectively. However, from the data it is difficult to infer the influence of the PEO chains at the surface on film collapse. The reported cross-sectional area of a fluorocarbon side chain is approximately 0.32 nm^2 .¹⁷⁵ If it is assumed that at the film collapse the air/water interface is occupied only by the FMA units of the copolymer chains, then the collapse areas ~ 0.31 , 1.31 , and

2.65 nm² indicate the presence of 1, 4, and 8 fluorocarbon side chains per molecule (of the respective copolymer) at the surface. Interestingly, the number of FMA units per PEO chain as calculated from ¹H-NMR data is ~ 1-2, 3-4, and 9 for PEO₅F15-D, PEO₁₀F11, and PEO₂₀F14, respectively. Therefore, these data tentatively exclude the influence of the PEO on the collapse area of the polymer film. The behavior of PEO₁₀F11 and PEO₂₀F14 at the interface is quite different from the telechelic poly(ethylene oxide) polymers end-capped with hydrophobic alkane groups. For example, Barentin et al.¹⁷⁴ have reported a second plateau in the brush regime of the π/A isotherm that was interpreted by the dissolution of the water surface attached polymer chains alkane groups. The second difference was that the surface pressure of the brush conformation was dependent on the PEO chain length, while we observed approximately the same brush pressure (surface pressure at the time of collapse) of approximately 60 mN/m for all the three polymers investigated here, i.e. independent of the PEO chain length. The difference can be due to the large difference in hydrophobicity of fluorine containing PFMA and alkane hydrocarbon chains.¹⁷⁶ The PFMA block anchors more strongly the PEO chains to the surface as compared to the hydrocarbon chains.

4.3.2. Penetration of lipid monolayer by block copolymer chains

Figure 4.5 shows the π/A isotherms of a pure DPhPC film and of PEO₁₀F11 block copolymer penetrated DPhPC films on the water surface. Taking into consideration the pure DPhPC isotherm, the gaseous phase of the monolayer, which is found at very low surface pressures (< 0.1 mN/m), cannot be detected with our setup. However, compression of the monolayer leads to a phase transition to the liquid-expanded phase state which is complete at an area of approximately 1.12 nm² per lipid molecule, which can be seen in Figure 4.5 (full line) by an increase of surface pressure from approximately 0 mN/m. The film collapses at π of approximately 40 mN/m and A of

approximately 0.66 nm^2 per molecule. After injecting the polymer solution into the

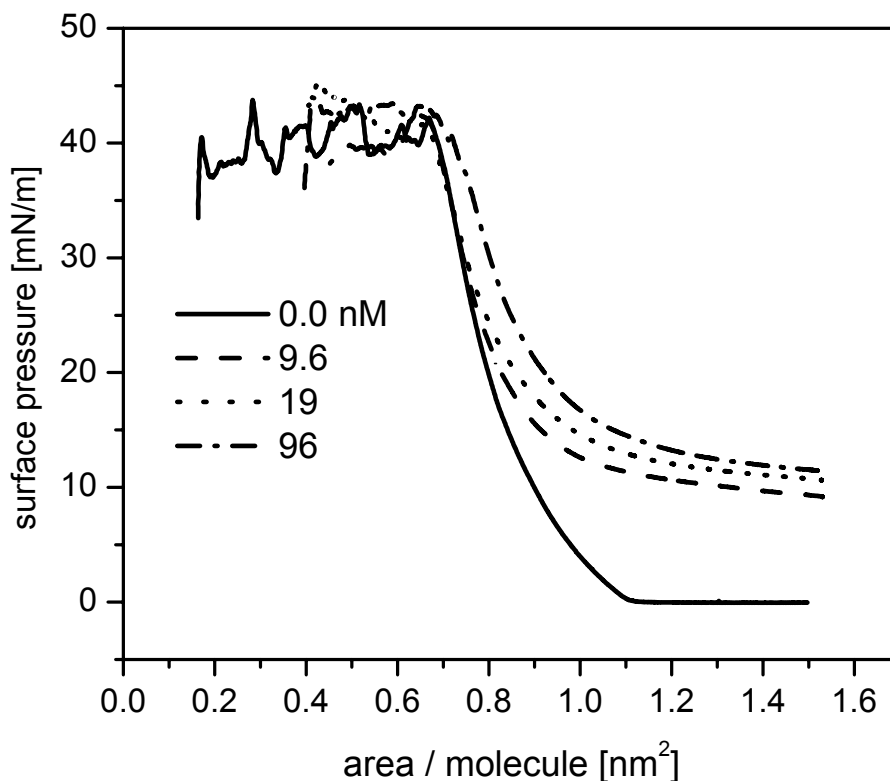


Figure 4.5. π/A isotherms of a pure DPhPC film and PEO₁₀F11 penetrated DPhPC films on the water surface at 20°C. DPhPC was spread and after 15 min waiting time for the solvent evaporation different amounts of PEO₁₀F11 block copolymer aqueous solution were injected into the subphase. The resultant polymer concentration in the trough in each experiment is given in the inset. The isotherms were recorded after 30 min in each case.

subphase under a fully expanded DPhPC film, a shift towards a higher area/molecule in the isotherms can be seen. This clearly indicates that PEO₁₀F11 copolymer chains insert into the DPhPC monolayer, thus increasing the apparent area per lipid molecule at a given surface pressure. There is also a considerable jump of the surface pressure from approximately 0.0 mN/m for pure DPhPC to approximately 9 – 11 mN/m (depending upon the final copolymer concentration in the trough) after the injection of the copolymer

solution into the water subphase. It is evident from Figure 4.5 that the shift in the isotherm increases with an increase in the copolymer concentration in the trough. For example, at $\pi \sim 17$ mN/m the (apparent) area per lipid molecule was increased from approximately 0.81 to 0.98 nm² with increase in polymer solution concentration from 0 nM to 96 nM, indicating an increasing number of polymer chains penetrating into the lipid monolayer. Furthermore, the effect of the polymer insertion on the isotherm is much stronger at low surface pressure. At a given polymer concentration, e.g. 96 nM, the increase in area per lipid molecule is ~ 0.52 nm² and ~ 0.06 nm² at 12 mN/m and 35 mN/m, respectively (the quantitative data were obtained by comparing the respective isotherms in Figure 4.5). In addition, at high surface pressures, depending upon the amount of the injected polymer solution, the isotherms (Figure 4) of the pure DPhPC and the polymer penetrated DPhPC overlap, indicating the expulsion of the polymer chains from the lipid film. Figure 4.5 also reveals that the surface pressure, at which the isotherms of the polymer penetrated DPhPC revert to the pure DPhPC isotherm, increases with the increase in polymer concentration in the trough, i.e. the copolymer chains retain their position in the lipid monolayer up to high surface pressures.

Figure 4.6 shows the results of the constant area experiments on the PEO₁₀F11 copolymer penetration into DPhPC monolayer at various initial surface pressures. In each experiment the same amount of the block copolymer solution was injected carefully through the lipid film. The resultant copolymer trough concentration was 0.22 μ M. The critical surface pressure of the lipid monolayer at or below which polymer chains could be inserted into the monolayer was determined approximately 38 mN/m.

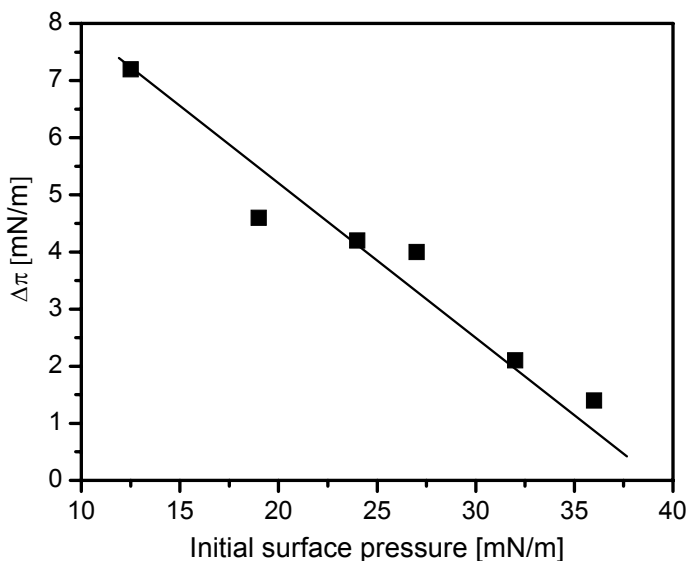


Figure 4.6. Increase in the surface pressure of DPhPC films having different initial surface pressures at constant area after injecting the same amount of the PEO₁₀F11 copolymer solution into the trough. The resultant trough concentration of the block copolymer in each experiment was 0.22 μ M. The experiments were performed at 20°C.

4.3.3. Infrared reflection absorption spectroscopy investigations

In recent years considerable progress has been made in the structural characterization of monolayers at the air/water interface, utilizing techniques such as X-ray and neutron reflection,¹⁷⁷⁻¹⁷⁸ Brewster angle microscopy (BAM),⁵⁴ and infrared reflection absorption spectroscopy (IRRAS).¹⁷⁹⁻¹⁸¹ One important aspect in the characterization of monolayers at the air/water interface is the determination of the conformation and the structure of the various molecular functional groups, and IRRAS has proved to be the key technique for this kind of investigations. Several groups have reported interactions between lipid monolayers at air/water interface and proteins or peptides using IRRAS.^{159,182-183} Figure 4.7 shows the IRRA spectra of a DPhPC (bold line) and a PEO₁₀F11 (full line) monolayer at the air/water interface. The spectra were recorded after compressing

the respective monolayers to $\pi = 36.7$ mN/m and 40 mN/m for DPhPC and PEO₁₀F11,

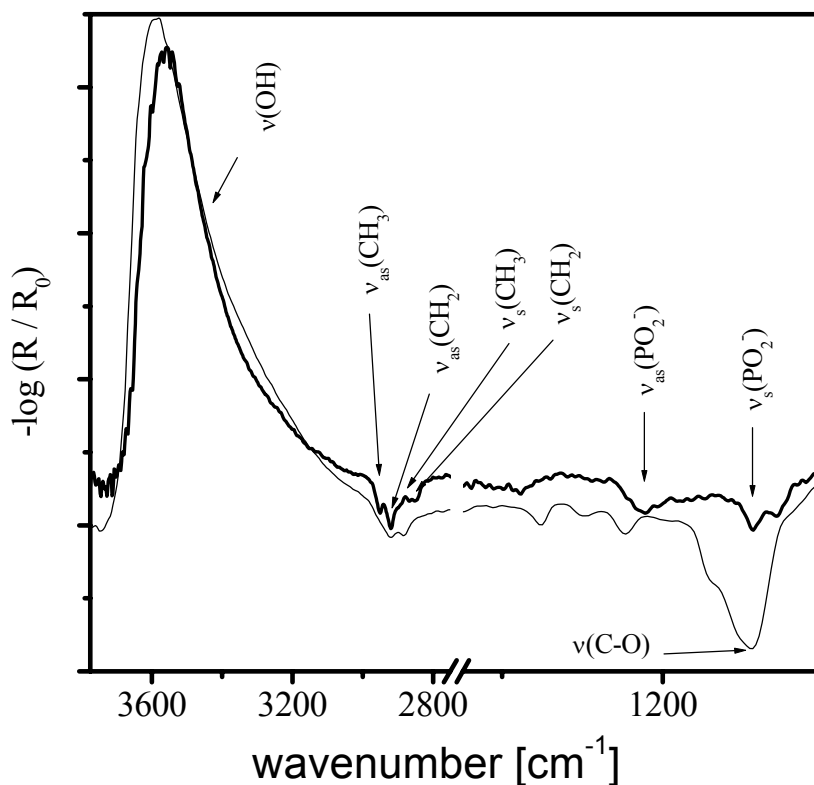


Figure 4.7. IRRA spectra of DPhPC (bold line) and PEO₁₀F11 (full line) film on water surface. The spectra were recorded at $\pi = 36.7$ mN/m and 40.0 mN/m for DPhPC and PEO₁₀F11, respectively.

respectively. Typical reflection-absorption bands for the lipid have been assigned to their respective groups as shown in Figure 4.7. The different vibration modes in the PEO₁₀F11 IRRA spectrum can be assigned as: the two bands at approximately 2920 cm⁻¹ and 2882 cm⁻¹ are attributed to $\nu_{\text{as}}(\text{CH}_2)$ and $\nu_{\text{s}}(\text{CH}_2)$ stretching vibration modes of the PEO chain, while the bands at 1352 cm⁻¹ and 1242 cm⁻¹ originate from the wagging (CH₂) and twisting (CH₂) vibrational modes.⁵⁶ The most prominent but broad peak in the copolymer IRRA spectrum can be seen at approximately 1090 cm⁻¹ for $\nu(\text{C-O})$ vibration. The

observed broad $\nu(\text{C-O})$ band shape is typical of PEO in an amorphous state,¹⁸⁴⁻¹⁸⁵ whereas crystalline PEO in this spectral region is characterized by a sharp peak. The reflection-absorption bands corresponding to the PFMA block could not be detected in the copolymer spectrum, because they are too weak (due to the low PFMA content in the copolymer) and also may be overlapped by the strong PEO reflection-absorption bands. Hence, no information about the PFMA itself can be deduced from the spectrum. A strong band at approximately 3600 cm^{-1} in both spectra in Figure 4.7 is due to the $\nu(\text{O-H})$ stretching vibration of water. Recently Kerth et al.¹⁷¹ correlated the intensity of this band with the film thickness at the air/water interface. They investigated the relation between the film thickness and the reflection-absorption intensity of the $\nu(\text{O-H})$ band and found that with an increase in the reflection-absorption intensity of the $\nu(\text{O-H})$ band the film thickness increases. Taking this into consideration, qualitative information about the film thickness and the behavior of the polymer chains at the air/water interface in the absence and presence of the DPhPC monolayer can be deduced from the IRRAS data. Figure 4.8 shows the IRRAS spectra of a $\text{PEO}_{10}\text{F11}$ film during the compression at different surface pressures. The arrows in Figure 4.8 serve as a guide to the eye pointing in the direction of increase in reflection-absorption intensity of the respective bands with compression. The reflection-absorption of both the $\nu(\text{C-O})$ and $\nu(\text{O-H})$ bands increases with compression. Similar behavior was observed for $\text{PEO}_5\text{F15-D}$ and $\text{PEO}_{20}\text{F14}$ block copolymer monolayers (data not shown). The reflection-absorption of the $\nu(\text{C-O})$ and $\nu(\text{O-H})$ bands at any given surface pressure was found to be dependent on PEO chain length, i.e. reflection-absorption order of the said bands was $\text{PEO}_{20}\text{F14} > \text{PEO}_{10}\text{F11} > \text{PEO}_5\text{F15-D}$. The increase in reflection-absorption intensity of the $\nu(\text{C-O})$ band and $\nu(\text{O-H})$ band with compression as shown in Figure 4.8 for three different surface pressures is due to the increase in surface density of the polymer chains⁵⁶ which subsequently forces the PEO chains to stretch in the water subphase to avoid steric repulsion between the neighboring

chains, resulting in the formation of a thicker and denser polymer brush at high surface pressures.

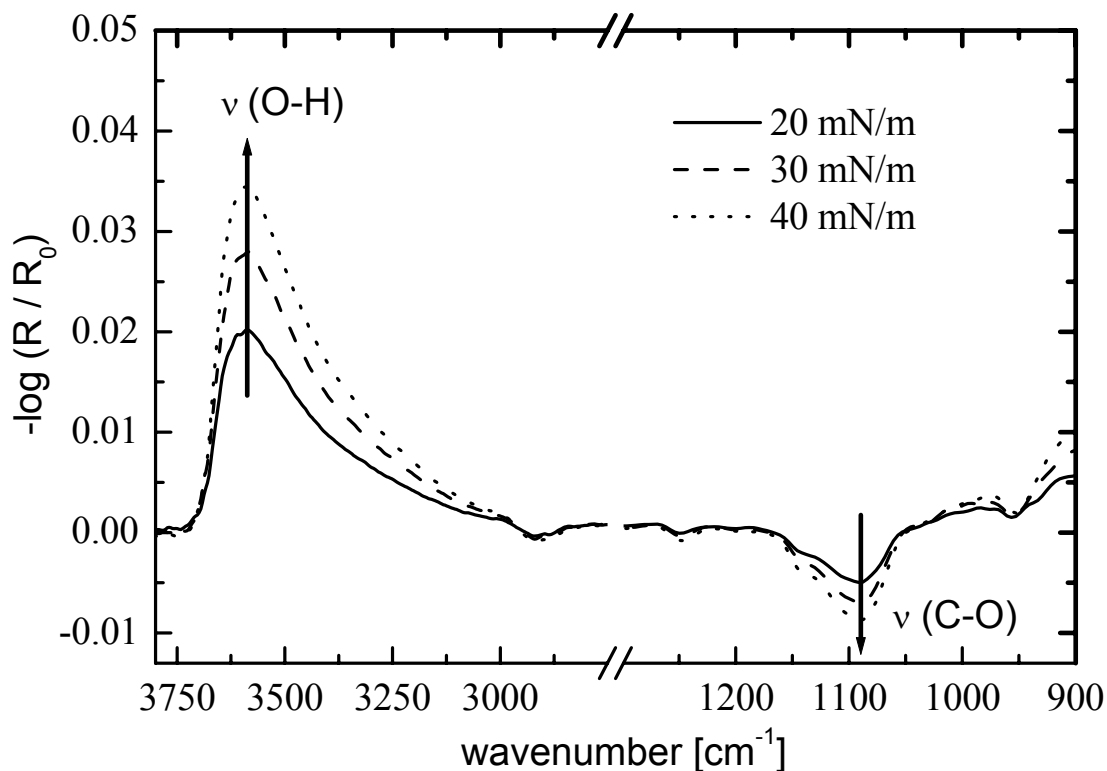
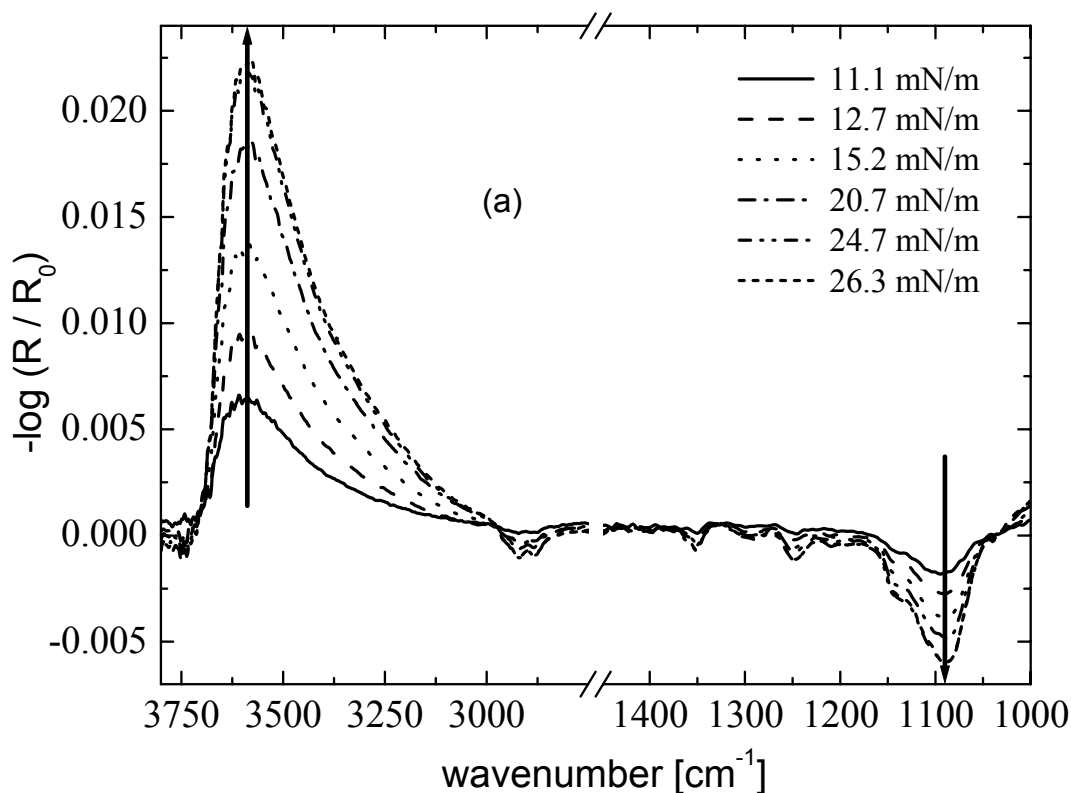


Figure 4.8. IRRA spectra of a PEO₁₀F11 film at the air/water interface at different surface pressures. The spectra were recorded after reaching the corresponding surface pressure during the compression mode. The arrows merely serve as a guide to the eye pointing in the direction of increase in reflection-absorption of the respective bands with compression. The surface pressures corresponding to each spectrum are given in the inset.

Figure 4.9 shows the behavior of PEO₁₀F11 block copolymer at the air/water interface in the presence of a DPhPC monolayer. For clarification of the data, they are presented in two parts (Figure 4.9a and Figure 4.9b). It is very difficult to detect the weak DPhPC reflection-absorption bands in comparison to the PEO reflection-absorption

bands in the IRRA spectra given in Figure 4.9. Figure 4.9a reveals the evolution of IRRA spectra of the PEO₁₀F11 block copolymer penetrated DPhPC monolayer. The arrows in Figure 4.9 serve again as a guide to the eye pointing in the direction of increase in reflection-absorption intensity of $\nu(\text{O-H})$ and $\nu(\text{C-O})$ band in Figure 4.9a and decrease in Figure 4.9b. As shown in Figure 4.9a a strong increase in the reflection absorption intensity of the $\nu(\text{O-H})$ band was observed when the film was compressed from $\pi = 11$ mN/m to 26 mN/m. A similar trend was observed also for the $\nu(\text{C-O})$ reflection-absorption band. However, with further compression of the film (see Figure 4.9b) a decreasing trend in reflection-absorption intensity of the said respective bands was observed. The intensity of the $\nu(\text{O-H})$ band reaches a minimum value at $\pi \sim 33$ mN/m and with no change in reflection-absorption on further compression to $\pi \sim 39.5$ mN/m. While the $\nu(\text{C-O})$ reflection-absorption band due to the PEO chains has almost vanished



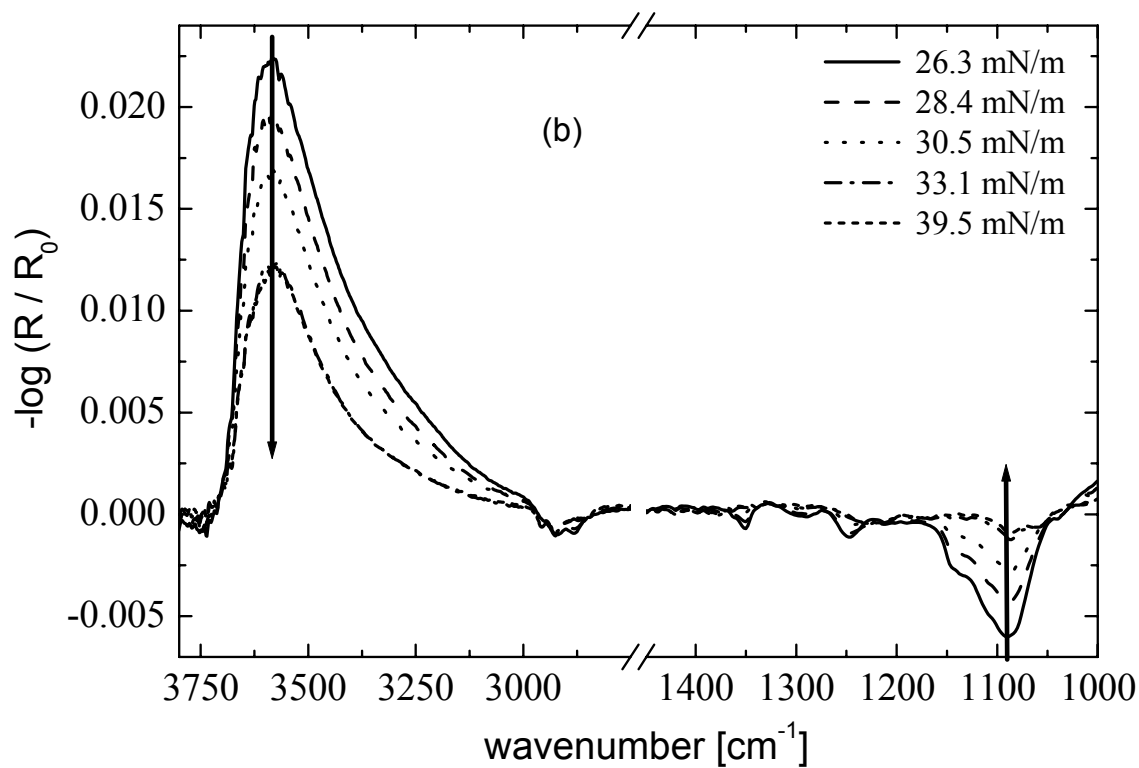


Figure 4.9. IRRA spectra of a PEO₁₀F11 penetrated DPhPC film at the air/water interface at different surface pressures during compression. The total polymer concentration in the trough after injection was 50 nM. The series of spectra has been separated into two parts: (a) increase in reflection-absorption intensity of the $\nu(\text{O-H})$ and $\nu(\text{C-O})$ band, and (b) decrease in reflection-absorption intensity of the corresponding bands with compression. The surface pressures corresponding to the different spectra are given in the inset.

at $\pi \sim 33$ mN/m, typical bands of the lipid DPhPC appeared, i.e. the $\nu_{\text{as}}(\text{PO}_2^-)$ band at approximately 1225 cm^{-1} and the $\nu_{\text{s}}(\text{PO}_2^-)$ band at approximately 1088 cm^{-1} .

Figure 4.10 summarizes these observations by comparing the reflection-absorption intensity of the corresponding $\nu(\text{O-H})$ bands of the IRRA spectra of the pure

DPhPC monolayer (open symbols) and the PEO₁₀F11 block copolymer penetrated DPhPC monolayer (filled symbols). The respective π/A isotherms are also given in Figure 4.10. The block copolymer trough concentration was 50 nM. A slight but

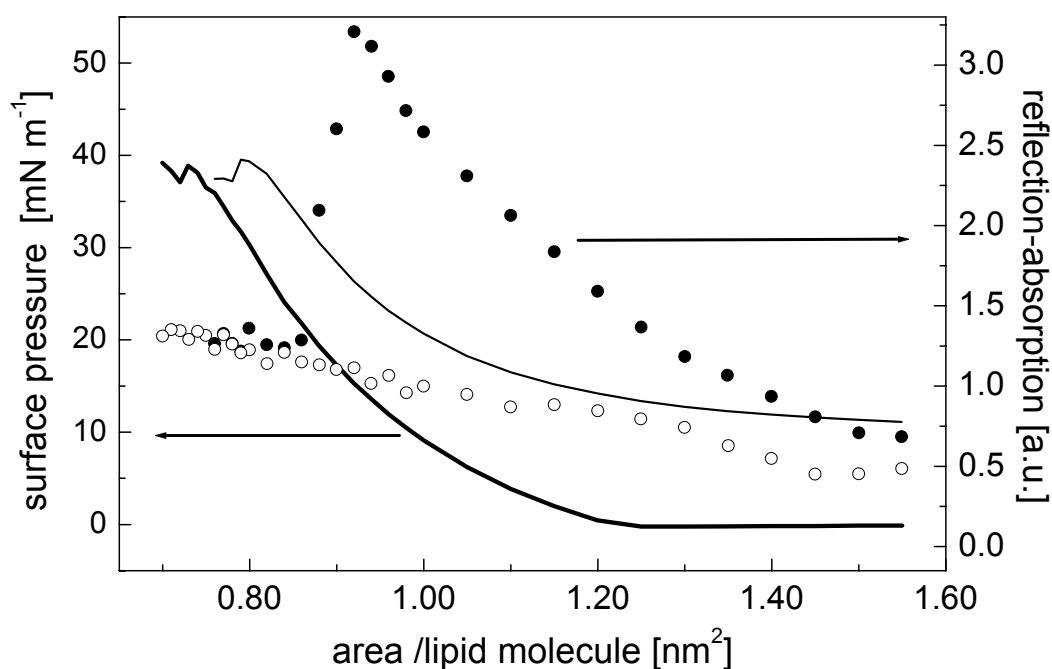


Figure 4.10. Comparison of the reflection-absorption intensity of the $\nu(\text{O-H})$ band from IRRA spectra of pure DPhPC monolayer (\circ) and PEO₁₀F11 block copolymer penetrated DPhPC monolayer (\bullet) on water surface during compression with the corresponding π/A isotherms [DPhPC (bold line), and PEO₁₀F11 copolymer penetrated DPhPC (full line)]. The block copolymer concentration in the trough was 50 nM.

significant increase in the reflection-absorption intensity of $\nu(\text{O-H})$ band can be seen when the pure DPhPC film is compressed from fully expanded state to approximately 37 mN/m surface pressure, which might be related to a change in the orientation of the lipid molecules to form a relatively dense phase as the surface pressure increases. However, as shown here and in Figure 4.9, the behavior of the reflection-absorption intensity of the

very same band was found quite different when the fully expanded PEO₁₀F11 block copolymer penetrated DPhPC monolayer was compressed. The initial increase in intensity of the $\nu(\text{C-O})$ (see Figure 4.9) and $\nu(\text{O-H})$ (Figure 4.9 and Figure 4.10) reflection-absorption bands in IRRA spectra from PEO₁₀F11 penetrated DPhPC monolayers with compression can be attributed to increase in surface density and the subsequent stretching of the PEO chains in water subphase due to the steric repulsion between the neighboring chains resulting into a more dense and extended conformation (i.e. thick film) with compression. However, due to the presence of the lipid molecules at the surface, the number density of the polymer chains would not be high enough to form a true brush like conformation. The decreasing trend in the reflection-absorption intensity of both the $\nu(\text{C-O})$ and $\nu(\text{O-H})$ bands above $\pi \sim 26\text{-mN/m}$, as shown in Figure 4.9b and Figure 4.10 (here only the $\nu(\text{O-H})$ band intensity is given), reveals that the polymer chains could not retain their position in the lipid monolayer. Furthermore, (1) the disappearance of the $\nu(\text{C-O})$ reflection-absorption band from the IRRA spectrum of the PEO₁₀F11 block copolymer penetrated DPhPC monolayer at high surface pressure of 33 mN/m (Figure 4.9b), and (2) the comparable reflection-absorption intensity of the $\nu(\text{O-H})$ band from the pure DPhPC and the PEO₁₀F11 penetrated DPhPC monolayer (Figure 4.10) indicate the almost complete expulsion of the polymer chains from the lipid monolayer. Therefore, little change in intensity was observed when the film was further compressed to π of approximately 39 mN/m. This observation also indicates that the mechanism of the PEO₁₀F11 penetration into the DPhPC monolayer might be dependent on the interaction of the block copolymer and the hydrophobic portion of the lipid monolayer, i.e. the PFMA block might penetrate the hydrophobic acyl chains of the lipid monolayer and that the block copolymer chains have no special interaction with the lipid molecule head group, otherwise IRRA spectra could detect PEO bands at $\pi \geq 33\text{ mN/m}$. However, it is difficult to determine from the present data the exact relation between the

$\nu(\text{O-H})$ reflection-absorption band intensity and the orientation of the lipid or the PEO₁₀F11 block copolymer chains at the air/water interface.

4.4. Conclusion

PEO and PFMA containing amphiphilic block copolymers have shown surface activity that leads to adsorption at the air/water interface. The kinetic adsorption isotherm of the PEO₁₀F11 block copolymer showed a slow increase regime (in surface pressure) after the sharp rise in surface pressure and prior to the plateau region. This regime was attributed to the rearrangement of the polymer chains at the water surface. All the three block copolymers show similar π/A isotherms, irrespective of the architecture of the copolymers. The π/A isotherms of the block copolymers indicate a pancake-like conformation at low surface coverage and a brush-like conformation at high surface pressures. A plateau in the π/A isotherms, indicating a phase transition from a low surface coverage conformation to a high surface density brush conformation, was found less pronounced with the decrease in the PEO chain length. The π/A isotherm of the DPhPC monolayer at the air/water interface exhibits only the liquid-expanded phase at high surface pressures. Penetration of the lipid monolayer by block copolymers was deduced from a shift of the lipid isotherm towards higher areas per lipid molecule after injecting the aqueous block copolymer solution into the subphase. The behavior of the PEO₁₀F11 block copolymer penetrated DPhPC monolayer during compression was also followed by monitoring the reflection-absorption intensity of the $\nu(\text{O-H})$ and $\nu(\text{C-O})$ bands in the IRRA spectra from the water subphase and the PEO chains, respectively. These observations are schematically summarized in Figure 4.11.

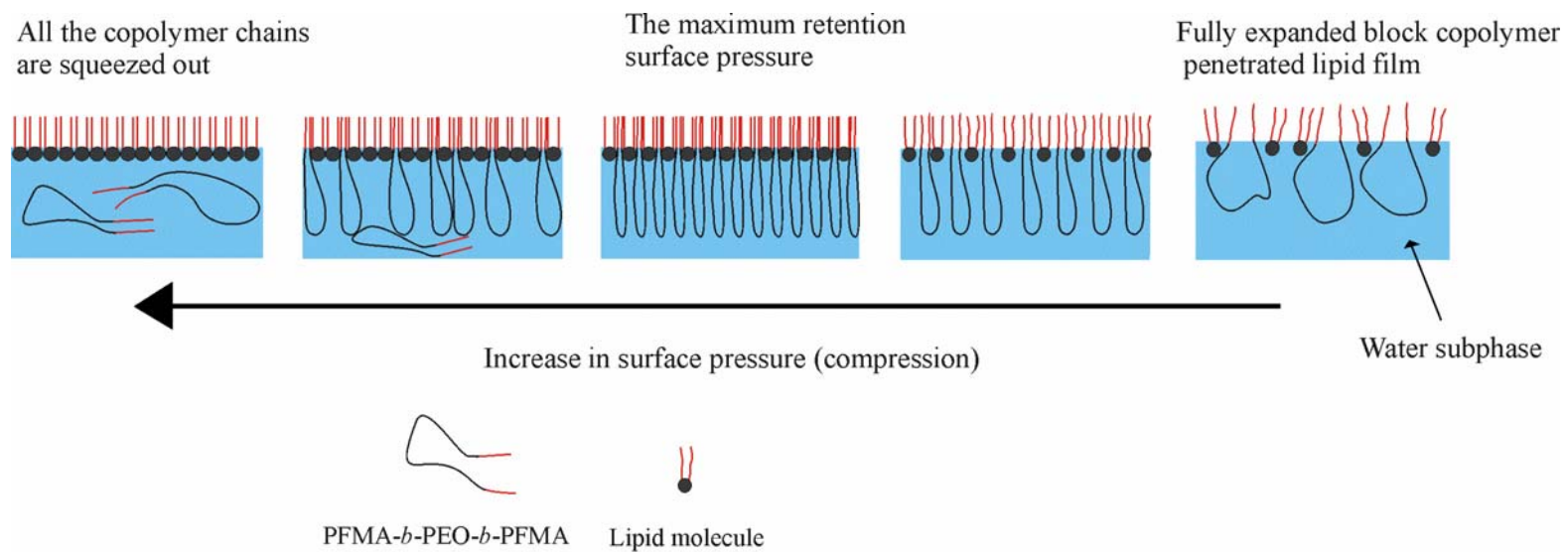


Figure 4.11. Schematic representation of the behavior of the tri block copolymer chains at the air/water interface in the presence of lipid monolayer during compression.

Chapter 5

Potential pharmaceutical applications of amphiphilic block copolymers of poly(ethylene oxide) and poly(perfluorohexylethylmethacrylate) or poly(*n*-decyl methacrylate)

5.1. Introduction

Amphiphilic block copolymers have attracted a great deal of attention for their pharmaceutical and biomedical applications. As with other industrial applications many uses of amphiphilic block copolymers in pharmaceutical formulations are largely related in one way or another to the amphiphilic nature of these materials.⁶² For example, the amphiphilic nature of block copolymers is responsible for the formation of self-assembled structures, e.g. micelles in selective solvents, which are attractive for pharmaceutical applications such as hydrophobic drug solubilization, controlled release of the drug after administration etc.^{63,186-187} Furthermore, amphiphilic block copolymers have been widely investigated for their use as steric stabilizers of pharmaceutically important colloidal dispersions, e.g. emulsions, and liposomes.¹⁸⁸⁻¹⁹⁰

Steric stabilization of colloidal system represents an important field of research because the colloidal stability of the particles often determines the applicability of the colloidal system in different types of applications. This can be achieved either by grafting of a polymer to the particle surface, or by physical adsorption of the polymer at the surface.¹⁹¹⁻¹⁹² Liposomes used for drug delivery are often sterically stabilized to prolong the circulation time in the blood stream.¹⁹³ Poly(ethylene oxide) (PEO) has been investigated extensively as the steric stabilizer of pharmaceutically important liposome systems. This has been accomplished in different ways, for example, in some liposome formulations, PEO is conjugated to a lipid anchor, which is subsequently incorporated into the lipid bilayer.¹⁹⁴⁻¹⁹⁶ An alternative that has been proposed is to use the physical

adsorption of PEO containing polymers particularly pluronic type of copolymers (triblock copolymers of PEO and PPO). This scheme has been reported extensively in the literature.^{191-192,197-199} Kostarelos et al.²⁰⁰⁻²⁰³ have systematically investigated the steric stabilization of phosphatidylcholine (PC) liposomes by pluronic block copolymers. They found that it is possible to induce steric stabilization of PC liposomes by use of block copolymers. The largest effect; however, was obtained when the triblock copolymer was added to the lipids before the liposome preparation. Johnsson et al.¹⁹¹ have concluded from their investigations on the physical adsorption of pluronic block copolymers on PC liposomes that pluronic type copolymers perturb the bilayer in terms of an increased permeability and that they can be easily displaced from the bilayer. These observations reflect a weak interaction between the PPO (hydrophobic) block of the copolymer and the lipid membrane, which was interpreted by them as the most likely reason for the weak in vivo performance of pluronic-treated liposomes. Rangelov et al.¹⁹⁶ have also recently reported the steric stabilization of liposomes by different PEO based block copolymers having short blocks of lipid-mimetic units. However, in addition to facilitate the drug delivery by liposomes, there has been a rising interest in self-assembled block copolymer structures as well for the controlled drug delivery over the past decade.²⁰⁴⁻²⁰⁷ This is due to the similarity of polymeric micelles to natural carriers, e.g. viruses. Polymeric micelles mimic aspects of biological transport systems in terms of structure and function. For example, a hydrophilic shell helps them to stay unrecognized during blood circulation.²⁰⁸ A viral-like size (<100 nm) prevents their uptake by the reticuloendothelial system and facilitates their passage through capillary walls, leading to passive accumulation in certain tissues.²⁰⁹⁻²¹⁰ The incorporation of a recognizable moiety on micellar surface or the development of thermo or pH sensitive block copolymers has been studied for site-specific drug delivery.²¹¹⁻²¹² More recently, polymeric micelles have been used for gene delivery and have shown a great potential in directing therapeutics to sub-cellular targets.²¹³⁻²¹⁴

Generally, the drug loading into the micelle core has been accomplished; by chemical conjugation,²¹⁵ i.e. introducing chemical bonding between the drug and the hydrophobic polymer core, or by physical entrapment.²¹⁶⁻²¹⁷ The simple equilibration of the drugs and micelles in water has been reported as an inefficient way of drug incorporation in polymeric micelles.²¹⁸⁻²¹⁹ The extent of drug incorporation in micelles by physical means is dependent on several factors, including the molecular volume of the solubilizate, its interfacial tension against water, length of the core, and shell forming blocks in the copolymer, and the polymer and the solubilizate concentration.¹⁸⁶ The partition coefficient of the hydrophobic drug molecules between the micellar core and surrounding aqueous medium describes the extent of drug encapsulation in micelles.²²⁰ The greatest degree of solubilization can be achieved however; when high compatibility exists between the micellar core and the solubilizate.

In almost all the amphiphilic block copolymers that have been investigated for drug delivery, PEO is the hydrophilic block, because PEO possesses a number of outstanding physicochemical and biological properties, including solubility in water and organic solvents, lack of toxicity,²²¹ and absence of antigenicity and immunogenicity.²²² In contrast, a wide range of hydrophobic blocks such as poly(β -benzyl-L-aspartate),²²³ poly(ϵ -caprolactone),²²⁴ poly(propylene oxide),²²⁵ poly(L-lysine),²²⁶ poly(D, L-lactide),²²⁷ and poly(aspartic acid),²²⁸ have been explored.

In this chapter, results are presented from the investigations on our amphiphilic di- and triblock copolymers of PEO (hydrophilic block) and poly(perfluorohexylethyl methacrylate) (PFMA) or poly(*n*-decyl methacrylate) (PDMA) (as hydrophobic block) with respect to their potential pharmaceutical applications:

(1) Cytotoxicity measurements of the block copolymers on K562 human erythroleucemia cells; (2) physical adsorption of the block copolymers on the liposome surface; (3) physical encapsulation of a model hydrophobic drug (testosterone undecanoate) by block copolymer micelles through dialysis technique. The results on the

toxicity measurements revealed that all the investigated block copolymers of PEO and PFMA had no measurable toxicity on sensitive K562 cells up to 0.2 wt.-% copolymer concentration. Observations on the physical adsorption of the block copolymers on liposome indicate that PEO_xFy (triblock) copolymers are more efficient in reducing the zeta (ζ) potential of the liposome surface as compared to PEO_xFy-D (diblock) copolymers. The PEO-*b*-PDMA diblock copolymer micelles were found to have a higher encapsulation capacity for the model hydrophobic drug testosterone undecanoate as compared to PEO_xFy-D or PEO_xFy block copolymers.

The naming schemes PEO_xFy, and PEO_xDy-D (i.e. *x* represents the molar mass of the PEO block in kg/mol, and *y* the wt.-% of the PFMA and PDMA content in the respective block copolymer, while *D* in the naming scheme means diblock copolymer) as used in this chapter for PEO/PFMA based, and PEO/PDMA based block copolymers are the same as discussed in *Chapter 2* and *Chapter 3*.

5.2. Experimental section

5.2.1. Cytotoxicity measurements

Toxicity effects of the block copolymers on K562 human erythroleucemia cells were measured as described below:

5.2.1.1. Purification of the copolymers

The block copolymers of PEO and PFMA, as discussed in *Chapter 2*, were synthesized by atom transfer radical polymerization using CuBr as catalyst. Immediately after the polymerization, the reaction mixture was filtered over silica gel to remove Cu complexes. However, even after this treatment, the blue color of the dried block copolymer powder indicates the presence of Cu compounds in the samples. Therefore, for cytotoxicity experiments the block copolymer samples were first purified from copper and sterilized as: The copolymers were dissolved in water and 50 mM EDTA (ethylenediaminetetraacetic acid) as chelator was added to bind all copper ions in solution. Then the preparations were dialyzed extensively against distilled water and lyophilized. The resulting samples were completely colorless. They were again dissolved in water (approximately 10 mg/mL) and filtered through sterile 0.2 μm pore size Millipore filters for sterilization. The polymer concentration of the sterilized solutions was determined using $\text{BaCl}_2/\text{KI}_3$ technique that was previously reported for PEO homopolymer and was found to be applicable for measuring concentration of any polymer containing ether bonds.²²⁹⁻²³⁰

5.2.1.2. Cell culturing

K562 human erythroleucemia cells were a gift of Prof. Saprin from Moscow Institute of theoretical problems of physico-chemical pharmacology. They were cultured in RPMI 1640 medium (Sigma) supplemented with 10 vol.-% fetal calf serum in an atmosphere containing 5 vol.-% CO_2 and 96% humidity. The cells density during culturing was maintained in 200 000–600 000 cells per mL range.

The toxic effect of the polymers on the sensitive cells was determined as reported.²³¹⁻²³² The polymer aqueous solutions were diluted with serum-free medium RPMI1640 (Sigma) up to the required concentration and 100 μL of the preparations were added to 100 μL of K562 cells ($\sim 10\,000$ cells per well) cultured in 96-well plates. The cells were incubated with the polymers for one hour and then centrifuged to remove the polymer. 200 μL of the fresh polymer-free medium, supplemented with 10 vol.-% of fetal calf serum was added to the cells and they were incubated for three days. Then 50 μL of methyl tetrazolium blue (MTT) dye was added to the cells up to final concentration of 0.2 $\mu\text{g}/\text{mL}$. The samples were incubated for four hours and sedimented on the centrifuge. The dye was reduced by mitochondria to give a colored product generally known as formazan. The medium was removed and 100 μL of dimethylsulfoxide was added to each well to dissolve formazan. Optical densities of the samples were measured on Titertek Multiscan multi-channell photometer (wavelength 550 nm) (Titertek, USA) and the relative amount of cells was calculated as a ratio of the optical density in the sample with polymer to that of control without any additives.

5.2.2. Interaction of block copolymers with lipid bilayers

Interaction of block copolymers with model lipid bilayer membranes; (1) planar bilayer membrane, and (2) liposomes was investigated as outlined below:

5.2.2.1. Planar bilayer membrane

For this purpose, the planar lipid bilayer was formed from 1,2-diphytanoyl-*sn*-glycero-3-phosphocholine (DPhPC) (Avanti Polar Lipids). The monolayer apposition technique²³³⁻²³⁴ was used to form solvent free membranes across an aperture (130–180 μm in diameter) in a Teflon septum (thickness 25 μm) separating two aqueous compartments. The septum was pretreated with 2 vol.-% solution of hexadecane in hexane. On top of the two aqueous phases, a 20 mg/mL solution of lipid in hexane was spread to form lipid monolayers. After solvent evaporation, the buffer solution levels in both compartments

were raised above the aperture by syringe. Within the aperture the two monolayers combined spontaneously to form a bilayer. The aqueous solution on both sides of the membrane contained 1 M KCl, 10 mM 4-(2-hydroxy ethyl)piperazine-1-ethane sulfonic acid (HEPES) (Fluka), and 10 mM tris (hydroxymethyl)aminoethane (Tris) (Aldrich). The medium had pH = 7.4. The transmembrane current was measured by a patch-clamp amplifier (model EPC9, HEKA Electronic, Lambrecht/Pflaz, Germany). The effect of block copolymers on the transmembrane current under voltage-clamp conditions was investigated. For this, first the current across the membrane was measured before adding copolymer solution. Then an aliquot of copolymer stock solution was added to both sides of the bilayer, agitated by stirring for 15-20 min, before measuring the current.

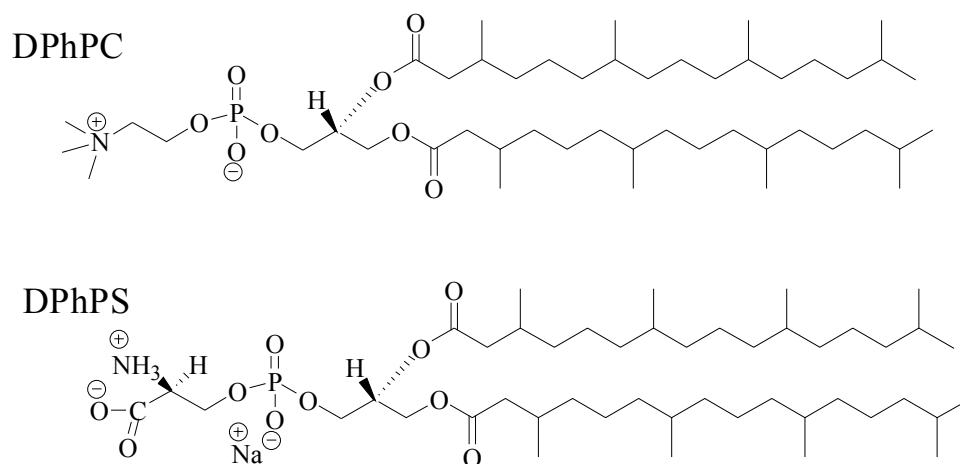


Figure 5.1. Chemical structures of the used lipids.

5.2.2.2. Liposomes

Physical adsorption of the amphiphilic block copolymers on liposomes was investigated by measuring the effect of copolymers on the ζ -potential and size of the liposomes. The liposomes were prepared from a mixture of DPhPC and 1,2-diphytanoyl-*sn*-glycero-3-[phospho-L-serine] (DPhPS). The chemical structures of the lipids are given in Figure 5.1. For the preparation of liposomes, aqueous dispersion of the mixture of 70 mol.-% DPhPC and 30 mol.-% DPhPS was prepared by adding the buffer solution (10 mM

HEPES and 20 mM KCl, having pH = 7.4) to the dried thin lipid film (the film was obtained by solvent evaporation from the CHCl_3 solutions of lipids) and subsequently vortexing of the samples for several minutes at room temperature. The dispersions were then extruded (19 times each sample) through the polycarbonate membrane of 100 nm pore size to obtain unilamellar liposomes. These freshly prepared liposome solutions were then diluted with appropriate amount of copolymer solutions. These systems were left for at least one hour before any measurement was carried out.

The interaction between the block copolymer and the liposome was studied by measuring the ζ -potential and size of the liposomes as a function of added copolymer concentration. The schematic illustration of the ζ -potential measurement is given in Figure 5.2.

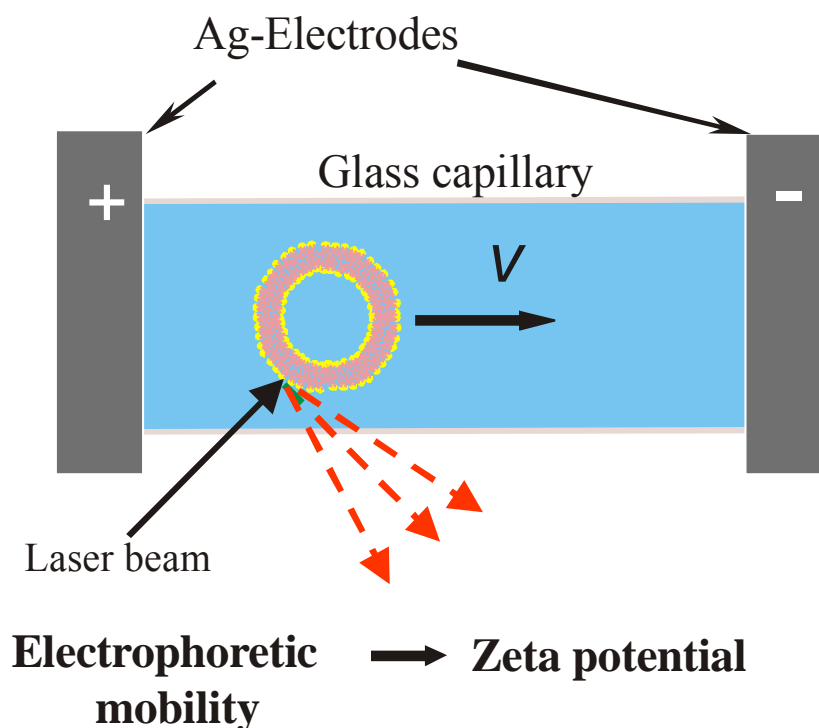


Figure 5.2. Schematic presentation of the ζ -potential measurement setup.

ζ -potential measurements were carried out with Coulter[®] Delsa 440SX, operating with a He-Ne (632 nm) laser beam (5 mW). The instrument measured the electrophoretic mobility (v) of the liposomes by measuring the Doppler shifts of scattered laser light at four angles simultaneously. A laser beam illuminates the liposome solution and the light scattered to various angles is compared to light in a reference beam to determine the Doppler shift of the scattered light. The Doppler shift of the light depends on the v of the liposomes and the angle of measurement. The electrophoretic mobility is related to the ζ -potential as:

$$\zeta = \eta v / \epsilon \epsilon_0 \quad (5.1)$$

Where η is the viscosity of the medium in which the particle is diffusing, ϵ_0 is the permittivity of free space, and ϵ is the relative permittivity of the medium. The size of the liposomes was investigated by Counter[®] N4 Plus Submicron Particle Size Analyzer having a laser source of 10 mW helium-neon at 632.8 nm. N4 Plus Particle Size Analyzer uses Photon Correlation Spectroscopy (PCS), which determines particle size by measuring the rate of fluctuations in laser light intensity scattered by particles as they diffuse through a fluid. All the experiments were carried out at room temperature and at an angle of 90°.

5.2.3. Encapsulation of a model hydrophobic drug by block copolymer micelles

5.2.3.1. Preparation of drug-loaded micelles

Physical entrapment of the model hydrophobic drug; testosterone undecanoate, (kindly given by Prof. Neubert of the Department of Pharmacy, Martin-Luther University Halle) by block copolymer micelles was accomplished by dialysis technique. Chemical structure of the testosterone undecanoate is given in Figure 5.3. In a typical experiment 100 mg of the block copolymer and calculated amount of the drug (2-60 mg) were dissolved in 10 mL of a water miscible organic solvent such as methanol (MeOH) (Fluka, $\geq 99.8\%$), N, N-Dimethyl formamide (DMF) (Fluka, $\geq 99.8\%$), tetrahydrofuran (THF) (Merck, 99.5

%), and dimethyl sulfoxide (DMSO) (Merck, >99 %), and stirred for about 4 h at room temperature to get complete solubility of the drug and polymer. The schematic

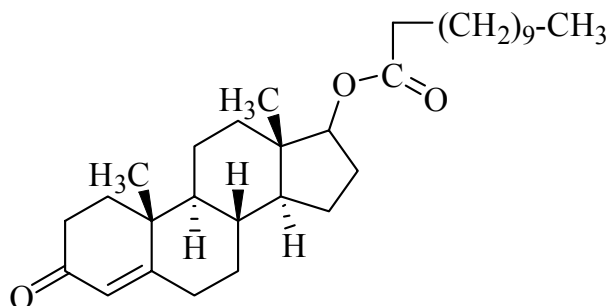


Figure 5.3. Chemical structure of testosterone undecanoate.

representation of the drug encapsulation into block copolymer micelles by dialysis method can be seen in Figure 5.4. To form drug-loaded micelles and remove the unsolubilized drug, the solution was dialyzed using dialysis membrane (molar mass cut-off 35 000 g/mol, Spectra/Pro3) against double distilled water (6x1 L) for more than 24 h.

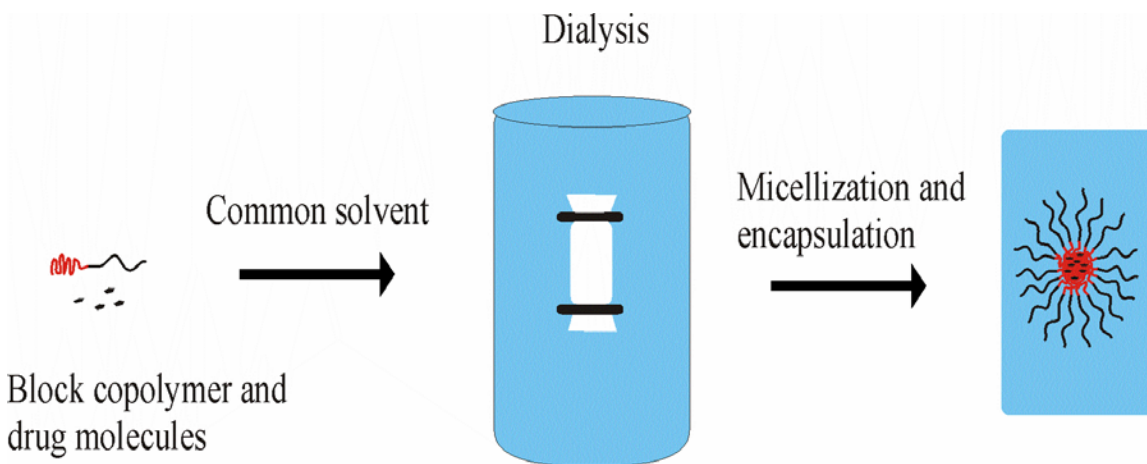


Figure 5.4. Schematic representation of the drug encapsulation into polymer micelles by dialysis technique.

After dialysis, each solution was filtered three times with micro filter (0.65 μm pore size, Millipore) to remove larger aggregates from the solution. Further purification of the solution from unbound drug molecules and low molecular weight impurities was carried out by ultrafiltration using centrifugal ultrafiltration devices (Amicon, YM-30). The resultant high concentrated solution was freeze-dried (VirTis, Gardner New York, USA), to obtain drug containing dried micelles (nanoparticles). The resultant powder was stored in refrigerator until further use.

5.2.3.2. Quantitative evaluation of the encapsulated drug content in dried micelles

A known amount of the dried micelles; obtained by lyophilization, was dissolved in methanol for quantitative investigation. Testosterone undecanoate had a strong absorption band at a wavelength of 240 nm. The solutions were measured by UV-Visible spectrophotometer (Ultra Spec3300) at this wavelength and the drug content in the dried micelle product was calculated by using a calibration curve of pure drug. The concentration of the solution of dried drug containing micelle powder in methanol was kept much lower to minimize the influence of block copolymer absorption in the respective wavelength range. The following characteristic parameters, i.e. yield, drug loading efficiency, and drug loading content in the dried micelle product were calculated as given below:

$$\text{Yield (\%)} = \frac{\text{weight of drug containing dried micelles}}{\text{weight of polymer and drug fed initially}} \times 100$$

$$\text{Drug loading efficiency(\%)} = \frac{\text{weight of drug in dried micelles}}{\text{weight of drug fed initially}} \times 100$$

$$\text{Drug loading content(\%)} = \frac{\text{weight of drug in dried micelles}}{\text{weight of dried micelles}} \times 100$$

5.2.3.3. Effect of freeze-thawing on drug loaded micelle size distribution

For this purpose, the drug containing micellar solution was measured by dynamic light scattering (DLS) before, and after freeze-thawing (i.e. The solution was frozen in a freezer for several days and the DLS experiments were carried out after thawing the frozen solution at 37°C in a water bath). The DLS set up was the same as discussed in *Chapter 3*. Additionally, drug containing nanoparticles obtained as a result of lyophilization were also characterized by DLS after dispersing in water at room temperature. The samples were prepared by filtering the solutions through cellulose acetate filters having 0.45 µm pore size directly into the dust free quartz cells.

5.3. Results and discussion

5.3.1. Cytotoxicity results

Toxicity of compounds or their metabolites is a major reason for the failure of a compound in medical or pharmaceutical applications. Therefore, the first step for any

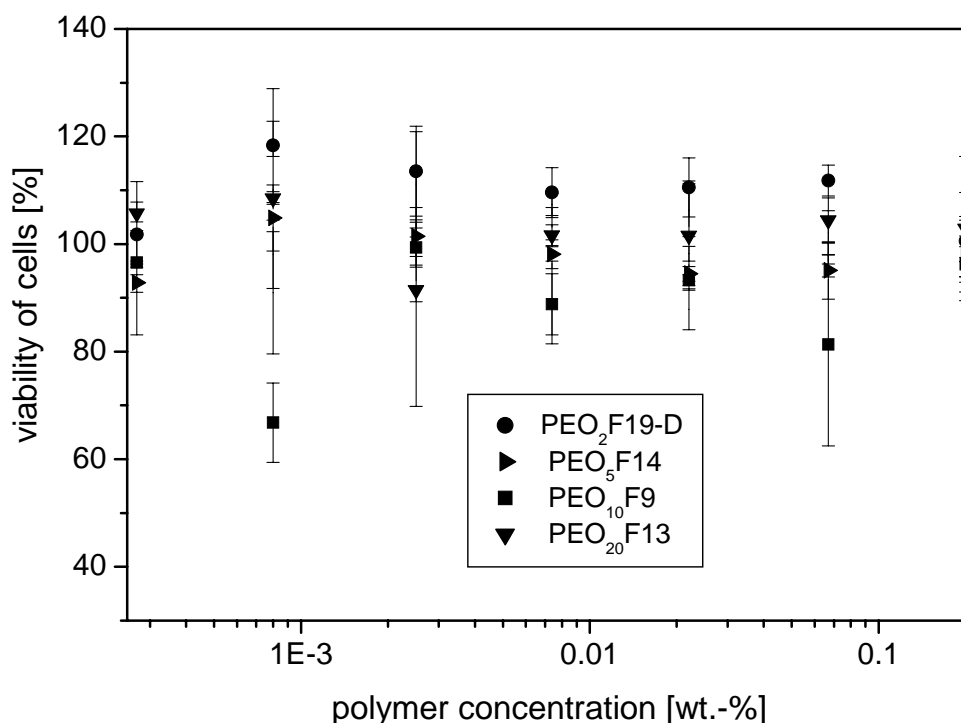


Figure 5.5. Concentration dependent cytotoxicity of different block copolymers as mentioned in the inset, for K562 human erythroleucemia cells. The Y-axis shows the percent of remaining living cells.

new polymer or any compound intended for pharmaceutical or medical application, should be the cytotoxicity investigation. The way the toxicity measurements (i.e. the toxic effect of the block copolymers on living cells) of the block copolymers have been carried out here, mimics the situation of rapid clearance of the polymer from the blood. In many cases it is really the case: the concentration of the substance administered into the animal blood decreases 5-10-fold during the first hour.²³⁵ Hence, the results of our

investigations would give information about the "acute" toxicity of the copolymers. Figure 5.5 shows the block copolymer concentration dependent viability of the K562 human erythroleucemia cells (the percent of remaining living cells) for four different block copolymers. Each experiment was repeated three times. The results indicate that all the copolymers are practically intoxic under the test conditions. The cell viability exceeding 100 %, as can be seen in Figure 5.5 for some samples, is the experimental error. The common error in these studies is as large as 15 to 20 %. Therefore, the sample that exhibits above 100 % of living cells simply means that the polymer has no toxicity and nothing else. The data of sample PEO₁₀F9 in Figure 5.5 shows a relatively low cell viability value at lower concentration. However, this cannot be assumed as the real toxicity of the sample. Generally, toxicity manifests as a regular decrease in the amount of living cells with the increase in the concentration of toxic agent. For example, exactly under similar test conditions, (i.e. one hour incubation and subsequent culturing for three days), the pluronic copolymers of L61 and L81 showed a real toxicity sigmoidal curve like behavior, having viability of cells value ~ 0 at 0.1 wt.-% copolymer concentration.²³⁶ Therefore, the behavior of the sample PEO₁₀F9 with relatively low viability of cell value as compared to other samples at lower copolymer concentration does not represent the real toxicity of the sample.

5.3.2. Block copolymers in contact with lipid bilayers

Interaction of amphiphilic block copolymers of PEO and PFMA with planar bilayer lipid membrane and liposomes has been investigated.

5.3.2.1. Interaction with planar lipid bilayer

The effect of copolymers on the ion permeability of the lipid bilayers was investigated by measuring the transmembrane current under voltage-clamp condition. Current traces were recorded before and after adding the PEO₁₀F11 copolymer aqueous solution on both sides of the bilayer. Some of the results from these investigations are given in Figure 5.6. The

data in Figure 5.6 show the current traces as function of applied voltage, for control (i.e. when no copolymer solution was added across the bilayer, black line) and after adding

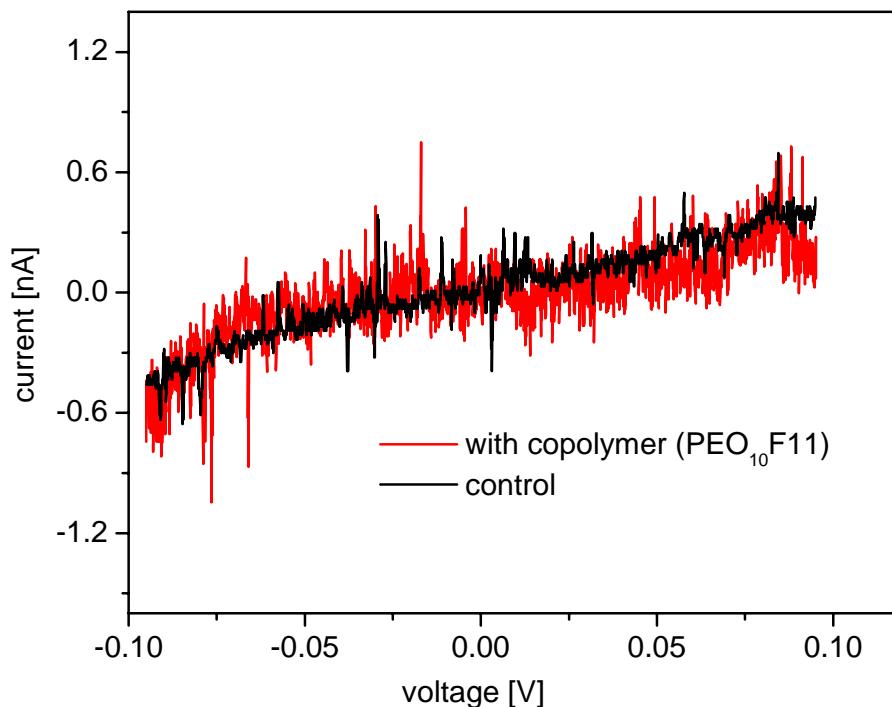


Figure 5.6. Traces of transmembrane current vs. applied voltage. The data were recorded before (control, black line), and after (red line) adding the copolymer (PEO₁₀F11) aqueous solution on both sides of the membrane. The final concentration of the copolymer on each side was 0.01 wt.-%.

the PEO₁₀F11 aqueous solution (final concentration = 0.01 wt.-%) (red line) on both sides of the planar bilayer. The data do not show any significant influence of block copolymer on the transmembrane current flow. Hence, there is no channel activity as observed for pluronic type of block copolymers.²³⁷ There could be two reasons for this behavior; either the polymers do not interact with the bilayer at all, or they do adsorb on the bilayer without causing any damage to the bilayer. If these polymers do interact with bilayers, then the low toxicity of the copolymers as discussed above could be due to the fact that these polymers adsorb on the bilayer, such that the integrity of the cell membrane

remains intact and obviously no solubilization of lipids from the cell membrane. Hence, to be sure that these polymers do interact with bilayers, further investigations were carried out with liposomes.

5.3.2.2. Interaction with liposomes

The interaction between the block copolymers under investigation and the liposomes has been studied by the ζ -potential and size measurements of the liposomes as function of added copolymer concentration. Figure 5.7a shows the variation of ζ -potential with added block copolymer concentration.

The data in Figure 5.7a show that the ζ -potential of the liposome decreases in absolute values with an increase in copolymer concentration. However, the triblock copolymers, i.e. PEO₁₀F9, PEO₁₀F11, PEO₂₀F10, have shown a strong effect on the liposome ζ -potential values, i.e. decreasing from -64 mV before adding the copolymer solution to close to zero at 0.2 wt.-% copolymer concentration. The saturation point,

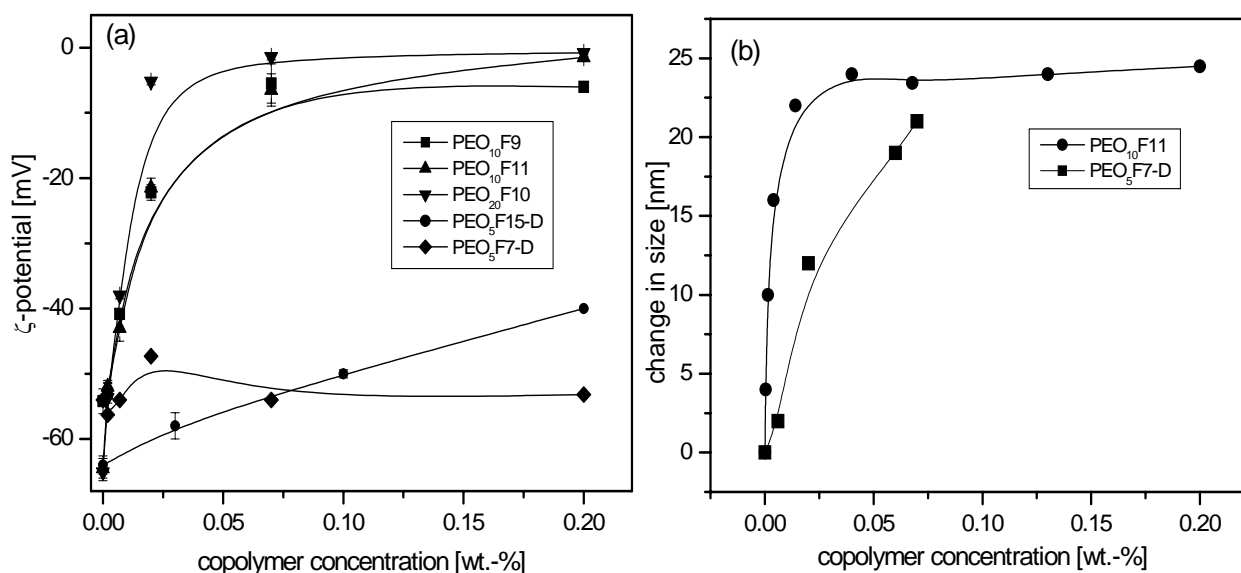


Figure 5.7. (a) Liposome ζ -potential (mV), and (b) change in liposome diameter as function of added block copolymer concentration. Several block copolymers as shown in the inset have been studied separately.

however, seems to be achieved at a copolymer concentration of less than 0.1 wt.-%. This reduction in ζ -potential in absolute values with increase in block copolymer concentration is consistent with the presence of the copolymer at the liposome/solution interface.¹⁸⁹ There could be two reasons for this effect, i.e. either adsorption or incorporation of the block copolymer chains, that may result in a shift in the shear plane outward from the surface and causes the reduction in ζ -potential. In contrast, the diblock copolymers (i.e. PEO₅F7-D and PEO₅F15-D) have reduced the ζ -potential value of the liposome to a much lesser extent (i.e. the least influence on the electrophoretic mobility of the liposomes) as shown in Figure 5.7a by the high ζ -potential value of the liposomes in presence of the copolymers mentioned. The observations on the interaction of these copolymers with DPhPC lipid monolayer on the water surface as discussed in *Chapter 4*, show that the block copolymers under investigation, penetrate the monolayer by hydrophobic interaction between the PFMA block of the copolymer and the acyl chains of the lipid molecules. It was also concluded that the copolymer chains do not have specific interactions with lipid head group. It can be concluded here that the interaction between the liposome bilayer and the block copolymer chains might be hydrophobic as well, i.e. PFMA block of the copolymer and hydrocarbon layer of the liposome wall may be involved. Therefore, the triblock copolymer chain will form a loop of PEO block on liposome surface while the PEO chains of the diblock copolymers will be dangling with one free end in solution. The data in Figure 5.7a reveal that the PEO loops on the liposome surface might be more effective in shielding the liposome surface and therefore, in shifting the shear plane outward from the liposome surface as compared to the free dangling chains of the diblock copolymer. Furthermore, the observations on ζ -potential measurements may reflect some change in size of the liposome with the adsorption of the copolymer chains. However, the real change in size as function of added block copolymer concentration can be measured by dynamic light scattering studies.

Figure 5.7b shows an increase in the mean diameter of the liposome with increasing the copolymer concentration for a triblock copolymer (PEO₁₀F11) and a diblock copolymer sample (PEO₅F15-D). The sample PEO₁₀F11 has shown a sharp increase in the liposome diameter until a plateau was reached at a concentration of approximately 0.05 wt.-%, and the liposome size changes from 120 nm to a maximum value of 144 nm (24 nm increase). The sample PEO₅F15-D also shows a strong increase in liposome size from 116 nm to 135 nm (21 nm increase) with 0.068 wt.-% concentration of the copolymer. These observations reinforce the ζ -potential results, i.e. the copolymers do adsorb on liposome surface such that the triblock copolymer chains forming loops of PEO and anchored to liposome bilayer by PFMA blocks and the diblock copolymer chain being attached to lipid bilayer through PFMA end while the PEO chain end remains free in solution around the liposome. Based on our observations, the schematic illustration of the physical adsorption of di- and triblock copolymer chains on liposome surfaces is shown in Figure 5.8.

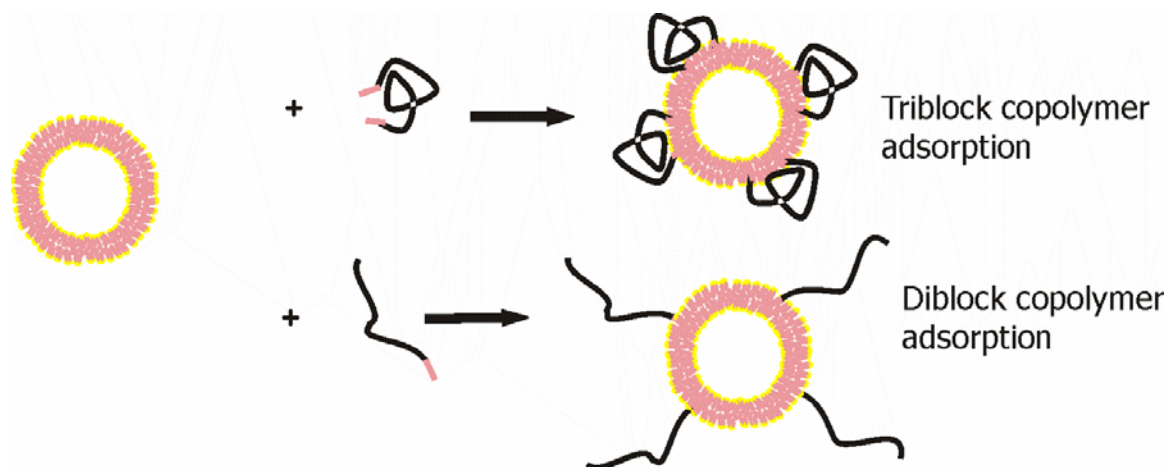


Figure 5.8. Schematic presentation of di- and triblock copolymer physical adsorption on the liposome surfaces.

5.3.3. Encapsulation of testosterone undecanoate as model hydrophobic drug by block copolymer micelles

To investigate the drug loading capability of the amphiphilic block copolymers under investigation, the encapsulation of a model hydrophobic drug, e.g. testosterone undecanoate, by dialysis technique was studied.

First experiments were performed on PEO₅F27-D block copolymer using DMF as the initial solvent for dialysis method. Table 5.1 shows the obtained results from these investigations. As given in Table 5.1, each experiment was started with 100 mg of the PEO₅F27-D copolymer and with different amounts of the testosterone undecanoate, ranging from 2.2 mg to 61 mg. The data in Table 5.1 reveal a decreasing trend in drug loading efficiency and yield, while the drug loading content remains almost the same after the initial decrease from 2.4wt.-% to 1.5 wt.-%, with increasing the initial amount (feed) of the drug. The drug loading efficiency has a maximum value with the minimum initial drug amount (2.2 mg). However, a large decrease in drug loading efficiency was observed when the initial drug amount was increased from 2.2 mg to 12 mg. Apparently

Table 5.1. Data of the encapsulation of testosterone undecanoate by PEO₅F27-D micelles using dialysis technique and DMF as the common solvent.

Polymer : Drug (mg)	Yield ⁺	Drug loading content ⁺	Drug loading efficiency ⁺
100 : 2.2	66	2.4	74.5
100 : 12	63	1.5	9.5
100 : 23	57	1.8	5.7
100 : 44	50	1.5	2.5
100 : 61	44	1.5	1.7

⁺in wt.-%

opposite trend have been reported by some authors^{64,238} for the amount of drug loading content and drug loading efficiency with the increase in the initial amount of the drug. They observed an initial increase in the loading efficiency as the ratio of probe to polymer increases, followed by a decrease in the loading efficiency. It was supposed that as the hydrophobic drug molecules become incorporated, the core becomes more similar to the probe and, consequently, there is an increase in the loading efficiency. However, as more drug molecules are incorporated, the core diameter increases, and without an increase in the aggregation number, the number of corona chains remains unchanged. Therefore, the number of contacts between the core and the water increases, leading to a decrease in the loading efficiency. From the drug loading data of testosterone undecanoate into the PEO₅F27-D copolymer micelles as given in Table 5.1, it can be argued that this block copolymer micelles have much lower capacity for the testosterone undecanoate. Furthermore, the large decrease in drug loading efficiency from 74 wt.-% to 9.5 wt.-%, and no significant effect on the drug loading content with the increase in the initial amount of the drug taken for solubilization, indicate that the micelles have already reached their maximum capacity level for testosterone undecanoate. The results of drug encapsulation by triblock copolymer (PEO₁₀F15) micelles were not much different from PEO₅F27-D block copolymer, i.e. comparable drug loading contents were obtained. For example, a maximum of only ~ 3 wt.-% drug content of testosterone undecanoate was achieved for PEO₁₀F15 copolymer. The obtained drug loading of testosterone undecanoate into PEO₅F27-D and PEO₁₀F15 block copolymer micelles is significantly lower when compared with much of the reported values for hydrophobic compounds by block copolymer micelles.²³⁹⁻²⁴⁰ There are a number of factors that influence the drug loading into copolymer micelles. The molar mass of the core, the corona block length, molecular volume of the solubilize, initial solvent for dialysis, and the partition coefficient are some of the factors that influence the drug loading. However, the most important factor is the compatibility between the drug and the core-forming polymer. Our observations suggest that PFMA is not a suitable core for testosterone undecanoate, and

one reason for the low drug loading would be the incompatibility between the fluorinated core and the nonfluorinated hydrophobic drug.²⁴¹ Hence, we investigated PEO₁₀D13-D and PEO₁₀D27-D block copolymers as well for testosterone undecanoate encapsulation.

Table 5.2 shows the results from the investigations on the drug loading of testosterone undecanoate into PEO₁₀D13-D and PEO₁₀D27-D copolymer micelles using different initial common solvents such as DMF, THF, MeOH, and DMSO. In all cases the initial polymer to drug weight ratio was kept constant (1 : 0.4) to observe the effect of different solvents and the hydrophobic block length on the drug loading of testosterone undecanoate in the copolymer micelles. Selecting an appropriate solvent is important in improving the drug loading into the hydrophobic core. The initial solvent in dialysis method has to be chosen for its ability to solubilize both the core and corona blocks of the polymer as well as the drug. The choice of the initial solvent has dramatic effects on the drug loading into micelles. For example, Nah et al.²⁴² have investigated the effect of initial solvent on drug loading into micelles of block copolymers of poly (γ -benzyl-L-glutamate) (PBLG) and PEO. They obtained 19 wt.-% and 24 wt.-% drug loading of Clonazepam using THF and 1,4-dioxane as common solvent respectively, compared to only 10 wt.-% drug loading using DMF or DMSO as the common solvent.

The data of PEO₁₀D13-D in Table 5.2 reveal approximately similar drug loading content of ~ 3 wt.-%, and approximately 6-7 wt.-% drug loading efficiency for the three solvents namely DMF, THF and Methanol. However, when DMSO was used as the initial common solvent for dissolving both the copolymer and drug the highest drug loading content of 19.4 wt.-% was achieved. The highest yield (84.5 wt.-%) was also achieved with DMSO as the initial solvent.

Another important factor in drug loading by copolymer micelles is the molar mass of the core forming block, because it is important in determining the core size. It can be said that the higher the length of the hydrophobic block the lower the critical micelle concentration and larger the core size of the micelle, which, in turn leads to higher drug

loading capacity of the micelle.²⁴⁴ This has been confirmed by different groups.

Table 5.2. Testosterone undecanoate entrapment in PEO₁₀Dy-D micelles by dialysis method.*

Sample	Solvent	Yield ⁺	Drug loading content ⁺	Drug loading efficiency ⁺
PEO ₁₀ D13-D	DMF	59	3.1	6.5
	THF	57.5	3.4	6.9
	MeOH	60	3	5.9
	DMSO	84.5	19.4	57.2
PEO ₁₀ D27-D	DMF	72.2	26	65
	THF	76.1	22	63
	MeOH	59	18	36
	DMSO	69	23.2	55.4

*for all the experiments the polymer to drug ratio was 1 : 0.4, ⁺in wt.-%

Kabanov's group found that increasing the block length of the PPO increases the aggregation number and the core size of the micelle, and subsequently the solubilization of hydrophobic substances.²⁴⁴ Hurter et al.²⁴⁵ have reported an increase in naphthalene uptake by pluronic block copolymer micelles with the increase of the PPO block length. In our experiments the drug loading of testosterone undecanoate in PEO₁₀D27-D block copolymer micelles (with relatively high hydrophobic content (long hydrophobic block)) shows the same behavior as given in Table 5.2. The data in Table 5.2 show the drug loading content in PEO₁₀D27-D copolymer micelles is over all higher than the PEO₁₀D13-D block copolymer micelles when comparing between identical solvents. The second observation was that with all the initial solvents reasonably higher values for drug

loading content and drug loading efficiency were achieved for PEO₁₀D27-D copolymer, indicating that length of the hydrophobic block plays the key role in drug encapsulation by micelles.

One possibility of storing the drug loaded micelles is freezing the aqueous micellar solution, and storing it in a refrigerator until use.²⁴⁶ Before use, frozen solution can be thawed in a water bath to obtain the drug containing micellar solution. The effect of freezing and thawing on micellar size distribution has been investigated for drug loaded micelles of PEO₅F27-D copolymer. Figure 5.9 depicts the data on the effect of freeze-thaw cycle on the size distribution of the drug loaded micelles of PEO₅F27-D

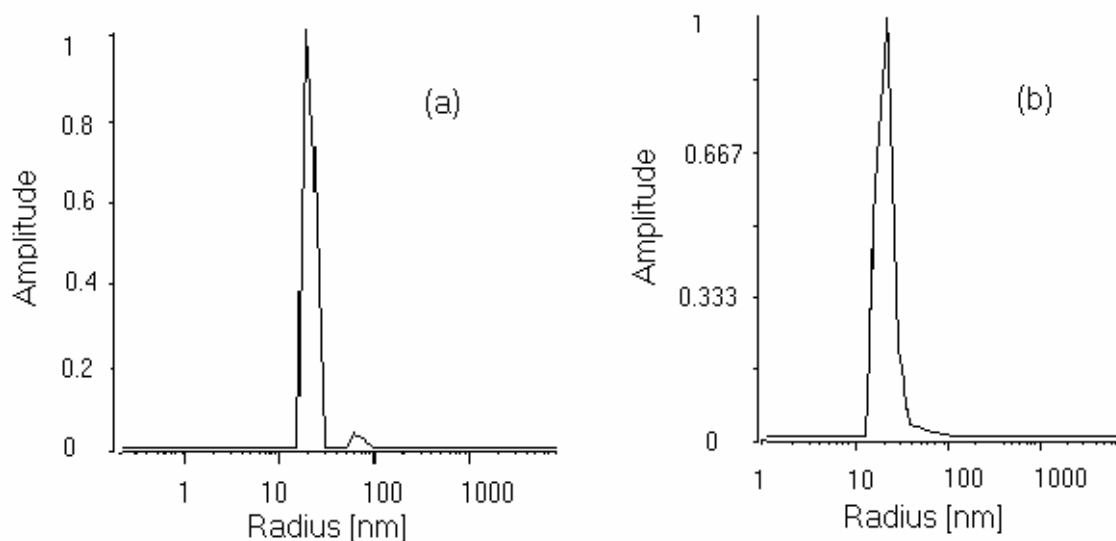


Figure 5.9. Number-averaged size distribution for testosterone undecanoate loaded PEO₅F27-D block copolymer micelles obtained by dialysis method (a) fresh solution (b) after freeze-thaw cycle. The measurements have been carried out at scattering angle of 90° and at 25°C.

copolymer solution. A fresh drug loaded (testosterone undecanoate) micellar solution was measured by dynamic light scattering for micelle size distribution. The number averaged micellar radius was calculated ~ 20 nm (Figure 5.9a). The solutions were then frozen in a

refrigerator for several days. After thawing the frozen micellar solution, the dynamic light scattering experiments were carried out to study the effect of freezing on the micelle size distribution. Although there is a small peak at around 70 nm, representing some secondary associations in fresh solution, which seems overlapped with the prominent peak after freeze-thaw cycle, the data do not show any significant change in size distribution of the drug loaded micelles after freeze-thaw cycle. Kwon et al.²¹⁸ have reported similar behavior for doxorubicin loaded poly(ethylene oxide)-*b*-poly(β -benzyl-L-aspartate) block copolymer micelles.

Nanoparticles obtained after freeze drying of the drug containing micellar solutions of PEO₁₀D13-D and PEO₁₀D27-D block copolymers were also characterized by dynamic light scattering after dispersing in double distilled water. Figure 5.10 shows the

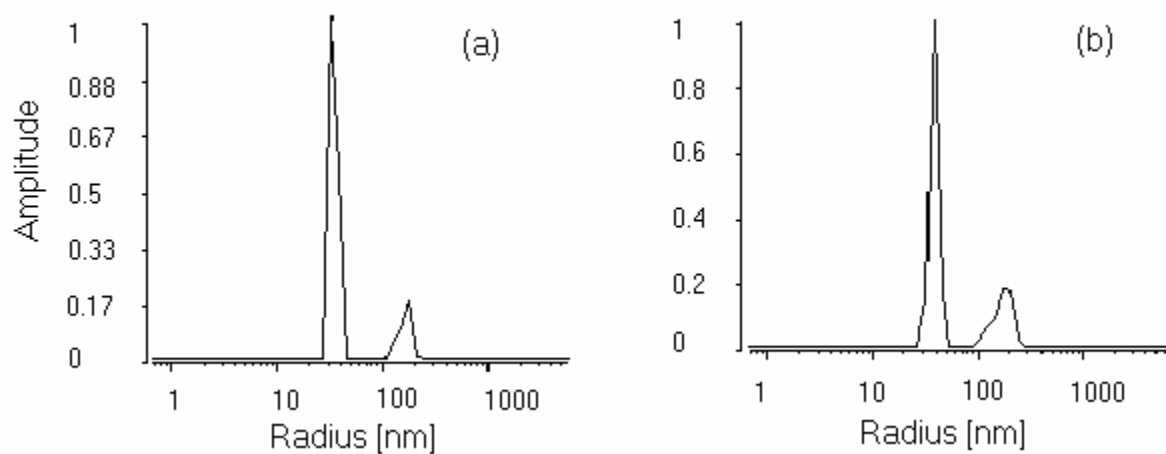


Figure 5.10. Number averaged size distribution of reconstituted nanoparticles of (a) PEO₁₀D13-D having 19 wt.-% drug content, and (b) PEO₁₀D27-D with 23 wt.-% drug content. The DLS experiments were carried out at angle 90° and at 25°C.

number-averaged size distribution data of the drug containing nanoparticle dispersion for (a) PEO₁₀D13-D copolymer having 19 wt.-%, and (b) PEO₁₀D27-D copolymer having 23 wt.-% drug content. The number averaged particle radii were calculated 34 nm (Figure

5.10a) and 38 nm (Figure 5.10b) respectively. There is a small fraction of large particles of approximately 170 nm, these may be assumed to be due to secondary association of individual particles. These results indicate that it is possible to reconstitute testosterone undecanoate loaded PEO₁₀Dy-D copolymer micelles after freeze-drying treatment.

5.4. Conclusion

The cytotoxicity results show that the PEO and PFMA containing block copolymers are nontoxic up to a copolymer concentration of 0.2 wt.-%, and hence safe for any pharmaceutical application.

The results on the interaction of block copolymers with planar lipid bilayer do not show any channel activity in planar bilayer membrane by the copolymer chains. However, the copolymers do interact with the bilayer as was confirmed by studying the effect of block copolymers on the ζ -potential and size of liposome. Triblock copolymers (i.e. PEO₁₀F9, PEO₁₀F11, and PEO₂₀F10) have reduced in absolute values the ζ -potential of the liposome from approximately -64 mV to a value close to 0.0 mV, indicating a strong interaction between the liposomes and block copolymers. In contrast, the observed effect of the diblock copolymers (PEO₅F7-D and PEO₅F15-D) on the liposome ζ -potential was significantly smaller than that produced by triblock copolymers. However, the DLS data revealed that both the di- and triblock copolymers have significantly increased the mean diameter of liposomes. It was concluded that both the di and triblock copolymers adsorb physically on the liposome surface, with PFMA block penetrating the hydrocarbon part of the liposome lipid bilayer wall, and that the PEO chain forming loop on liposome surface in case of triblock copolymer, and dangling as free chain end in solution in case of diblock copolymer.

Investigations on solubilization of a model hydrophobic drug (testosterone undecanoate) by the block copolymer micelles reveal that a much lower drug loading was achieved by PFMA containing copolymers as compared to PDMA containing block

copolymer micelles. The data show that the PFMA core of the micelle has much lower capacity for testosterone undecanoate and it was suggested that the PFMA is not a suitable core for this drug. The incompatibility between the fluorine containing micelle core and the non-fluorinated drug was assumed to be one of the main reasons for this behavior. On the contrary, no such incompatibility should exist between the PDMA core of the PEO_xDy-D copolymer micelle and the testosterone undecanoate. Accordingly, the PEO₁₀Dy-D block copolymer micelles were found more effective in drug loading of testosterone undecanoate in comparison to PEO_xFy block copolymers. Different initial common solvents (e.g. DMSO, THF, DMF, and MeOH, to dissolve both the copolymer and the drug) were used for the preparation of the drug loaded micelles. For PEO₁₀D27-D copolymer in particular, a significantly higher drug loading content was achieved with all the initial solvents. In contrast, for PEO₁₀D13-D, a significantly higher drug loading was achieved only when DMSO was used as the initial common solvent. Furthermore, no significant effect of freeze-thaw cycle on the size distribution of drug loaded micelles was found and a successful reconstitution of the drug containing dried micelles was achieved after dispersing in water

Chapter 6

Summary and perspectives

Block copolymers are macromolecules that consist of different and often immiscible blocks obtained from chemically different monomers. The immiscibility of the constituent blocks leads to microphase separation in block copolymers, which in turn is responsible for the formation of ordered structures in bulk, micelle formation in selective solvents, and adsorption at different interfaces (e.g. air/liquid and liquid/solid). The most suitable method for the synthesis of block copolymers with well-defined structures is anionic polymerization. However, the more recent techniques of controlled radical polymerization, such as atom transfer radical polymerization (ATRP) and nitroxide-mediated polymerization have been successfully adopted as well to synthesize block copolymers with well-defined compositions, and molar masses. This project is mainly focused on a new series of poly(ethylene oxide) (PEO) and poly(perfluorohexylethyl methacrylate) (PFMA) based di- and triblock copolymer synthesis and characterization of bulk, solution and interfacial properties.

A new series of amphiphilic di- and triblock copolymers of PEO and PFMA has been synthesized by atom transfer radical polymerization using mono- or bifunctional PEO macroinitiators. The molecular structure of the block copolymers was confirmed by ^1H NMR spectroscopy and size exclusion chromatography. X-ray scattering studies were carried out to investigate their bulk properties. Small angle X-ray scattering (SAXS) studies at temperature above the melting temperature of PEO have revealed composition dependent classical block copolymer ordered morphologies of cubic arrangement of spheres (bcc), hexagonally packed cylinders (hpc) and lamellar microdomains. Crystallization was, however, found to destroy the ordered melt morphology, and imposes a lamellar crystalline structure. Transmission electron microscopy (TEM) studies have confirmed the crystalline lamellar morphology of the isothermally crystallized block copolymer samples. Wide angle X-ray scattering (WAXS) investigations on isothermally crystallized samples show no effect of PFMA block on the crystal structure of the PEO

segment, i.e. PEO crystallizes in its usual monoclinic form. WAXS and differential scanning calorimetry (DSC) have confirmed that the PEO block could not be hindered completely from crystallization even with the highest PFMA content (wt.% = 62) in block copolymer. However, the crystallinity, as calculated from the WAXS and DSC data, was found significantly low in block copolymers with high PFMA content as compared to PEO homopolymer. Depression in melting point of block copolymers as compared to PEO homopolymer was observed by DSC measurements, however, no systematic effect of PFMA content on melting temperature of the copolymers was established. Polarized light microscopy experiments have also confirmed the crystallization of PEO segment in block copolymers as the sample was allowed to crystallize isothermally below the melting temperature of the PEO (after fast cooling from the melt to the desired temperature). The formation of large Maltese cross spherulitic texture on crystallization from the melt reinforced the SAXS observation, i.e. the formation of the crystalline lamellar morphology after crystallization. Furthermore, the formation of the distorted spherulitic texture by the block copolymer sample with high PFMA content (wt.% = 35) also suggests the confined crystallization of PEO segments within the volume defined by the microphase separated melt morphology.

The block copolymers under investigation are amphiphilic in nature having PEO as the hydrophilic block and the PFMA as the hydrophobic block. Therefore, after characterization of their bulk properties, behavior in aqueous solution was studied as well. Self-association in aqueous solution has been investigated using different techniques such as surface tension measurements, dynamic light scattering (DLS), and TEM. Surface tension measurements have shown a clear inflection point in surface tension vs. concentration plots. The characteristic concentration (c^*) corresponding to the inflection point was interpreted as the critical micelle concentration (CMC). The CMC was found decreasing with an increase in fluoro content in the block copolymer up to 11 wt.% PFMA (solubility limit). DLS studies have been carried out on different samples above the CMC, showing small aggregates (micelles) and single chains in diblock copolymer solutions. In triblock copolymer aqueous solution, large clusters were the dominant scatterers in addition to the micelles and single chains. The effect of temperature and concentration on the micelle and cluster formation has been investigated

by DLS studies. Micelle size was found to be resistant to any change by temperature, however, a slight but significant increase in apparent hydrodynamic radius was observed with an increase in concentration, while both temperature and concentration affected the formation of large clusters, especially in concentrated solutions. Investigations on the same sample solutions after a long storage time at room temperature, the DLS investigations revealed the dissolution of large clusters into micellar aggregates, i.e. the micelles were the dominant scatterers in copolymer solution. Similar behavior was observed when a freshly prepared triblock copolymer solution was given an ultrasonic treatment for approximately one hour before the DLS experiments were carried out. The individual micelles were assumed flower-like micelle having some chains dangling in solution and the large clusters as the loose aggregates formed by the intermicellar connection through bridges (formed by the dangling chain ends). TEM studies were carried out to visualize the morphology of the aggregates after transferring the solution to carbon film. The initial concentration for the preparation of TEM samples was found to influence the morphology of the aggregates for the investigated PEO₁₀F11 triblock copolymer. With the increase in initial concentration for the sample preparation (a) individual micelles, (b) fibrous network and circular structures, and (c) disordered structure (i.e. a tendency towards film formation at high concentration) were observed.

Amphiphilic block copolymers have attracted a great deal of attention for their adsorption at the interface and interaction with model membranes for a wide variety of applications in pharmacy, biophysics, and biomedicine. Therefore, these PEO and PFMA based amphiphilic block copolymers were investigated for their interfacial behavior and their penetration into 1,2-diphytanoyl-*sn*-glycero-3-phosphocholine (DPhPC) monolayer at the air/water interface by measuring surface pressure (π)-area (A) isotherms in conjunction with infrared reflection absorption spectroscopy (IRRAS). The π/A isotherms of the block copolymers show pressure regimes corresponding to different conformations of the polymer chains, i.e. a pancake like conformation at low surface coverage, and a brush conformation at high surface pressures. The plateau in π/A isotherms of the block copolymers, (i.e. a phase transition from the pancake like conformation to the brush conformation) becomes less and less pronounced with a decrease in the PEO block length. The π/A isotherm of the DPhPC monolayer shows only a liquid expanded phase

state at the air/water interface at all surface pressures. The DPhPC monolayer penetration by the block copolymer chains was investigated by measuring π/A isotherms and IRRA spectra of the pure DPhPC and the block copolymer penetrated DPhPC monolayers. The behavior of the block copolymer chains at the water surface in the presence of the DPhPC monolayer during compression was monitored by following the IRRA signals [$-\log(R/R_0)$, where R is the reflectivity of the sample and R_0 is the reflectivity of pure water surface] of the $\nu(\text{O-H})$ and the $\nu(\text{C-O})$ vibrational bands of the water subphase and the PEO chains, respectively. The intensity of the $\nu(\text{O-H})$ band increased with compression of the fully expanded film and the negative $\nu(\text{C-O})$ band increased also in its absolute value. However, after reaching a maximum value at a surface pressure of approximately 26 mN/m, the intensity of the both bands decreased again with further compression. The initial intensity increase in the reflection-absorption bands with compression was attributed to the increased surface density and the subsequent stretching of the PEO chains in the water subphase forming a more dense and extended conformation. The subsequent decrease is due to the expulsion of the block copolymer chains from the lipid monolayer. At $\pi \approx 33$ mN/m (where the $\nu(\text{C-O})$ reflection-absorption band from PEO was not detected any more) all the polymer chains are probably squeezed out of the lipid film.

Toxicity of compounds or their metabolites is a major reason for the failure of a compound in medical or pharmaceutical applications. Therefore, the first step for any new polymer or any compound intended for pharmaceutical or medical application, should be the cytotoxicity measurements. The results on the cytotoxicity of PEO and PFMA containing block copolymers on K562 human erythroleucemia cells reveal that these materials are nontoxic up to a copolymer concentration of 0.2 wt.-%, and hence safe for any pharmaceutical application. The data on the interaction of block copolymers with planar lipid bilayer of DPhPC; determined by studying the effect of block copolymers on the transmembrane current, do not show any channel activity in planar bilayer membrane by the copolymer chains. However, the copolymers do interact with the bilayer as confirmed by studying the effect of block copolymers on the ζ -potential value and size of the liposomes. Triblock copolymers (i.e. PEO₁₀F9, PEO₁₀F11, and PEO₂₀F10) have reduced in absolute values the ζ -potential of the liposome from

approximately -64 mV (when no copolymer solution was added) to a value close to 0.0 mV, indicating a strong interaction between the liposomes and block copolymers. In contrast, the observed effect of the diblock copolymers (PEO₅F7-D and PEO₅F15-D) on the liposome ζ -potential was significantly smaller than that produced by triblock copolymers. However, the DLS data revealed that both the di- and triblock copolymers significantly increase the mean diameter of the liposomes. It was concluded that both the di- and triblock copolymers adsorb physically on the liposome surface, with PFMA block penetrating the hydrocarbon part of the liposome lipid bilayer wall, and that the PEO chain forming loop in case of triblock copolymer, and dangling as free chain end in solution in case of diblock copolymer. These observations indicate that the mentioned block copolymers might find potential applications as the steric stabilizers of pharmaceutically important colloidal dispersions, e.g. liposomes.

The micelles formed by the amphiphilic block copolymers in aqueous medium have great potential as hydrophobic drug carrier in pharmaceutical applications. Therefore, the encapsulation of a model hydrophobic drug testosterone undecanoate by the amphiphilic block copolymer micelles by dialysis technique was explored. Two types of block copolymers, i.e. PEO_xFy and PEO_xDy-D, were investigated for this purpose. The results reveal that a much lower drug loading was achieved by PFMA containing copolymers as compared to PDMA containing block copolymer micelles. The data show that the PFMA core of the micelle has much lower capacity for testosterone undecanoate and it was suggested that the PFMA is not a suitable core for this drug. The incompatibility between the fluorine containing micelle core and the non-fluorinated drug was assumed one of the main reasons for this behavior. On the contrary, no such incompatibility should exist between the PDMA core of the PEO_xDy-D copolymer micelle and the testosterone undecanoate. Accordingly, the PEO₁₀Dy-D block copolymer micelles were found more effective in drug loading of testosterone undecanoate in comparison to PEO_xFy block copolymers. Different initial common solvents (e.g. DMSO, THF, DMF, and MeOH, to dissolve both the copolymer and the drug) were used for the preparation of drug loaded micelles. For PEO₁₀D27-D copolymer in particular, a significantly higher drug loading content was achieved with all the initial solvents. In contrast, for PEO₁₀D13-D, a significantly higher drug loading was achieved only when

DMSO was used as the initial common solvent. Furthermore, no significant effect of freeze-thaw cycle on the size distribution of the drug loaded micelles was found and a successful reconstitution of the drug containing dried micelles was achieved after dispersing in water.

Future perspectives

Many issues regarding the behavior of this new class of block copolymers in bulk and in selective solvents remain unresolved. In order to fully understand the behavior of these materials and to explore their potential pharmaceutical and biomedical application, the future works should be focused on the following points.

1. To get complete phase diagram, detailed investigations on the microphase separation of the block copolymers are needed to be done. Furthermore, the crystallization of the PEO chains in confined geometry, particularly in samples with high PFMA content, could be explored.
2. To explore the detailed structure of the various self-assembled structures of the block copolymers in water using neutron and small angle X. Ray scattering (synchrotron).
3. A systematic study on the phase behavior of the block copolymers having various compositions and molar masses at the air/water interface using π/A measurements in conjunction with IRRAS, neutron, and X-Ray reflection.
4. To get insight into the interaction between the block copolymers of various compositions and architectures and the lipid monolayer at the air/water interface by measuring the π/A isotherms in conjunction with IRRAS and various microscopic techniques.
5. To explore the chemosensitizing effect of the block copolymers on multidrug resistance tissues for anticancer agents.
6. To study the effect of block copolymers on the permeability of the liposome membrane for various pharmaceutical probes.
7. Detailed studies on the steric stabilization of the liposomes by block copolymers.

8. Investigations on the block copolymers as artificial oxygen carriers.
9. To study the gelation behavior of the triblock copolymers in water by rheology and light scattering, and to get insight in to their structures by SAXS and SANS.

Chapter 7

Zusammenfassung

Blockcopolymere sind Makromoleküle, die aus unterschiedlichen und häufig nicht mischbaren Teilblöcken bestehen, die auch chemisch unterschiedliche Monomeren erhalten werden. Die Unmischbarkeit der Blöcke führt zu einer Mikrophasenseparation von Blockcopolymeren, wie zum Beispiel zu selbstgeordneten Strukturen im Bulk, Mizellbildung in den selektiven Lösungsmitteln und Adsorption an unterschiedlichen Grenzflächen (z.B. Gas/Flüssigkeit und Flüssigkeit/Festkörper). Die gängigste Methode für die Synthese der Blockcopolymere mit definierter Struktur ist die anionische Polymerisation. Jedoch sind mit der kontrollierten radikalischen Polymerisation, wie Atom Transfer Radical Polymerization (ATRP) und Nitroxid vermittelten Polymerisation, erfolgreich neue Blockcopolymere mit gut definiertem Aufbau und Molmasse synthetisiert worden. Diese Arbeit basiert hauptsächlich auf der Synthese von Di- und Triblock-Copolymeren aus Poly(ethylenoxid) (PEO) und Poly(perfluor-hexyl-ethyl-methacrylat) (PFMA) sowie der Charakterisierung von Bulk-, Lösungs- und Grenzflächeneigenschaften.

Eine neue Reihe amphiphiler Di- und Triblock-Copolymere aus PEO und PFMA ist mittels ATRP aus mono- und bifunktionellen PEO Makroinitiatoren synthetisiert worden. Die molekulare Struktur der Blockcopolymere wurde durch ^1H NMR Spektroskopie und Größenausschlußchromatographie bestimmt. Mit Röntgenstreuung wurden die Bulkeigenschaften untersucht. Mit Röntgenkleinwinkelstreuung (SAXS) wurde bei Temperaturen oberhalb der Schmelztemperatur von PEO die klassische Morphologiebildung der Blockcopolymere unterschiedlicher Zusammensetzung mit kubischen Gittern (bcc), hexagonal gepackten Zylindern (hpc) und lamellaren Mikrodomänen gefunden.

Es stellte sich jedoch heraus, dass die PEO-Kristallisation die bestehende Morphologie in der Schmelze zerstört und eine lamellare Struktur aufprägt. Untersuchungen der Transmissionselektronenmikroskopie (TEM) haben diese Lamellenmorphologie der isotherm kristallisierten Blockcopolymerproben bestätigt. Messungen der Röntgenweitwinkelstreuung (WAXS) an isotherm kristallisierten Proben zeigten keinen Einfluss des PFMA-Blockes auf die Kristallstruktur des PEO-Segments, d.h. PEO kristallisiert in seiner üblichen Form. WAXS und Differential Scanning Calorimetry (DSC) haben bestätigt, dass der PEO-Block nicht vollständig an der Kristallisation gehindert werden konnte, selbst bei der Probe mit höchstem PFMA-Gehalt dieser Untersuchung (62 Gew.-%).

Jedoch wurde die aus WAXS- und DSC-Daten erhaltene Kristallinität bei den Blockcopolymeren mit hohem PFMA-Inhalt gegenüber reinem PEO erheblich verringert. Ebenso wurde mit DSC Messungen eine Schmelzpunktniedrigung gefunden, jedoch wurde kein systematischer Zusammenhang des PFMA-Anteils mit der Schmelztemperatur der Copolymere festgestellt. Mittels Polarisationslichtmikroskopie (PLM) konnte auch die Kristallisation des PEO-Segments in den Blockcopolymeren bestätigt werden, wenn die Probe unterhalb der Schmelztemperatur des PEO isotherm kristallisiert wurde (nach dem schnellen Abkühlen aus der Schmelze zur gewünschten Temperatur).

Die Bildung von großen sphärolitischen Strukturen (Malteser Kreuz) bei der Kristallisation aus der Schmelze unterstützte die Ergebnisse aus SAXS-Messungen, dass die Kristallisation eine Lamellenmorphologie aufprägt. Außerdem lässt die Bildung von verzerrten Sphäroliten bei Blockcopolymeren mit hohem PFMA-Gehalt (35 wt.-%) vermuten, dass die Kristallisation der PEO-Segmente durch das Volumen eingeschränkt wird, dass durch die Mikrophasenseparation definiert ist.

Die Blockcopolymere dieser Untersuchung sind amphiphil, mit PEO als dem hydrophilen und PFMA als dem hydrophoben Block. Daher wurde nach der Bestimmung der Bulkeigenschaften auch das Verhalten in der wässrigen Lösung studiert. Die Strukturbildung in der wässrigen Lösung wurde mit unterschiedlichen Techniken

untersucht, wie der Oberflächenspannungsmessung, dynamischer Lichtstreuung (DLS) und TEM. Die Oberflächenspannung zeigte einen deutlichen Übergang in der Abhängigkeit von der Konzentration. Die charakteristische Konzentration (c^*) am Übergangspunkt wurde als die kritische Mizellkonzentration gedeutet (cmc). Die cmc zeigte bei einer Zunahme des Fluorgehalts im Blockcopolymer bis zu 11 wt.-% PFMA (Löslichkeitsgrenze) eine stetige Verringerung. DLS-Studien sind an unterschiedlichen Proben oberhalb cmc durchgeführt worden und es konnten kleine Aggregate (Mizellen) und einzelne Ketten in den Lösungen von Diblock-Copolymeren beobachtet werden. In wässrigen Lösungen von Triblock-Copolymeren traten zusätzlich große Cluster als dominierende Streuzentren neben den Mizellen und den Einzelketten auf. Der Einfluss von Temperatur und Konzentration auf die Mizell- und Clusterbildung ist durch DLS-Studien untersucht worden. Hierbei war die Mizellgröße unabhängig von der Temperatur, jedoch wurde eine geringfügige aber signifikante Zunahme des hydrodynamischen Radius bei steigender Konzentration beobachtet. Die großen Cluster wurden von Temperatur- und Konzentrationsänderungen deutlich stärker beeinflusst.

DLS-Untersuchungen an denselben Proben nach einer langen Lagerung bei Raumtemperatur zeigten weniger große Cluster bei deutlicherem Signal der Mizellen, d.h. die Mizellen waren nun die dominierenden Streuzentren in der Copolymerlösung. Ein ähnliches Verhalten konnte durch ein etwa einstündiges Ultraschallbad der frisch vorbereiteten Triblock-Copolymerlösung erzielt werden. Die Struktur der Mizellen kann als flower-like angenommen werden, wobei freie Enden einzelner Ketten in die Lösung zeigen. Die großen Cluster können als Anhäufungen von Mizellen mit intermizellaren Brücken durch einzelne Moleküle angesehen werden. TEM Untersuchungen wurden an Proben auf Kohlenstofffilm durchgeführt, um die Morphologie der Aggregate sichtbar zu machen. Die Ausgangskonzentration der Lösungen für die TEM-Untersuchungen hatte einen starken Einfluss auf die Morphologie der Aggregate der untersuchten Triblock-Copolymere. Mit der Zunahme der Ausgangskonzentration konnten (a) einzelne

Micellen, (b) aufgereichte und kreisförmige Strukturen, und (c) ungeordnete Strukturen (mit Tendenz zur Filmbildung bei hoher Konzentration) beobachtet werden.

Amphiphile Blockcopolymere haben große Bedeutung bei der Adsorption an Grenzflächen und bei der Wechselwirkung mit Modellmembranen für eine breite Vielzahl von Anwendungen in der Pharmazie, der Biophysik und der Biomedizin. Daher wurden die auf PEO und PFMA basierenden amphiphilen Blockcopolymere für ihr Grenzflächenverhalten und ihre Durchdringung von 1,2-diphytanoyl-*sn*-glycero-3-phosphocholin (DPhPC) Monolayern an der Luft-/Wassergrenzfläche untersucht. Hierbei fand die Infrarotreflexionsabsorptionsspektroskopie (IRRAS) in Verbindung mit Oberflächendruckmessungen (π/A -Isothermen) Verwendung. Die π/A -Isothermen der Blockcopolymere zeigen Druckbereiche mit unterschiedlichen Konformationen der Polymerketten, einer 'pan-cake' Struktur bei geringer Oberflächenbedeckung und einer Bürstenstruktur mit hohem Oberflächendruck. Das Plateau in den π/A Isothermen der Blockcopolymere beim Phasenübergang von der 'pan-cake' zur Bürstenstruktur wird bei längeren PEO-Blöcken stärker ausgeprägt. Die π/A Isotherme des DPhPC Monolayers zeigt nur einen Phasenzustand an der Luft-/Wasser-Grenzfläche unabhängig vom Oberflächendruck. Die Durchdringung des DPhPC Monolayers durch die Blockcopolymerketten wurde zusätzlich mit IRRAS beobachtet. Die Intensität der $\nu(\text{O-H})$ Bande erhöhte sich mit Kompression des Filmes und die negative $\nu(\text{C-O})$ Bande verstärkte sich ebenfalls. Nachdem jedoch der Oberflächendruck einen Maximalwert von ungefähr 26 mN/m erreicht hatte, verringerte sich die Intensität der beider Banden wieder mit weiterer Kompression. Die Zunahme der Intensität der Reflexions-Absorptionsbanden bei Kompression wurde der erhöhten Oberflächendichte und dem folgenden Ausdehnen der PEO-Ketten in der Wassersubphase zugeschrieben. Die nachfolgende Abnahme beruht auf dem Herausdrängen der Blockcopolymerketten aus der Lipidmonolayer. Bei $\pi \approx 33$ mN/m konnte keine $\nu(\text{C-O})$ Reflexions-Absorptionsbande des PEO mehr beobachtet werden, da nun alle Polymerketten aus dem Lipidfilm herausgedrückt worden sind.

Der Hauptgrund für die Nichtverwertbarkeit eines Mittels in medizinischen oder pharmazeutischen Anwendungen liegt in der toxischen Wirkung der Bestandteile oder der Stoffwechselprodukte. Folglich liegt der erste Schritt für jedes neue Material oder jeden neuen Wirkstoff für pharmazeutische oder medizinische Anwendungen bei der Bestimmung der Cytotoxizität. Messungen der Cytotoxizität von Blockcopolymeren aus PEO und PFMA auf menschlichen Zellen (Erythroleucemia K562) zeigen, dass die verwendeten Materialien bis zu einer Copolymerkonzentration von 0.2 Gew.-% praktisch nicht toxisch, und somit sicher für pharmazeutische Anwendung sind. Die Wechselwirkung der Blockcopolymeren mit planaren Lipidbilayern aus DPhPC, führt nicht zu einer Kanalbildung in der Membran, wie durch Messung des Transmembranstrom festgestellt werden konnte. Jedoch wirken die Copolymeren auf das ζ -Potential und die Größe der Liposomen. Triblock-Copolymeren (d.h. PEO₁₀F9, PEO₁₀F11 und PEO₂₀F10) haben in den Absolutwerten das ζ -Potential des Liposoms von ungefähr -64 mV auf einen Wert nahe an 0,0 mV verringert, was für eine starke Wechselwirkung zwischen den Liposomen und den Blockcopolymeren spricht. Demgegenüber war der beobachtete Effekt der Diblock-Copolymeren (PEO₅F7-D und PEO₅F15-D) auf das ζ -Potential des Liposoms erheblich kleiner. Jedoch zeigten die DLS-Daten, dass sowohl Di- als auch Triblock-Copolymeren den Mitteldurchmesser der Liposomen signifikant erhöhen. Man kann vermuten, dass Di- und Triblock-Copolymeren physikalisch auf der Liposomenoberfläche absorbieren, indem der PFMA-Block die Kohlenwasserstoffschicht der Lipidwand durchdringt und dass der PEO-Block als gelöste Hülle (bei Triblock-Copolymeren als Schleifen und bei Diblock-Copolymeren mit freiem Kettenende) vorliegt.

Die Mizellen amphiphiler Block-Copolymeren in Wasser haben ein großes Potential als hydrophobe Drug-Release Systeme in pharmazeutischen Anwendungen. Folglich wurde die Verkapselung des hydrophoben Testosteronundecanoate durch die amphiphilen Block-Copolymermizellen durch Dialysetechnik exemplarisch erforscht.

Zwei Arten der Blockcopolymeren, PEO_xFy und PEO_xDy-D (Blockcopolymer aus PEO und einem Methacrylat mit langer n-Alkylseitenkette), wurden für diese Untersuchungen herangezogen. Die Resultate zeigen, dass bei den PFMA-Copolymeren viel weniger Arzneistoff in den Mizellen enthalten war, als bei den Copolymeren mit PDMA. Die Unverträglichkeit zwischen dem Fluor im Mizellkern und dem nicht-fluorierten Arzneistoff scheint einer der Hauptgründe für dieses Verhalten zu sein. Unterschiedliche Lösungsmittel (z.B. DMSO, THF, DMF und MeOH), geeignet für Arzneistoff und Copolymer, wurden zusätzlich zur Probenpräparation herangezogen. Beim PEO₁₀D27-D konnten dadurch erheblich höhere Arzneistoffmengen eingebunden werden. Beim PEO₁₀D13-D konnte dieser Effekt nur durch DMSO hervorgerufen werden. Weiterhin konnte kein signifikanter Effekt des Einfrier-Auftau-Zyklus auf die Korngrößenverteilung der Mizellen gefunden werden. Die so getrockneten Mizellen konnten durch Dispergieren in Wasser wieder hergestellt werden.

Literature

1. M. Szwarc, M. Levy, R. Milkovich, *J. Am. Chem. Soc.* **1956**, 78, 2656.
2. Y. Matsushita, *Structure and Properties of Multiphase Polymeric Materials*, T. Araki, Q. T. Cong, M. Shibayama (Eds.), Marcel Dekker, New York, 1998, p.121.
3. M. Bouix, J. Gouzi, B. Charleux, J. P. Vairon, P. Guinot, *Macromol. Rapid Commun.* **1998**, 19, 209.
4. C. Burguière, S. Pascual, B. Coutin, A. Polton, M. Tardi, B. Charleux, K. Matyjaszewski, J. P. Vairon, *Macromol. Symp.* **2000**, 150, 39.
5. K. A. Davis, B. Charleux, K. Matyjaszewski, *J. Polym. Sci., Polym. Chem.* **2000**, 38, 2274.
6. F. S. Bates, G. H. Fredrickson, *Annu. Rev. Phys. Chem.* **1990**, 41, 525.
7. P. Bahadur, *Curr. Sci.* **2001**, 80, 1002.
8. G. Strobl, *The Physics of Polymers* (2nd ed.) Springer, Berlin, 1997.
9. L. Leibler, *Macromolecules* **1980**, 13, 1602.
10. A. K. Khandpur, S. Förster, F. S. Bates, I. W. Hamley, A. J. Ryan, W. Bras, K. Almdal, K. Mortensen, *Macromolecules* **1995**, 28, 8796.
11. S. Förster, A. K. Khandpur, J. Zhao, F. S. Bates, I. W. Hamley, A. J. Ryan, W. Bras, *Macromolecules*, **1994**, 27, 6922.
12. M. W. Matsen, F. S. Bates, *Macromolecules* **1996**, 29, 1091.
13. G. H. Fredrickson, E. Helfand, *J. Chem. Phys.* **1987**, 87, 697.
14. K. R. Shull, *Macromolecules* **1992**, 25, 2122.
15. A. Hale, H. E. Bair, *Thermal Characterization of Polymeric Materials*, E. A. Turi (Ed.), (2nd ed.) Academic Press, San Diego, 1997, vol. 1, p. 745.
16. M. Banaszak, S. Woloszczuk, T. Pakula, S. Jurga, *Phys. Rev. E* **2002**, 66, 031804, and A. V. Dobrynin, I. Y. Erukhimovich, *Macromolecules* **1993**, 26, 276.
17. I. W. Hamley, J. P. A. Fairclough, N. J. Terrill, A. J. Ryan, P. M. Lipic, F. S. Bates, E. T. Andrews, *Macromolecules* **1996**, 29, 8835.
18. S. Hong, W. J. MacKnight, T. P. Russell, S. P. Gido, *Macromolecules* **2001**, 34, 2876.
19. E. A. DiMarzio, C. M. Guttman, J. D. Hoffman, *Macromolecules* **1980**, 13, 1194.

20. M. D. Whitmore, J. Noolandi, *Macromolecules* **1988**, *21*, 1482.
21. T. Vilgis, A. Halperin, *Macromolecules* **1991**, *24*, 2090.
22. C. Park, C. D. Rosa, L. J. Fetters, E. L. Thomas, *Macromolecules* **2000**, *33*, 7931.
23. L. Li, Y. Serero, M. H. J. Koch, W. H. de Jeu, *Macromolecules* **2003**, *36*, 529.
24. S. Nojima, K. Kato, S. Yamamoto, T. Ashida, *Macromolecules* **1992**, *25*, 2237.
25. D. J. Quiram, R. A. Register, G. R. Marchand, *Macromolecules* **1997**, *30*, 4551.
26. A. J. Ryan, I. W. Hamley, W. Bras, F. S. Bates, *Macromolecules* **1995**, *28*, 3860.
27. T. Shiomi, H. Takeshita, H. Kawaguchi, M. Nagai, K. Takenaka, M. Miya, *Macromolecules* **2002**, *35*, 8056.
28. T. P. Lodge, *Macromol. Chem. Phys.* **2003**, *204*, 265.
29. T. Hashimoto, S. Suehiro, M. Shibayama, K. Saijo, H. Kawai, *Polym. J.* **1981**, *13*, 501.
30. C. Booth, D. Attwood, *Macromol. Rapid. Commun.* **2000**, *21*, 501.
31. J. Preuschen, S. Menchen, M. A. Winnik, A. Heuer, H. W. Spiess, *Macromolecules* **1999**, *32*, 2690.
32. J. F. Berret, D. Calvet, A. Collet, M. Viguier, *Curr. Opin. Colloid Interf. Sci.* **2003**, *8*, 296.
33. F. M. Merrett, *J. Polym. Sci.* **1957**, *24*, 467.
34. I. E. Climie, E. F. T. White, *J. Polym. Sci.* **1960**, *47*, 149.
35. G. M. Burnett, P. Meares, C. Paton, *Trans. Faraday Soc.* **1961**, *58*, 737.
36. P. Alexandridis, T. A. Hatton, *Polymeric Material Encyclopedia*, J. C. Salamone (Ed.), CRC Press, Boca Raton, FL, 1996, p. 743.
37. Z. Zhou, B. Chu, *J. Colloid. Interf. Sci.* **1988**, *126*, 171
38. Z. Tuzar, P. Kratochvil, *Surface and Colloid Science*, E. Matjevic (ed.), Plenum Press, New York, 1993, vol. 15.
39. J. R. Quintana, M. Villacampa, I. Katime, *Polymeric Material Encyclopedia*, J. C. Salamone (Ed.), CRC Press, Boca Raton, FL, 1996, p. 815.
40. G. Riess, *Prog. Polym. Sci.* **2003**, *28*, 1107.
41. T. Liu, Z. Zhou, C. Wu, V. M. Nace, B. Chu, *J. Phys. Chem. B* **1998**, *102*, 2875.
42. Z. Tuzar, *Solvents and Self-Organization of Polymer*, NATO ASI series, serie E: applied sciences, Kluwer Academic Publisher, Dordrecht, 1996, vol. 327, p. 1.

-
43. T. Liu, L. Z. Liu, B. Chu, *Amphiphilic Block Copolymers*, P. Alexandridis, B. Lindman (Eds.), Elsevier Science, Amsterdam, 2000, p. 115.
 44. K. Mortensen, Y. Talman, B. Gao, J. Kops, *Macromolecules*, **1997**, *30*, 6764.
 45. C. Price, *Pure Appl. Chem.* **1983**, *55*, 1563.
 46. W. Huang, J. B. Kim, G. L. Baker, M. L. Bruening, *Nanotech.* **2003**, *14*, 1075.
 47. M. Moffitt, L., Zhang, K. Khougaz, A. Eisenberg, *Solvents and Self-Organization of Polymer*, S. E. Webber, P. Munk, Z. Tuzar (Eds.) NATO ASI series, serie E: applied sciences, Kluwer Academic Publisher, Dordrecht, 1996, vol. 327, p. 53.
 48. J. J. Yuan, Y. S. Li, X. Q. Li, S. Y. Cheng, L. Jiang, L. X. Feng, Z. Q. Fan, *Eur. Polym. J.* **2003**, *39*, 767.
 49. Z. Yang, M. Crothers, N. M. P. S. Ricardo, C. Chaibundit, P. Taboada, V. Mosquera, A. Kellarakis, V. Havredaki, L. Martini, C. Valder, J. H. Collett, D. Attwood, F. Heatley, C. Booth, *Langmuir* **2003**, *19*, 943.
 50. W. Brown, K. Schillen, M. Almgren, S. Hvidt, P. Bahadur, *J. Phys. Chem.* **1991**, *95*, 1850.
 51. G. -E. Yu, Z. -K. Zhou, D. Attwood, C. Price, C. Booth, P. C. Griffiths, P. Stilbs, *J. Chem. Soc. Faraday Trans.* **1996**, *92*, 5021, and G. Fleischer, *J. Phys. Chem.* **1993**, *97*, 517.
 52. A. D. Bedells, R. M. Arafah, Z. Yang, D. Attwood, F. Heatley, J. C. Padget, C. Price, C. Booth, *J. Chem. Soc. Faraday Trans.* **1993**, *89*, 1235.
 53. K. Mortensen, *Amphiphilic Block Copolymers*, P. Alexandridis, B. Lindman (Eds.), Elsevier Science, Amsterdam, 2000, p. 191.
 54. M. C. Faure, P. Bassereau, L. T. Lee, A. Menelle, C. Lheveder, *Macromolecules* **1999**, *32*, 8538.
 55. G. J. Fleer, M. A. C. Stuart, J. M. H. M. Scheutjens, T. Cosgrove, B. Vincent, *Polymer at Interfaces*, Chapman and Hall, London, 1993.
 56. M. C. Faure, P. Bassereau, B. Desbat, *Eur. Phys. J. E* **2000**, *2*, 145.
 57. S. Rivillon, M. G. Munoz, F. Monroy, F. Ortega, R. G. Rubio, *Macromolecules* **2003**, *36*, 4068.
 58. M. S. Kent, J. Majewski, G. S. Smith, L. T. Lee, S. Satija, *J. Chem. Phys.* **1998**, *108*, 5635.

-
59. G. Riess, G. Hurtrez, P. Bahadur, *Encyclopedia of Polymer Science and Engineering*, H. F. Mark, N. Bikales, C. G. Overberger, G. Menges, J. I. Kroschwitz (Eds.), Wiley, New York, 1985, vol. 2. P. 324.
 60. V. Y. Alakhov, E. Y. Moskaleva, E. V. Batrakova, A. V. Kabanov, *Bioconjug. Chem.* **1996**, 7, 209.
 61. A. Venne, S. Li, R. Mandeville, A. V. Kabanov, V. Y. Alakhov, *Cancer Res.* **1996**, 56, 3626.
 62. M. Malmsten, *Amphiphilic Block Copolymers*, P. Alexandridis, B. Lindman (Eds.), Elsevier Science, Amsterdam, 2000, p. 319.
 63. N. Rapoport, W. G. Pitt, H. Sun, J. L. Nelson, *J. Control. Release* **2003**, 91, 85.
 64. P. L. Soo, L. Luo, D. Maysinger, A. Eisenberg, *Langmuir* **2002**, 18, 9996.
 65. L. J. Goldstein, M. M. Gottesman, I. Pastan, *Cancer Treat. Res.* **1991**, 57, 101.
 66. A. V. Kabanov, E. V. Batrakova, V. Y. Alakhov, *J. Control. Release* **2003**, 91, 75.
 67. I. Szleifer, *Curr. Opin. Solid State and Mat. Sci.* **1997**, 2, 337.
 68. *Stealth Liposomes*, D. D. Lasic, F. Martin (Eds.) CRC Press, Boca Raton, FL, 1995.
 69. R. Nagarajan, *Curr. Opin. Colloid and Interf. Sci.* **1996**, 1, 391.
 70. M. Svensson, H. O. Johansson, F. Tjerneld, *Amphiphilic Block Copolymers*, P. Alexandridis, B. Lindman (Eds.), Elsevier Science, Amsterdam, 2000, p. 377.
 71. K. Matsumoto, M. Kubota, H. Matsuoka, H. Yamaoka, *Macromolecules* **1999**, 32, 7122
 72. A. Menelle, T. P. Russell, S. H. Anastasiadis, *Phys. Rev. Lett.* **1992**, 68, 67
 73. S. Sheiko, A. A. Turetskii, J. Höpken, M. Möller, *Macromolecular Engineering*, M. K. Mishra (Ed.), Plenum Press, New York, 1995, p. 219.
 74. W. P. Hems, T. M. Yong, J. L. M. Nunen, A. I. Cooper, A. B. Holmes, D. A. Griffin, *J. Mater. Chem.* **1999**, 9, 1403.
 75. J. N. Meussdoerffer, H. Niederprüm, *Chem. Zeit.* **1980**, 104, 45.
 76. T. J. Romack, E. E. Maury, J. M. DeSimone, *Macromolecules* **1995**, 28, 912.
 77. M. R. Giles, R. M. T. Griffiths, A. A. Ricardo, M. M. C. G. Silva, S. M. Howdle, *Macromolecules* **2001**, 34, 20.
 78. M. J. Krupers, C. F. Bartelink, H. J. M. Grünhauer, M. Möller, *Polymer* **1998**, 39, 2049.

-
79. K. Busse, J. Kressler, D. Eck, S. Höring, *Macromolecules* **2002**, *35*, 178.
 80. K. Matsumoto, H. Mazakai, R. Nishimura, H. Matsuoka, H. Yamaoka, *Macromolecules* **2000**, *33*, 8295.
 81. S. J. McLain, B. B. Sauer, L. E. Firment, *Macromolecules* **1996**, *29*, 8211.
 82. Z. B. Guan, J. M. DeSimone, *Macromolecules* **1994**, *27*, 5527.
 83. M. Krupers, M. Möller, *Macromol. Chem. Phys.* **1997**, *198*, 2163.
 84. H. S. Hwang, J. Y. Heo, Y. T. Jeong, S. H. Jin, D. Cho, T. Chang, K. T. Lim, *Polymer* **2003**, *44*, 5153.
 85. Z. B. Zhang, S. K. Ying, Z. Q. Shi, *Polymer* **1999**, *40*, 5439.
 86. K. T. Lim, M. Y. Lee, M. J. Moon, G. D. Lee, S. S. Hong, J. L. Dickson, K. P. Johnston, *Polymer* **2002**, *43*, 7049.
 87. Y. Ren, T. P. Lodge, M. A. Hillmyer, *Macromolecules* **2001**, *34*, 4780.
 88. T. Imae, H. Tabuchi, K. Funayama, A. Sato, T. Nakamura, N. Amaya, *Colloids Surf. A* **2000**, *167*, 73.
 89. T. Imae, *Kobunshi Ronbunshu* **2001**, *58*, 178.
 90. T. Hayakawa, J. G. Wang, N. Sundararajan, M. L. Xiang, X. F. Li, B. Glusen, G. C. Leung, M. Ueda, C. K. Ober, *J. Phy. Org. Chem.* **2000**, *13*, 787.
 91. D. R. Iyengar, S. M. Perutz, C. A. Dai, C. K. Ober, E. J. Kramer, *Macromolecules* **1996**, *29*, 1229.
 92. G. Floudas, C. Tsitsilianis, *Macromolecules* **1997**, *30*, 4381.
 93. S. Hong, A. A. Bushelman, W. J. MacKnight, S. P. Gido, D. J. Lohse, L. J. Fetters, *Polymer* **2001**, *42*, 5909.
 94. J. K. Kim, D. J. Park, M. S. Lee, K. J. Ihn, *Polymer* **2001**, *42*, 7429.
 95. G. Kim, C. C. Han, M. Libera, C. L. Jackson, *Macromolecules* **2001**, *34*, 7336.
 96. A. J. Ryan, J. P. A. Fairclough, I. W. Hamley, S. M. Mai, C. Booth, *Macromolecules* **1997**, *30*, 1723.
 97. L. Zhu, S. Z. D. Cheng, B. H. Calhoun, Q. Ge, R. P. Quirk, E. L. Thomas, B. S. Hsiao, F. Yeh, B. Lotz, *Polymer* **2001**, *42*, 5829.
 98. P. Rangarajan, R. A. Register, L. J. Fetters, W. Bras, S. Naylor, A. J. Ryan, *Macromolecules* **1995**, *28*, 4932.
 99. M. A. Hillmyer, F. S. Bates, *Macromol. Symp.* **1997**, *117*, 121.

-
100. S. Mahajan, S. Renker, P. F. W. Simon, J. S. Gutmann, A. Jain, S. M. Gruner, *Macromol. Chem. Phys.* **2003**, *204*, 1047.
 101. J. S. Wang, K. Matyjaszewski, *J. Am. Chem. Soc.* **1995**, *117*, 5614.
 102. K. Matyjaszewski, J. Xia, *Chem. Rev.* **2001**, *101*, 2921.
 103. G. Strobl, *Acta Crystallogr.* **1970**, *A26*, 367.
 104. Y. Takahashi, H. Tadokoro, *Macromolecules* **1973**, *6*, 672.
 105. V. V. Volkov, N. A. Plate, A. Takahara, T. Kajiyama, N. Amaya, Y. Murata, *Polymer* **1992**, *33*, 1316.
 106. M. Beiner, K. Schröter, E. Hempel, S. Reissig, E. Donth, *Macromolecules* **1999**, *32*, 6278.
 107. C. Campbell, K. Viras, M. J. Richardson, A. J. Masters, C. Booth, *Makromol. Chem.* **1993**, *194*, 799.
 108. E. Donth, H. Kretzschmar, G. Schulze, D. Garg, S. Höring, J. Ulbricht, *Acta Polym.* **1987**, *38*, 260.
 109. V. Balsamo, F. V. Gyldenfeldt, R. Stadler, *Macromol. Chem. Phys.* **1996**, *197*, 3317.
 110. S. Hong, L. Yang, W. J. MacKnight, S. P. Gido, *Macromolecules* **2001**, *34*, 7009.
 111. Y. Y. Won, H. T. Davis, F. S. Bates, *Science* **1999**, *283*, 960.
 112. J. R. Harris, C. Roos, R. Djalali, O. Rheingans, M. Maskos, M. Schmidt, *Micron* **1999**, *30*, 289.
 113. M. Maskos, J. R. Harris, *Macromol. Rapid. Commun.* **2001**, *22*, 271.
 114. V. P. Torchilin, *J. Control. Release* **2001**, *73*, 133.
 115. S. Förster, M. Antonietti, *Adv. Mat.* **1998**, *10*, 195.
 116. E. Alami, M. Almgren, W. Brown, J. Francois, *Macromolecules* **1996**, *29*, 2229.
 117. K. Thuresson, S. Nilsson, A. L. Kjoniksen, H. Walderhaug, B. Lindman, B. Nystrom, *J. Phys. Chem. B* **1999**, *103*, 1425.
 118. S. Maiti, P. R. Chatterji, *J. Phys. Chem. B* **2000**, *104*, 10253.
 119. W. T. Tang, G. Hadziioannou, P. M. Cotts, B. A. Smith, C. W. Frank, *Polym. Prepr.* **1986**, *27*, 107.
 120. E. Raspaud, D. Lairez, M. Adam, J. P. Carton, *Macromolecules* **1994**, *27*, 2956.

-
121. G. Fleischer, C. Konak, A. Puhmann, F. Rittig, J. Karger, *Macromolecules* **2000**, *33*, 7066.
 122. Y. Y. Won, A. K. Brannan, H. T. Davis, F. S. Bates, *J. Phys. Chem. B* **2002**, *106*, 3354.
 123. X. Zushun, Y. Changfeng, C. Shiyuan, F. Linxian, *Polym. Bull.* **2000**, *44*, 215.
 124. G. Marinov, B. Michels, R. Zana, *Langmuir* **1998**, *14*, 2639.
 125. C. Chaibundit, S. M. Mai, F. Heatley, C. Booth, *Langmuir* **2000**, *16*, 9645.
 126. W. Brown, K. Schillen, S. Hvidt, *J. Phys. Chem.* **1992**, *96*, 6038.
 127. K. Yu, A. Eisenberg, *Macromolecules* **1998**, *31*, 3509.
 128. P. Petit, I. Iliopoulos, R. Audebert, S. Szonyi, *Langmuir* **1997**, *13*, 4229.
 129. J. Zhou, D. Zhuang, X. Yuan, M. Jiang, Y. Zhang, *Langmuir* **2000**, *16*, 9653.
 130. G. Tae, J. A. Kornfield, J. A. Hubbell, D. Johannsmann, T. E. H. Esch, *Macromolecules* **2001**, *34*, 6409.
 131. A. J. F. Siegert, *MIT Rad. Lab. Rep.* **1943**, 465.
 132. S. W Provencher, *Macromol. Chem.* **1979**, *180*, 201.
 133. J. C. Ravey, M. J. Stébé, *Colloids Surf. A* **1994**, *84*, 11.
 134. K. Devanand, J. C. Selser, *Macromolecules* **1991**, *24*, 5943.
 135. Y. W. Yang, Z. Yang, Z. Zhou, D. Attwood, C. Booth, *Macromolecules* **1996**, *29*, 670.
 136. M. Polverari, T. G. M. Vandeven, *J. Phys. Chem.* **1996**, *100*, 13687. D. K. Carpenter, G. Santiago, A. H. Hunt, *J. Polym. Sci., Polym. Symp.* **1974**, *44*, 75.
 137. M. Duval, *Macromolecules* **2000**, *33*, 7862.
 138. B. Xu, L. Li, A. Yekta, Z. Masoumi, S. Kanagalingam, M. A. Winnik, K. W. Zhang, P. M. Macdonald, *Langmuir*, **1997**, *13*, 2447.
 139. O. Vorobyova, W. Lau, M. A. Winnik, *Langmuir*, **2001**, *17*, 1357.
 140. D. Calvet, A. Collet, M. Viguier, J. F. Berret, Y. Serero, *Macromolecules* **2003**, *36*, 449.
 141. T. T. Lee, A. Cooper, R. Apkarian, V. Conticello, *Adv. Mat.* **2000**, *12*, 1105.
 142. *Nanoparticles and Nanostructured Films* J. H. Fendler (Ed.), Wiley-VCH Weinheim, Germany 1998.
 143. S. Alexander, *J. Phys. (Paris)* **1977**, *38*, 977.

-
144. A. Haplerin, *Europhys. Lett.* **1987**, *4*, 439.
145. G. Rother, G. H. Findenegg, *Colloid Polym. Sci.* **1998**, *276*, 496.
146. A. Malzert, F. Boury, P. Saulnier, J. P. Benoit, J. E. Proust, *Langmuir*, **2001**, *17*, 7837.
147. C. Ligoure, *J. Phys. II* **1993**, *3*, 1607.
148. S. K. Peace, R. W. Richards, M. R. Taylor, J. R. P. W. Webster, N. Williams, *Macromolecules* **1998**, *31*, 1261.
149. A. M. G. da Silva, E. J. M. Filipe, J. M. R. d'Oliveira, J. M. G. Martinho, *Langmuir*, **1996** *12*, 6547.
150. M. C. Faure, P. Bassereau, M. Carignano, I. Szleifer, Y. Gallot, D. Andelman, *Eur. Phys. J. B* **1998**, *3*, 365.
151. W. Hanke, W. R. Schlue, *Planar Lipid Bilayers*, Academic Press, 1993.
152. H. Möhwald, *Annu. Rev. Phys. Chem.* **1990**, *41*, 441.
153. S. A. Maskarinec, J. Hannig, R. C. Lee, K. Y. C. Lee, *Biophys. J.* **2002**, *82*, 1453.
154. X. Bi, C. R. Flach, J. P. Gil, I. Plasencia, D. Andreu, E. Oliveira, R. Mendelsohn, *Biochemistry* **2002**, *41*, 8385.
155. J. Hannig, D. Zhang, D. J. Canaday, M. A. Beckett, R. D. Austumian, R. R. Weichselbaum, R. C. Lee, *Radiat. Res.* **2000**, *154*, 171.
156. M. A. Terry, J. Hannig, C. S. Carrillo, M. A. Beckett, R. R. Weichselbaum, R. C. Lee, *Ann. N. Y. Acad. Sci.* **1999**, 888, 274.
157. X. Bi, S. Taneva, K. M. W. Keough, R. Mendelsohn, C. R. Flach, *Biochemistry* **2001**, *40*, 13659.
158. J. M. Brockman, Z. D. Wang, R. H. Notter, R. A. Dluhy, *Biophys. J.* **2003**, *84*, 326.
159. P. Cai, C. R. Flach, R. Mendelsohn, *Biochemistry* **2003**, *42*, 9446.
160. D. Vollhardt, V. B. Fainerman, *Adv. Colloids. Interf. Sci.* **2000**, *86*, 103.
161. A. Wiese, M. Munstermann, T. Gutschmann, B. Lindner, K. Kawahara, U. Zahringer, U. Seydel, *J. Membr. Biol.* **1998**, *162*, 127.
162. A. M. O'Connell, R. E. Koeppe, O. S. Andersen, *Science* **1990**, *250*, 1256.
163. H. Abrecht, R. Wattiez, J. M. Ruyschaert, F. Homble, *Plant Physiol.* **2000**, *124*, 1181.
164. A. Vescovi, A. Knoll, U. Koert, *Org. Biomol. Chem.* **2003**, *1*, 2983.

-
165. H. Lindsey, N. O. Petersen, S. I. Chan, *Biochim. Biophys. Acta* **1979**, 555, 147.
166. C. H. Hsieh, S. C. Sue, P. C. Lyu, W. G. Wu, *Biophys. J.* **1997**, 73, 870.
167. M. Winterhalter, H. Burner, S. Marzinka, R. Benz, J. J. Kasianowicz, *Biophys. J.* **1995**, 69, 1372.
168. R. Cseh, R. Benz, *Biophys. J.* **1999**, 77, 1477.
169. C. R. Flach, J. W. Brauner, J. W. Taylor, R. C. Baldwin, R. Mendelsohn, *Biophys. J.* **1994**, 67, 402.
170. R. Mendelsohn, J. W. Brauner, A. Gericke, *Annu. Rev. Phys. Chem.* **1995**, 46, 334.
171. A. Kerth, A. Gericke, A. Blume, (to be published).
172. P. G. de Gennes, *Macromolecules* **1980**, 13, 1069.
173. K. Paeng, J. Choi, Y. Park, D. Sohn, *Colloids Surf.* **2003**, 220, 1.
174. C. Barentin, P. Muller, J. F. Joanny, *Macromolecules* **1998**, 31, 2198.
175. Y. Ren, K. Iimura, T. Kato, *J. Phys. Chem. B* **2002**, 106, 1327.
176. J. C. Ravey, M. J. Stebe, *Colloids Surf. A* **1994**, 84, 11.
177. W. J. Pao, F. Zhang, P. A. Heiney, C. Mitchell, W. D. Cho, V. Percec, *Phys. Rev. E* **2003**, 67, 021601.
178. J. Alsnielsen, D. Jacquemain, K. Kjaer, F. Leveiller, M. Lahav, L. Leiserowitz, *Phys. Reports* **1994**, 246, 251.
179. A. Pinazo, X. Y. Wen, Y. C. Liao, A. J. Prosser, E. I. Franses, *Langmuir*, **2002**, 18, 8888.
180. H. Bourque, I. Laurin, M. Pezolet, J. M. Klass, R. B. Lennox, G. R. Brown, *Langmuir* **2001**, 17, 5842.
181. R. Mendelsohn, C. R. Flach, in *Infrared Reflection-Absorption Spectroscopy of Lipids, Peptides, and Proteins in Aqueous Monolayers*, S. A. Simon, T. J. McIntosh (Eds.), Elsevier Science, San Diego, 2002, p. 57.
182. S. Castano, B. Desbat, J. Dufourcq, *Biochim Biophys. Acta* **2000**, 1463, 65.
183. M. Weygand, M. Schalke, M. Weygand, M. Schalke, P. B. Howes, K. Kjaer, J. Friedmann, B. Wetzler, D. Pum, U. B. Sleytr, M. Losche, *J. Mater. Chem.* **2000**, 10, 141.
184. M. A. K. L. Dissanayake, R. Frech, *Macromolecules* **1995**, 28, 5312.
185. K. J. Lin, J. L. Parsons, *Macromolecules* **1969**, 2, 529.

-
186. A. Lavasanifar, J. Samuel, G. S. Kwon, *Adv. Drug. Delv. Rev.* **2002**, *54*, 169.
187. M. F. Francis, L. Lavoie, F. M. Winnik, J. C. Leroux, *Eur. J. Pharm. Biopharm.* **2003**, *56*, 337.
188. K. Kostarelos, P. Luckam, T. Tadros, *J. Colloid Interf. Sci.* **1997**, *191*, 341.
189. K. Kostarelos, T. Tadros, P. Luckam, *Langmuir*, **1999**, *15*, 369.
190. J. C. M. Lee, H. Bermudez, B. M. Discher, M. A. Sheehan, Y. Y. Won, F. S. Bates, D. E. Discher, *Biotech. Bioeng.* **2001**, *73*, 135.
191. M. Johnsson, N. Bergstrand, K. Edwards, J. J. R. Stalgren, *Langmuir*, **2001**, *17*, 3902.
192. M. Johnsson, M. Silvander, G. Karlsson, K. Edwards, *Langmuir*, **1999**, *15*, 6314.
193. D. Papahadjopoulos, *Stealth Liposomes*, D. D. Lasic, F. Martin, (Eds.), CRC Press Inc., Boca Raton, FL, 1995, Chapter 1.
194. M. C. Woodle, D. D. Lasic, *Biochim. Biophys. Acta* **1992**, *1113*, 171.
195. A. Chonn, P. R. Cullis, *Curr. Opin. Biotechnol.* **1995**, *6*, 698.
196. S. Rangelov, K. Edwards, M. Almgren, G. Karlsson, *Langmuir* **2003**, *19*, 172.
197. P. Chandaroy, A. Sen, P. Alexandridis, S. W. Hui, *Biochim. Biophys. Acta* **2002**, *1559*, 32.
198. J. D. Castile, K. M. G. Taylor, G. Buckton, *Inter. J. Pharm.* **2001**, *221*, 197.
199. T. K. Bronich, S. V. Solomatin, A. A. Yaroslavov, A. Eisenberg, V. A. Kabanov, A. V. Kabanov, *Langmuir* **2000**, *16*, 4877.
200. K. Kostarelos, M. Kipps, T. F. Tadros, P. F. Luckham, *Colloids Surf. A* **1998**, *136*, 1
201. K. Kostarelos, P. F. Luckham, T. F. Tadros, *J. Lipos. Res.* **1995**, *5*, 117.
202. K. Kostarelos, T. F. Tadros, P. F. Luckham, *Langmuir* **1999**, *15*, 369.
203. K. Kostarelos, P. F. Luckham, T. F. Tadros, *J. Chem. Soc., Faraday Trans.* **1998**, *94*, 2159.
204. K. Kataoka, G. S. Kwon, M. Yokoyama, T. Okano, Y. Sakurai, *J. Control. Release* **1993**, *24*, 119.
205. K. Kataoka, *J. Macromol. Sci. Pure Appl. Chem.* **1994**, *11*, 213.
206. G. S. Kwon, *Crit. Rev. Ther. Drug Carrier Sys.* **1998**, *15*, 481.
207. V. P. Torchilin, *J. Control. Release* **2001**, *73*, 137.

-
208. S. E. Dunn, A. Brindley, S. S. Davis, M. C. Davies, L. Illum, *Pharm. Res.* **1994**, *11*, 1016.
209. D. C. Litzinger, A. M. Buiting, N. V. Rooijen, L. Huang, *Biochim. Biophys. Acta* **1994**, *1190*, 99.
210. R. K. Jain, *Adv. Drug. Deliv.* **1997**, *26*, 71.
211. K. Yamamoto, Y. Nagasaki, M. Kato, K. Kataoka, *Colloids Surf. B* **1999**, *16*, 135.
212. J. Taillefer, M. C. Jones, N. Basseur, J. E. V. Lieer, J. C. Leroux, *J. Pharm. Sci.* **2000**, *89*, 52.
213. M. H. Shiba, K. Yamauchi, A. Harada, I. Takamisawa¹, K. Shimokado¹ and K. Kataoka, *Gene Ther.* **2002**, *9*, 407.
214. K. Kataoka, A. Harada, Y. Nagasaki, *Adv. Drug. Deliv. Rev.* **2001**, *47*, 113.
215. Y. Li, G. S. Kwon, *Pharm. Res.* **2000**, *17*, 607.
216. S. Bumla, T. Okano, K. Kataoka, *J. Pharm. Sci.* **1996**, *85*, 85.
217. A. Benahmed, M. Ranger, J. C. Leroux, *Pharm. Res.* **2001**, *18*, 323.
218. G. S. Kwon, M. Naito, M. Yokoyama, T. Okano, Y. Sakurai, K. Kataoka, *J. Control. Rel.* **1997**, *48*, 195.
219. G. S. Kwon, M. Naito, M. Yokoyama, T. Okano, Y. Sakurai, K. Kataoka, *Pharm. Res.* **1995**, *12*, 192.
220. R. Nagarajan, M. Barry, E. Ruckenstein, *Langmuir* **1986**, *2*, 210.
221. D. A. Herold, K. Keil, D. E. Bruns, *Biochem. Pharmacol.* **1989**, *38*, 73.
222. A. W. Richter, E. Akerblom, *Int. Arch. Allergy Appl. Immunol.* **1983**, *70*, 124.
223. B.G. Yu, T. Okano, K. Kataoka, S. Sardari, G. S. Kwon, *J. Control. Release* **1998**, *56*, 285.
224. H. Ge, Y. Hu, X. Jiang, D. Cheng, Y. Yuan, H. Bi, C. Yang, *J. Pharm. Sci.* **2002**, *91*, 1463.
225. D. W. Miller, E. V. Batrakova, T. O. Waltner, V. Y. Alakhov, A. V. Kabanov, *Bioconjugate. Chem.* **1997**, *8*, 649.
226. S. Katayose, K. Kataoka, *J. Pharm. Sci.* **1998**, *78*, 160.
227. M. Ramaswami, X. Zhang, H. M. Burt, K. M. Wasan, *J. Pharm. Sci.* **1997**, *86*, 460.
228. A. Harada, K. Kataoka, *Macromolecules* **1998**, *31*, 288.
229. B. Skoog, *Vox Sang* **1979**, *37*, 345.

-
230. S. C. Cole, G. A. Christensen, W. P. Olson, *Anal. Biochem.* **1983**, *134*, 368.
231. J. Carmichael, W. D. DeGraff, A. F. Gazdar, J. D. Minna, J. B. Mitchell, *Cancer Res.* **1987**, *47*, 936.
232. S. P. C. Cole, *Cancer Chemother. Pharmacol.* **1986**, *17*, 259.
233. M. Montal, P. Mueller, *Proc. Natl. Acad. Sci. USA.* 1972, *69*, 3561.
234. A. V. Krylov, P. Pohl, M. L. Zeidel, W. G. Hill, *J. Gen. Physiol.* **2001** *118*, 333.
235. E. V. Batrakova, T. Y. Dorodnych, E. Y. Klinskii, E. N. Kliushnenkova, O. B. Shemchukova, O. N. Goncharova, S. A. Arjakov, V. Y. Alakhov, A. V. Kabanov *Br. J. Cancer* **1996**, *74*, 1545.
236. T. Demina et al. (unpublished results).
237. O. Krylova, P. Pohl., *Biophys. J.* **2003**, *84*:191A.
238. C. Allen, J. Han, Y. Yu, D. Maysinger, A. Eisenberg, *J. Controlled Release* **2000**, *63*, 275.
239. X. Zhang, J. K. Jackson, H. M. Burt, *Int. J. Pharm.* **1996**, *132*, 195.
240. S. A. Hagan, A. G. Coombes, M. C. Garnett, M. C. Davies, L. Illum, S. S. Davis, *Langmuir*, **1996**, *12*, 2153.
241. R. Oda, I. Huc, D. Danino, Y. Talmon, *Langmuir* **2000**, *16*, 9759.
242. J. W. Nah, Y. I. Jeong, C. S. Cho, S. I. Kim, *J. Appl. Polym. Sci.* **2000**, *75*, 1115.
243. F. Gadelle, W. J. Koros, R. S. Schechter, *Macromolecules* **1995**, *28*, 4883.
244. M. Y. Kozlov, N. S. M. Nubarov, E. V. Batrakova, A. V. Kabanov, *Macromolecules* **2000**, *33*, 3305.
245. P. N. Hurter, T. A. Hatton, *Langmuir* **1992**, *8*, 1291.
246. Y. I. Jeong, J. G. Ryu, Y. H. Kim, S. H. Kim, *Bull Korean Chem. Soc.* **2002**, *23*, 872.

Resume

Name: Hazrat Hussain
Date of Birth: 05-01-1973
Place of Birth: Nawan Killi-Dist. Swabi (Pakistan)

Academic Qualifications:

August 2000-2004 Martin-Luther University, Halle (Saale) Germany.
Doctor of Engineering

1997-1999 Quaid-i-Azam University, Islamabad Pakistan.
M. Phil. Degree in Physical Chemistry.

1995-1996 Quaid-i-Azam University, Islamabad Pakistan.
M. Sc. Degree in Chemistry.

Awards and Honors:

1. Deutsche Forschungsgemeinschaft (DFG), Scholarship for Ph.D. studies (August 2000-September 2002).
2. Certificate of Merit and Chancellors Medal for First Position in M.Sc. Chemistry Examinations.
3. Merit Scholarship during M. Sc. and M.Phil. studies at Quaid-i-Azam University, Islamabad Pakistan.

Statement

I certify that this thesis is based on my own work. I also certify that to the best of my knowledge any help received in preparing this work, and all sources used, have been acknowledged in this Thesis.

M.Phil. Hazrat Hussain